Effect of Carbon nanotubes/nanofibers Reinforcement on Mechanical and Thermal Properties of CFRPs

I. Srikanth

(MS10P002)

A Dissertation Submitted to

Indian Institute of Technology Hyderabad

In Partial Fulfillment of the Requirements for
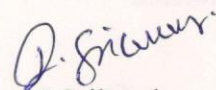
The Degree of Doctor of Philosophy

भारतीय प्रौद्योगिकी संस्थान हैदराबाद
Indian Institute of Technology Hyderabad

Department of Materials Science and Metallurgical Engineering

July 2014

Declaration

I declare that this written submission represents my ideas in my own words, and where others ideas or words have been included, I have adequately cited and referenced the original sources. I also declare that I have adhered to all principles of academic honesty and integrity and have not misrepresented or fabricated or falsified any idea/data/fact/source in my submission. I understand that any violation of the above will be a cause for disciplinary action by the Institute and can also evoke penal action from the sources that have thus not been properly cited, or from whom proper permission has not been taken when needed.
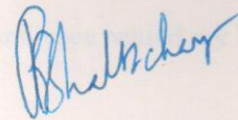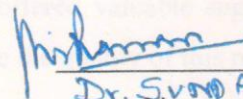
I.Srikanth

(MS10P002)

Approval Sheet

This thesis entitled **"Effect of Carbon nanotubes/nanofibers Reinforcement on Mechanical and Thermal Properties of CFRPs"** by I.Srikanth is approved for the degree of Doctor of Philosophy from IIT Hyderabad.
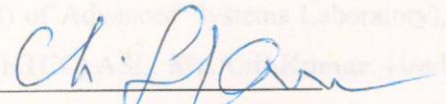
-Name and affiliation-
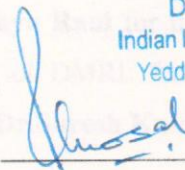
Examiner

BAIDURYA BHATTACHARYA
PROFESSOR, IIT KHARAGPUR

Dr. SVND ARABATAN M.
-Name and affiliation-
PROFESSOR, IIT Madras.
Examiner

-Name and affiliation-
Dr. Ch. Subrahmanyam
Associate Professor
Adviser
Department of Chemistry
Indian Institute of Technology, Hyderabad
Yeddumailaram, 502 205, A. P., INDIA

-Name and affiliation-
Dr Partha Ghosal
Scientist 'F' & Head, Electron Microscopy Group   Co-Adviser
Defence Metallurgical Research Laboratory
Kanchanbagh-P.O., Hyderabad-500 008.

-Name and affiliation-

Chairman

Acknowledgements

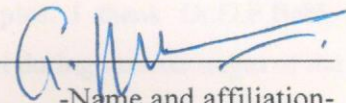Lotus blooms only when the rays of moon invokes it, beautiful songs of the nightingales comes out effortlessly, when the spring inspires it with its exciting colours, rocks comes out with life when the sculptors carefully carves them. Thus every beautiful aspect that we see is seconded either by right people or right ambience. It is my sincere duty to acknowledge those people and the ambience behind my Ph.D work.

Dedicated to

Ever blossoming science

&

All those great minds who nurtured it

Abstract

Multiwalled carbon nanotubes (MWCNTs) were purified to ultra high purity levels (99.9%) by high temperature (2600^0C) heat treatment method. It was observed that, the structural perfection of MWCNTs increased besides improvement in their purity. Based on the TGA, XRD, TEM and Raman spectroscopy studies mechanisms are proposed for the observed structural changes to MWCNTs. These mechanisms says that, during high temperature treatment, the innermost walls of the MWCNTs collapse due to thermal stresses. However, it was observed that, as long as some traces of the metallic impurities are present, they suppress the collapse of the internal walls. Once the metallic impurities are removed, structural distortion of MWCNTs takes place. It was observed that heat treatment for 60 mins is optimum to obtain highly pure and structurally perfect MWCNTs. These purified MWCNTs were subsequently amino functionalised. FT-IR and XPS methods were used to ascertain the functional groups present on the MWCNTs. These functionalised MWCNTs were used to reinforce carbon fiber reinforced plastics (CFRPs). Two kinds of CFRPs were studied in the present work, namely

      i) Carbon fiber reinforced epoxy (C-epoxy) composites,
      ii) Carbon fiber reinforced phenolic (C-Ph) composites.

C-epoxy composites were studied for their mechanical properties when reinforced with carbon nanotubes and nanofibers. C-Ph composites were studied for thermal and ablative properties when reinforced with carbon nanotubes and zirconia. For the C-epoxy based CFRPs, studies were carried out on how MWCNTs influence the crosslink density and toughness of the epoxy matrix. It was observed that, toughness improvement to epoxy due to addition of A_f-MWCNTs is primarily due to the improved crosslink density of the matrix due to of amino groups present on MWCNTs. It was observed that upto certain critical crosslink density, toughness of the matrix increases and beyond this matrix embrittlement was observed. Based on the toughness changes observed with the amino functionalised MWCNTs (A_f-MWCNTs) addition to epoxy, new mechanisms are proposed on the mechanical property improvements for C-epoxy reinforced with A_f-MWCNTs. These mechanisms emphasize the role of MWCNTs in toughening the fiber - matrix interface as the primary reason in improving the mechanical properties of C-epoxy composites. It was observed that, beyond a certain critical loading of A_f-MWCNTs, they embrittle the interface of the composites and decreases the

mechanical properties. A_f-CNF reinforced C-epoxy composites were also made with different fiber volume fractions and tested for their mechanical properties. Typical results highlighted that, A_f-CNFs can increase the mechanical properties of the CFRPs, especially at lower fiber volume fraction, probably due to more matrix content. Fiber - matrix interface zones and matrix rich zones are the weakest zones in the composites. Hence, during the mechanical loads, cracks may initiate preferentially at interface and propagate in a facile manner along the interface thereby leading to a premature failure of the composites. When A_f-CNFs are present, they strengthen the matrix pockets present along the interface zones. Hence, crack can not easily propagate along the interface. This makes the cracks to propagate through the thickness of the composite, which involves rupturing the fibrous reinforcements which consumes more energy. However, as the fiber volume fraction of the CFRPs increases, there is lesser matrix present in the CFRPs and hence A_f-CNFs lose their significance as reinforcements. On the other hand, studies on the mechanical, thermal properties of A_f-MWCNTs reinforced C-phenolic composites have shown that A_f-MWCNTs increases the inter laminar shear strength (ILSS) of C-Ph composites besides increasing the thermal conductivity. As increase in the thermal conductivity is not intended for this class of composites, experiments were carried out to reduce the thermal conductivity of these composites by using zirconia as an additive (Zr-C-Ph). Zirconia introduction to CFRPs was carried out through sol-gel method. It was observed that, when carbon fabrics were coated with zirconia, the thermal conductivity of the resultant composite (Zr-C-Ph) decreased significantly due to insulating properties of zirconia. A functionally graded C-Phenolic composite (FG-C-Ph) was made by a varying the composition of C-Ph composite across its thickness which involves introducing MWCNTs upto certain thickness followed by zirconia in the remaining thickness. Thermal and ablative properties of the prepared C-Ph composites were studied and ablation mechanisms of the C-Ph composites in presence of A_f-MWCNTs and zirconia were proposed.

Nomenclature

Abbreviation/Symbol	Description
A_f-MWCNTs	Amino functionalised MWCNTs
ASTM	American society for testing and materials
CFRPs	Carbon fiber reinforced plastics
CNFs	Carbon nanofibers
CNTs	Carbon nanotubes
CVD	Chemical vapour deposition
cP	Centi Poise
C-epoxy	Carbon fiber reinforced epoxy composite
C-Ph	Carbon fiber reinforced phenolic composite
DSC	Differential scanning calorimeter
FT-IR	Fourier transform infrared spectroscopy
FG-C-Ph	Functionally graded C-Ph composite
FWHM	Full width half maximum
GPa	Gega Pascal
g/cc	grams per cubic centimeter
ILSS	Interlaminar shear strength
K_{IC}	Plane strain fracture toughness
MW/m^2	Megawatt per square meter
MPa	Mega Pascal
MWCNTs	Multiwalled carbon nanotubes
mW	Milliwatts
nm	Nanometers
p-MWCNTs	Purified MWCNTs
SWCNTs	Singlewalled carbon nanotubes
SEM	Scanning electron microscope
TEM	Transmission electron microscope
TGA	Thermo gravimetric analysis

Abbreviation/Symbol	Description
UD	Uni directional
2D	Bi directional
V_f	Fiber volume fraction
Wt%	Weight percentage
XPS	X-ray photo electron spectroscopy
XRF	X-ray fluorescence spectroscopy
XRD	X-ray diffraction
μm	Micrometres
ΔH	Enthalpy change
σ	Stress
ρ	Density
θ	Bragg angle

CONTENTS

Chapter: IV: MWCNT Reinforced Carbon – Epoxy Composites

Chapter: V: CNF Reinforced Carbon-Epoxy Composites

Chapter: VI: CNT-Zirconia Reinforced Carbon-Phenolic Composites

Chapter: VII: Concluding Remarks and Future Scope of Work

Chapter: I

Introduction and Literature Review

Introduction and Literature Review

This chapter introduces various forms of composites in general and CFRPs in particular. Brief overview of carbon nanotubes (CNTs) and carbon nanofibers (CNFs) along with the challenges in tapping their potential as reinforcements in CFRPs is included in this chapter. Significance of structural grade CFRPs (Carbon-epoxy composites) and the ablative grade CFRPs (Carbon-phenolic composites) are highlighted. Research trends in the CNT/CNF reinforced structural grade CFRPs as well as ablative grade CFRPs are summarized from the published literature. Chapter identifies the gaps in the reported literature which forms the basis for the present research.

1. Introduction: Composite is a multiphase material made up of a continuous phase called as the matrix and discontinuous phase called as the reinforcement. Composites generally exhibit significant proportion of properties of both the constituent phases. Among various types of composites, continuous carbon fiber reinforced plastics (CFRPs) are preferred for aerospace applications where high specific strength is required. These CFRPs having high specific strength are generally called as structural grade CFRPs. All structural grade CFRPs are invariably made with epoxy matrix system. This is because epoxy matrix shows excellent environmental stability, moisture resistance, durability besides its cost effectiveness. Hence, all the grades of carbon fibers that are commercially available are made to be compatible with the epoxy matrix. With increasing availability of carbon fibers; epoxy based CFRPs i.e. carbon fiber reinforced epoxy (C-epoxy) composites are finding increasing number applications in the aerospace, and automotive industries to replace conventional materials like metals. Though C-epoxy composites have got high specific strength as compared to the other conventional materials like metals, there is further scope to improve their specific strength. This is because, their true mechanical properties are lower than the theoretically predicted mechanical properties.

The main reason for lower mechanical properties for CFRPs as compared to the theoretically predicted values is due to weak interface between the fiber and matrix, which leads to premature failure. Interface strengthening is expected to give significant improvement in mechanical properties of CFRPs. Especially, matrix dominated properties like inter laminar shear strength and flexural strengths should increase significantly, while the fiber dominated properties like tensile strength also should improve considerably. This could result in overall improvement in the specific strength of CFRPs. There have been attempts to achieve this goal by incorporating nanomoities, such as

nanoclay, graphite nanoparticles, carbon nanotubes (CNTs) and carbon nanofibers (CNFs) [1-5]. Among all these, CNTs and CNFs have emerged as the attractive reinforcing materials for CFRPs due to their superior mechanical properties and high aspect ratio, which suits for composite applications.

On the other hand, most of the aerospace grade structures are exposed to high temperatures generated due to friction with the atmosphere and also due to the high temperature and high velocity gases coming from the exhaust of the motors/engines. CFRPs used under such environments should have high temperature stability, low thermal conductivity (to protect the sub-systems that are behind the CFRPs) and also high shear strength (to withstand, high aerodynamic shear loads of the environment). This class of CFRPs are called as ablative composites which are generally made with the phenolic resin system. The reason to choose the phenolic resin system for this purpose is that phenolic resin is a high char yielding system, which can undergo endothermic pyrolysis at high temperatures thereby offering ablative cooling and thus protect other sub-systems that lie behind it. Any further improvement in the mechanical properties and reduction in thermal conductivity of CFRPs that are used for ablative applications can offer a significant weight saving to the aerospace systems. Many researchers have attempted to enhance the mechanical properties, especially shear strength of ablative grade CFRPs by introducing CNTs/CNFs, as they are known to enhance the shear strength by locking the fiber – matrix interface [6]. Efforts are also going on worldwide to reduce the thermal conductivity of the ablative CFRPs by introducing ceramic powders like nanosilica, nanoclay, zirconium diboride etc [7, 8].

Present research is aimed at understanding the role of CNTs/CNFs as additional reinforcements to structural grade CFRPs (C-epoxy) and also the possibility of deriving the combined benefits of CNTs and other ceramic additives to ablative grade CFRPs (C-phenolic).

1.1. Introduction to composites: A composite is a multiphase material, wherein, the constituent phases are chemically dissimilar and separated by a distinct interface. The phase that is continuous is called as the matrix phase. Matrix surrounds and holds together the other phase called dispersed phase or reinforcement phase. The properties of the composite are mainly dependent on the following aspects.

- Relative amounts of matrix and reinforcements phase

- Geometry of the reinforcements
- Interface bond strength and compatibility between the phases
- Uniform dispersion/spread of the reinforcement phase in the matrix

1.2. Classification of the composites: Composites can be classified based on the type of matrix phase or the type/orientation of the reinforcement phase [9].

1.2.1. Classification based on the matrix: Based on the matrix phase, composites may be classified as following

- Polymer matrix composites
- Ceramic matrix composites
- Metal matrix composites

1.2.2. Classification based on the reinforcements: Based on the reinforcement phase, composites may be classified as following

1.2.2.1. Particle reinforced composites: Particle phase is generally harder and stiffer than matrix. The reinforcing particles tend to restrain movement of matrix phase in the vicinity of each particle. Generally particles, act as hindrances to propagating cracks. Particle reinforced composites are divided in to large particle reinforced composites and dispersion strengthened composites.

1.2.2.2. Fiber reinforced composites: Most important class of composites are fiber reinforced composites. They are generally designed for high strength and high stiffness. Various fibers that are generally used as reinforcements in composites are listed below.

- **Glass fibers**   : Used for low cost industrial applications
- **Aramid fibers**   : Used in applications where high impact strength is required
- **Carbon fibers**   : Used in applications where high specific strength is required. In general carbon fibers are used in aerospace applications where lightweight is the primary requirement.

Fiber reinforced composites are subdivided in to the following.

Continuous fiber reinforced composites: These composites are made by using continuous fibers/fabrics either by filament winding or fabric layup processes. These composites are again subdivided in to following categories.

- Filament wound composites (Uni directional fiber reinforced/UD composites)
- Laminated composites (Layered structures / 2D composites)

Discontinuous fiber reinforced composites: Fibers used in these composites are generally short fibers made by chopping the continuous fibers. These composites can be made either by aligned or randomly dispersed discontinuous fibers.

In general, for most of the structural applications where high specific strengths are essential, CFRP with either UD (filament wound structure) or 2D (laminated structures) are used.

In general, CFRPs contains two phases (matrix phase and the reinforcement phase). Advent of nanomaterials like CNTs/CNFs offer scope for realizing multiphase composites. CNT-C-epoxy or CNF – C-epoxy comes under category of multiphase composites. They are expected to posses much better specific strength than conventional CFRPs. The opportunities and challenges associated with CNT/CNF reinforcement to CFRPs and the global scenario as seen through the published literature is discussed in the subsequent sections.

2. Literature review: The following section gives thorough literature review on the state of the art of the CNTs/CNFs and their reinforced composites.

2.1. Introduction to carbon nanotubes (CNTs): Elemental Carbon in SP^2 hybridized state can form a variety of structures such as graphite, graphene, carbon nanotubes (CNTs), carbon nanofibers (CNFs), fullerenes, etc. CNTs can be treated as rolled graphene sheets with ends closed with the hemisphere of the fullerenes. The uniqueness of their structure is tubular structure having nanometer scale diameters and large length/diameter ratios and low defect densities [10]. Two kinds of CNTs are generally popular. They are single walled carbon nanotubes (SWCNTs) which contain single rolled up hexagonal graphene plane and multiwalled CNTs (MWCNTs) which consists of concentric cylindrical layers of hexagonal graphene planes with an inter layer spacing close to graphite (0.3348 nm). Owing to the strong carbon – carbon bond present between the carbon atoms, CNTs are stiffer and stronger than any other known materials. SWCNTs are reported to have ultra

high modulus (1 – 5 TPa) and high tensile strength (200GPa) with strain to failure up to 10% [11]. Mechanical properties for MWCNTs are known to be inferior to SWCNTs due to more defect concentration. Experimentally measured tensile modulus values for the MWCNTs are in the range of 1TPa and tensile strength is of the order of 80GPa [12]. Mechanical properties of both SWCNTs and MWCNTs are much higher compared to high strength carbon fibers like T-700 grade carbon fibers (Tensile strength 4.8 GPa and modulus 230 GPa). This makes the CNTs promising reinforcement materials for composites. As compared to SWCNTs, MWCNTs have emerged as the preferred materials for reinforcing CFRPs due to cost effectiveness and ease of dispersion.

2.2. Introduction to carbon nanofibers (CNFs): In general, CNFs can be viewed as crude form of MWCNTs with a thick pyrolitic carbon deposition on the initially formed hollow core. They are made up of a hollow core surrounded by a cylindrical fiber comprised of graphite basal planes stacked at about 25^0 from the longitudinal axis of the fiber. The inner walls of the nanofiber consists of stacked up cup morphology formed by nested conical graphene planes canted with respect to the longitudinal fiber axis. These interior cones are completely graphitized but oriented along off-axis of the fiber length. Generally their diameters are in the range of 100-200 nm. They possess excellent mechanical properties with Young's modulus in the range of 300-1000 GPa, tensile strength up to 3.5 Gpa [13]. CNFs are also widely explored as additional reinforcements to CFRPs. The factors which made them compete with CNTs as additional reinforcements to CFRPs are

i)   Low cost and ease of availability
ii)   Ease of dispersion in polymer matrices as compared to CNTs.

Generally large scale synthesis of CNTs and CNFs is carried out by chemical vapor deposition (CVD) method. Hydrocarbon gas or vapors are used as the carbon source/precursor. Synthesis process involves passing hydrocarbon gas or vaporizing the catalyst dissolved organic liquid in to a high temperature chamber and cracking the precursor. The carbonaceous material that forms during cracking, deposits on the metal catalyst surface and grow in the form of CNTs or CNFs depending on the conditions employed in the CVD chamber [14].

CVD is the most preferred method for producing CNTs/CNFs in bulk quantities with a better control over the purity, diameter, and length. CNTs synthesized by CVD method are more suitable as composite reinforcements due to their longer lengths (in microns) compared to the arc discharge

method synthesized CNTs which generally possess sub-micron lengths. However, the main drawback of this method is that, it gives CNTs with high defect density. As a result of this the mechanical properties of the CNTs synthesized by this method are poor [11]. Higher defect density for CVD derived CNTs is due to low operating temperatures of CVD process which lies between 600^0C - 1200^0C depending on the precursor material used as the source for carbon. In the present study, both MWCNTs and CNFs are explored as additional reinforcements to FRPs to understand how MWCNTs/CNFs contribute to the mechanical properties of CFRPs.

2.3. Purification: As synthesized CNTs/CNFs usually contain carbonaceous or metallic impurities. Their purification is an essential issue to be addressed. Considerable progress in purification of these materials is made. A number of purification methods like chemical oxidation, physical separation and combination of chemical and physical techniques have been developed for obtaining CNTs/CNFs with desired purity. Various purification methods available along with their advantages and disadvantages are summarized by Peng – Xiang Ho etal. [15]. Chemical method of purification of CNTs is the most widely followed method due to ease of processing and less infrastructure requirements. This is a two step process. In the first step, raw CNTs/CNFs are exposed to approximately 450^0C temperature in air to remove amorphous carbon by selective oxidation

Carbonaceous impurities get selectively oxidized in this step because of their high reactivity with air as compared to CNTs which are thermally stable up to higher temperatures (up to 550^0C). In the second step, metallic impurities are selectively dissolved by refluxing in strong acids. The disadvantage of chemical purification method is that, it imparts enhanced structural defects to CNTs. Hence, for effective purification of CNTs, skillful optimization of the processes is essential.
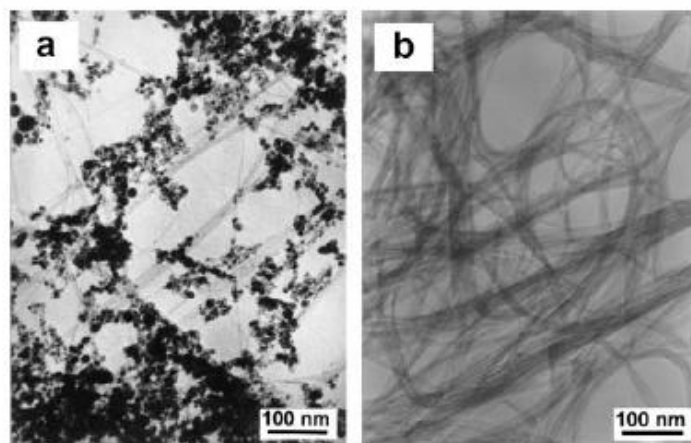
Figure.1.1.TEM images of (a) As synthesized CNTs (b) CNTs after purification [Peng-Xiang et al. [15]. [Reproduced with permission from Elsevier. License. No: 3492590582806 dated 19-10-2014].

To overcome the disadvantages of chemical purification methods, physical purification methods like centrifugation, magnetic separation of metallic impurities, high temperature (up to 2600^{0}C) treatment method were explored by some research groups [16-18].

To study the purity of CNTs, thermo gravimetric analysis (TGA) is widely used. Raman spectroscopy is also generally employed to understand the structural changes of CNTs due to purification/high temperature treatments [19].

2.4. Functionalisation: Performance of the CNTs / CNFs in polymer nanocomposites depends on the interfacial interaction of these materials with the polymer, besides their dispersion. Carbon atoms on the CNTs walls are chemically inert and do not bond well to the polymer matrix thereby seriously impeding the load transfer across the CNT/matrix interface. Reactive functional groups should be generated on CNT surface (functionalisation) which can provide multiple bonding sites to the polymer matrix. Functionalisation gives improved interfacial interaction between the nanotubes and the matrix besides aiding in better dispersion [20, 21]. Hence, functionalisation of CNTs is essential. Functionalisation methods can be divided in to covalent and non-covalent functionalisation methods.

2.4.1. Covalent functionalisation: It involves treating CNTs with oxidising inorganic acids like nitric acid, sulphuric acid or ozone, reactive plasma etc-- to generate carboxylic groups on the CNT surface [10]. These carboxylic groups can act as precursors for further chemical reactions such as

8

silanation, polymer grafting, esterification, alkylation, amination etc-. For reinforcing CNTs with epoxy matrix, amino functionalisation is to be carried out. This is because, amine functional groups on CNTs are reported to show high reactivity and ability to incorporate directly in to the epoxy resin system [22, 23].

The following figure shows the schematic of the amine functionalisation process for CNTs.
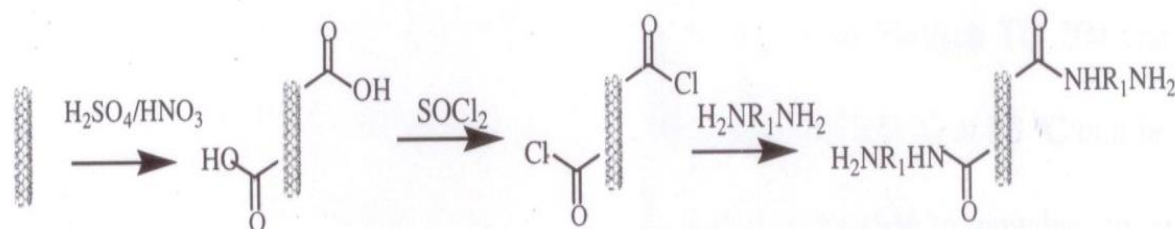
Fig.1.2. Schematic of amino functionalisation process for CNTs /CNFs ([J.Shen.W.Huang et al.[24]). [Reproduced with permission from Elsevier. License. No: 3490121317822 dated 15-10-2014].

The negative side of the covalent functionalisation is that, it often induces the defects in the CNT structure, thereby lowering its mechanical strength.

2.4.2. Non covalent functionalisation: This involves wrapping of polymer around the CNTs to form super molecular complexes of CNTs through van der Waals interaction and $\pi - \pi$ stacking between the CNTs and polymer chains containing aromatic rings. The advantage of this method is that, it do not damage the CNT walls [25]. However, this method can not ensure strong bonding between the CNT surface to the matrix. Hence this method is not popular in composite applications. Peng − Cheng Ma et al. summarized various functionalisation processes for CNTs [26]. Priya et al. reported systematic studies on the functionalisation process of CNFs [27].

2.5. Dispersion in resin system: CNTs and CNFs tend to agglomerate in polymer matrices. This is due to cumulative effect of their large surface area, Van der Waals forces of interactions and their incompatibility with polar matrices (in pristine/non-functionalised state). However, to realize the full potential of these additives as the reinforcements, a stable and homogeneous dispersion in the polymer matrix is desirable [28]. Different dispersion methods reported in the literature are summarized below.

2.5.1: Sonication: In this method, a pulsed ultrasound exfoliates the agglomerated CNTs and disperses them in the matrix effectively [29,30]. For better sonic efficiency, it is recommended to

reduce the viscosity of the polymer resin systems with solvent like acetone, and then add CNTs/CNFs instead of adding them directly in to the resin systems [31]. Drawback of sonication method is that, it is suitable for small batches only. Moreover there is possibility of rupture of CNTs due to the local energy input leading to a reduction of the effective length of CNTs.

2.5.2. Shear mixing/ calendaring: In this method, CNTs/CNFs are dispersed by shear stresses generated by the adjacent cylinders which are rotating at different velocities. Advantage of this method is that it gives uniform shear to the entire volume of the material because the mixture (resin mixed with CNTs/CNFs) must pass through the gap between the rotating cylinders. It is cost effective and suitable for large batches [32]. However, dispersion efficiency is less due to minimum gap that is to be maintained between the rotating cylinders.

2.5.3. Deagglomerator/ Homogenizer: This process involves forcing CNT/CNF mixed fluid to flow at high velocities (up to 500 m/s) in microchannels in a turbulent flow conditions. High shear generated between the agglomerates and walls of the chambers helps in dispersing CNTs/CNFs effectively [33].

Direct evidence for good dispersion of CNTs/CNFs in polymer matrices can be obtained from the electron microscope (scanning electron microscope/SEM and transmission electron microscope/TEM). SEM/TEM observation of the fractured surfaces for CNT/CNF two phase/ three phase composite, is the most reliable and widely used technique. Indirect methods which could give insight on dispersion of CNTs/CNFs in polymers are UV–Vis spectroscopic method [34], Rheological methods [35] Raman spectroscopic method [36] and DSC method [37].

2.6. CNT/CNF reinforced polymer composites (CNT/CNF-CFRPs): The nanometric size and high surface area (up to 1000 m^2/g for SWCNTs, 150m^2/g for MWCNTs, 40 m^2/g for CNFs) make these nanomaterials unique reinforcing materials that can increase the mechanical and physical properties of polymer composites. The advantage of nanoscale compared to micro scale fillers is their enormous surface area which can offer large interface area for stress transfer.

Many researchers have explored the possibility of using CNTs/CNFs as reinforcements in neat epoxy (two phase nanocomposites) and CFRP (three phase nanocomposites) composites. The following section gives the brief necessity/ significance of the study and the summary of the published literature in this area.

2.6.1. Two phase nanocomposites: When CNTs or CNFs are added to the epoxy resin and cured to make a composite, it becomes a two phase nancomposite.

2.6.1.1. Significance of the study: Fabrication and testing of two phase nanocomposites gives a thorough understanding on the various important aspects of nanocomposites which are listed below.

    i) Interaction of nanomaterials with the matrix in terms of formation of chemical

           bonds, retardation/acceleration of cure rate, degree of cure.

    ii) Dispersion of the nanomaterials in the resin system

    iii)   Role of nanomaterials in deflecting/bridging the micro-cracks prior to the failure of

           the composite.

    iv)   Improvement of various properties of the matrix Viz. toughness, impact strength,

           conductivity etc- and the related mechanisms.

A firm knowledge of the above aspects enable us to understand the role of nanomaterials as additional reinforcements in CFRPs (three phase composites). This is because, two phase (CNT-epoxy/CNF-epoxy) composites becomes main constituents of three phase (CNT-C-epoxy/CNF-C-epoxy). The following section gives brief glimpse of reported literature trends in the area of two phase nanocomposites.

2.6.1.2. State of the art in two phase nanocomposites: It is widely reported that, addition of CNTs/CNFs to polymeric systems results in significant improvements in the mechanical properties. For instance, 43% improvement in the fracture toughness, 35% improvement in the flexural strength and 40% improvement in the flexural modulus were reported for CNT – epoxy systems that employed shear mixing method [32]. Impact strength improvements up to 84%, bending strength up to 150 % were reported in MWCNT- epoxy composites when sonication method was employed for dispersion [38]. Impact strength improvement up to 80%, flexural strength and modulus improvements up to 36% and 58% respectively were reported with micro fluidizer based dispersion for CNT-epoxy systems [32].

It is also reported that CNTs show a significant reinforcement effect in soft and ductile matrices. As the stiffness of the matrix increases, CNTs role as reinforcements will diminish due to weak interaction between the CNTs and the matrix [39,40]. On the other hand, J.Cho et al. reported that the length of CNTs that are used as reinforcements also has a significant effect on the final

mechanical properties. They reported that long CNTs are able to enhance the mechanical properties of the composites as they are better able to bridge the micro-cracks [41]. P.C.Ma et al. reported significant improvements in the toughness of the two phase nanocomposites containing functionalised CNTs due to their ability to deflect, bridge the cracks[42] [Fig.1.3]. However enhancement in the fracture toughness ceases when agglomeration of the nano additives takes place [43]. In general functionalised MWCNTs are found to increase the toughness of the matrix and thus give rough fracture surfaces [44]. Failure analysis and modeling studies have proved that, it is the optimal interfacial chemical bond density and the CNT length that lead to the enhancement in the fracture toughness CNTs/CNFs beyond 20-30 micron lengths will self fold and cluster thereby making dispersion difficult[45]. This leads to a reduction in toughness and other mechanical properties.

Most of the published literature in the area of two phase composites (CNT-epoxy) has focused on achieving uniform dispersion of CNTs in epoxy and to understand the mechanisms of strength improvement due to CNTs. These mechanisms primarily revolve around crack deflection/bridging/ load bearing role of CNTs in improving the mechanical properties.

Significant efforts were not made to understand how CNTs influence the cure behavior of the polymeric resin systems, as this will have a significant impact on the final properties. Curing reaction of the polymeric resins, especially epoxy follows a two stage process [46]. In the first stage, the crosslinking reaction is chemically controlled where in hydrogen bearing electron donor molecules (curing agent which is generally amine based chemical) breaks the epoxy ring and sets in the reaction with the formation of hydroxyl groups. Along with the progress of the crosslinking reaction, the viscosity of the system increases. When the viscosity reaches to a critical value, curing reaction becomes diffusion controlled, which is considered as the second stage of curing reaction [46].
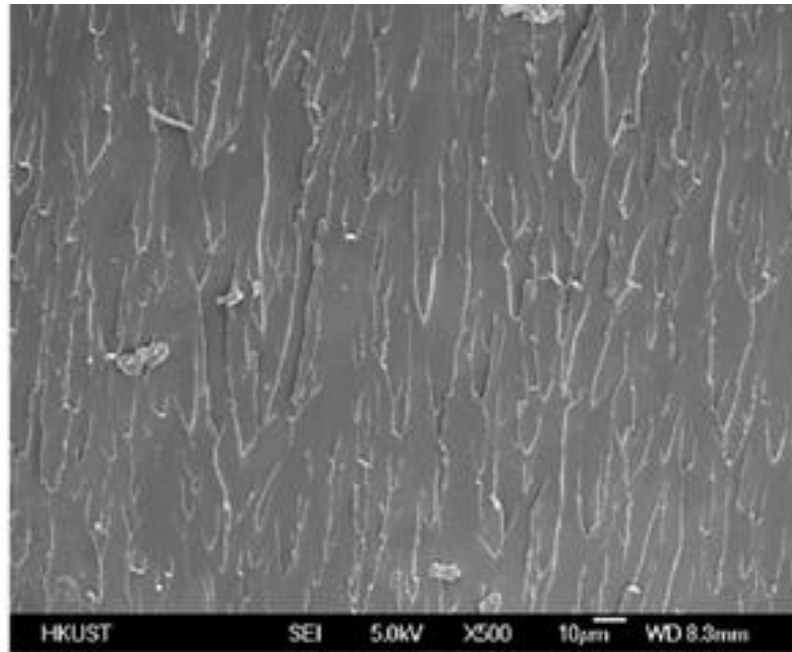
Figure.1.3. Showing CNTs-Epoxy two phase with rough fracture surface indicating crack deflection by CNTs (After Peng-Cheng Ma et al. [42].). [Reproduced with permission from Elsevier. License. No: 3490120713964 dated 15-10-2014].
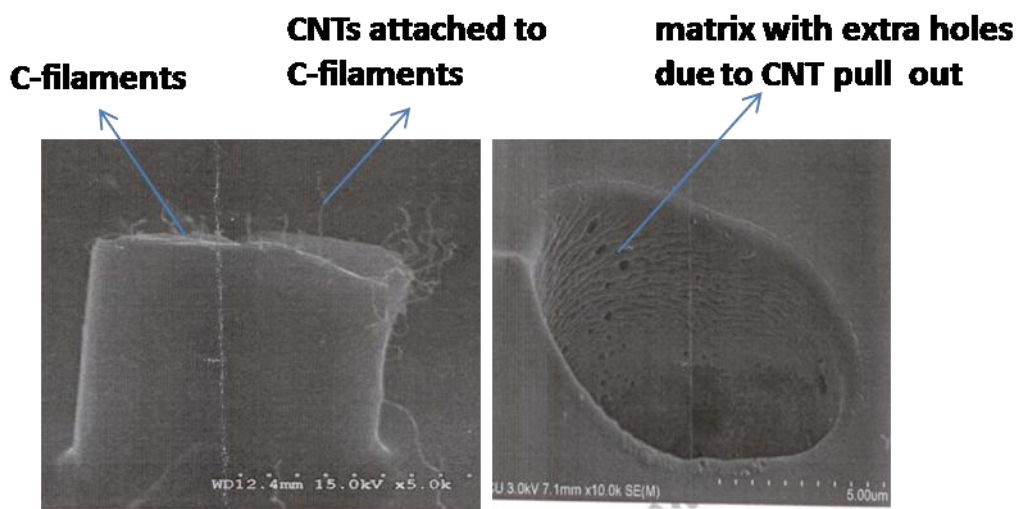
Figure. 1.4. Showing CNTs anchoring effect to the matrix in three phase composites (After K.H. Hung et al.[51]). [Reproduced with permission from Elsevier. License. No: 3490130325332 dated 15-10-2014].

Presence of CNTs increases the viscosity, and makes the mobility of the polymer chains difficult as compared to the resin systems cured without CNTs. Thus resin system having CNTs enters to the diffusion control stage early. This brings down the overall degree of curing. However, the curing

reaction becomes complex when the CNTs are functionalised and contain reactive functional groups which can react with the polymer matrix in which they are dispersed. For instance, if the CNTs/CNFs are functionalised with amino groups they can participate in the crosslinking reactions with epoxy resin [24]. In general, presence of amino groups on CNT/CNF surfaces ensures the initiation of crosslinking during the early stage of the reaction due to the availability of more number of epoxy groups. Besides this, when the reaction reaches the diffusion controlled stage, the amino groups offer more crosslinking sites to the diffusing epoxy species, thereby increasing overall degree of cure of the epoxy. This aspect is not studied thoroughly by any research group.

2.6.2. Three phase nanocomposites: CFRPs having additional reinforcements like CNTs/CNFs along with the conventional reinforcements like carbon fibers are referred as three phase composites.

2.6.2.1. Significance of the study: In general, CFRPs are used to make structural subsystems of aerospace vehicles. The main purpose of these structures is to bear the load. Any improvement in the mechanical properties of CFRPs can result in a significant weight saving for aerospace systems. In CFRPs, among various possible matrix systems, epoxy matrix reinforced with carbon fiber (C-epoxy) is the most preferred because of its high specific strength. Hence, most of the research in the area of CNT-CFRPs is focused around improving the mechanical properties of C-epoxy by using CNTs/CNFs, as additional reinforcements. On the other hand, CFRPs, made with phenolic matrix reinforced with carbon fiber (C-phenolic) are used for protecting the aerospace vehicles from high temperatures generated due to friction of high velocity vehicle with the atmosphere and/or due to high temperature generated from the motor/engine exhausts. These composites (C-phenolic) are known as ablative composites. Significant efforts were made by many groups to understand the suitability of CNT/CNF reinforced C-phenolic three phase composites for ablative applications. Following sections presents the international scenario in the area of CNT/CNF reinforced CFRPs with a focus on structural and ablative applications.

2.6.2.2. State of the art in three phase nanocomposites (CNT/CNF-CFRPs): In CFRPs, weakest zone is the interface zone between carbon fiber and matrix**.** Micro cracks that get initiated at the fiber-matrix interface propagate easily which leads to delamination and premature failure of CFRPs. Improvement the interfacial bond strength is expected to boost the mechanical properties of CFRPs. Hence, the main aim of the research in this area is to understand how the CNTs/CNFs can strengthen

the fiber – matrix interface area [47-50]. It is reported that, introduction of CNTs/CNFs in the CFRPs results in strengthened fiber-matrix interface as these nanomaterials occupy the interface zones and anchor the fiber to the matrix in a manner similar to what roots can do to a tree as shown in Fig1.4. [51].

Under the applied loads, when the fiber is pulled, the load can be transferred to the matrix uniformly across the interface through the CNTs in the form of both shear and tensile forces. The off axis CNTs which spread into matrix tend to resist pull out of C-fiber and thus offer more shear resistance across the interface. Thus in CNT/ CNF reinforced CFRPs, pull out of the C-fiber involves simultaneous pulling of the CNTs/CNFs which are spread in to much larger matrix area. Hence, the pulling process consumes a higher amount of energy at the fracture zone. This results in higher mechanical properties for CFRPs reinforced with CNTs/CNFs. Other possible reasons for improved mechanical properties of CFRPs due to CNT addition includes the ability of CNTs to offer retardation effect on matrix micro-cracks by bridging the cracks [51]. Some reports even suggested that CNTs can take the load and thus enhance the mechanical properties [52].

Due to cumulative effect of the above mechanisms, significant improvement in the mechanical properties of CFRPs due to CNTs was observed. For instance, F.H.Gojny et al. reported flexural strength and ILSS improvements up to ~26% for CNT reinforced FRPs processed by vacuum assisted resin infusion molding (VARIM) at 1wt% loading of CNTs [53]. Zhianhang et al. reported 20-25% improvement in the matrix dominated properties for glass fiber reinforced polymers (GFRP) with nanotube reinforcements [54]. These GFRPs were processed by vacuum assisted resin transfer molding (RTM).M.Nadler et al. emphasized that higher loading of nanofillers may be essential for nanocomposites to exceed the mechanical properties of the existing composites [23]. However, achieving better dispersion at higher nanofiller loading may be complicated. Moreover, increased resin viscosity at higher loadings may also complicate the processing of the epoxy resin [55].

On the other hand, CNF reinforcements to C-epoxy composites also resulted in a similar degree of improvement in mechanical properties. For instance, Sohel Rana et al. reported 18% improvement in the tensile strength for the 2D C-epoxy composites with the addition of 0.5wt%CNFs, while the compressive strength and toughness also improved significantly [56]. Flexural strength improvement for CFRPs up to 22% was reported by Zhou et al., while ILSS improvements of the same degree

were reported many research groups [57]. Kieth.J.Green et al., reported flexural strength improvement up to 16% and ILSS improvement up to 25% with 1wt% addition of functionalised CNF to FRPs made of epoxy matrix [58]. Mechanisms for the improved mechanical properties due to addition of CNFs to CFRPs are same as reported for CNT - CFRPs. In essence, the improvements are due to strengthened matrix and improved fiber-matrix interfacial strength. As the degree of improvements in mechanical properties to CFRPs due to either CNTs or CNFs is more or less of same degree, the later were also widely explored as additional reinforcements to CFRPs. Moreover, lower cost, ease of dispersion in polymer matrices made CNFs more attractive than CNTs. Hence, in the present study, systematic experimental studies were carried out to understand, the role of CNFs as reinforcements to CFRPs along with the CNT reinforcement studies to CFRPs.

2.6.2.2.1. Novel trends in three phase composites: To overcome the problem of CNT dispersion in the resin systems, some researchers have adopted novel method of depositing CNTs on the C-fibers by using chemical vapor deposition (CVD) method. These CNT deposited C-fibers are subsequently used to realize composites [59]**.** CFRPs made of this method, have shown a multiscale fracture behavior, where CNTs pulled out along with the fibers have left nanoscale holes indicating the strengthening of the interface. Enrique J.Garcia et al. have transferred the aligned CNT forest on to a epoxy C-fabric prepeg and made unidirectional carbon tape composites while maintaining the CNT alignment in the through thickness direction [47]. Fracture toughness improvements up to 1.5 to 2.5 times was reported by them. Tomohiro Yokozeki et al. reported addition of 5wt% amine CNTs to epoxy resin and made carbon - prepegs with this resin. They reported improvement in stiffness for the composites made with these prepregs [48]. Large variations in the reported mechanical property enhancements can be attributed to the variations in the quality of raw materials, functionalisation, and dispersion methods etc. Design methods used for conventional CFRPs based on the rule of mixtures are not suitable for nanocomposites. Hence new design methods are proposed for nanocomposites [60].

2.6.2.3. State of the art in Carbon-Phenolic three phase composites: The following sections gives a brief overview on the state of the art in this area.

2.6.2.3.1. Two phase CNT/CNF-phenolic composites: Yeh et al. mixed MWCNTs to the phenolic matrix by using sonicator. Various weight percentages (wt %) of MWCNTs (from 0.5wt% to 4.0wt

16

%) were added to phenolic matrix and made two phase composites. They reported up to 64% improvement in the tensile modulus and 46% improvement in the tensile strength at 2wt% loading of MWCNTs for two phase MWCNT-phenolic composites [61]. R.D.Patton et al. evaluated the ablation, mechanical and thermal properties of the CNF reinforced phenolic composites [62]. In the ablation testing, it was observed that, CNF-phenolic two phase composites have shown good erosion resistance. In general, thermal conductivity of the both CNT/CNF-phenolic (two – phase) are observed to increase as compared to the corresponding blank composites [63].

2.6.2.3.2. Three phase CNT/CNF-phenolic composites: R.B.Mathur et al. have deposited up to 8wt% of MWCNTs on the carbon cloth and used this CNT deposited cloth to reinforce phenolic matrix to realize CNT-C-Phenolic CFRPs. They reported 75% improvement in the flexural strength and 54% improvement in the flexural modulus of the C-Phenolic composites due introduction of CNTs [64]. The reason for such high magnitude of improvement in the flexural strength is attributed to strengthening of the cross over points (crossing points of warp and weft tows) by CNTs. J.M.Park et al. studied optimizing CNT dispersion conditions in phenolic resin and improved adhesion between the carbon fibers and the CNT-Phenolic resin by treating the carbon fiber surfaces with plasma treatment. They reported increased ILSS for CNT-C-phenolics made with plasma treated carbon fibers [6]. CNTs are also reported to facilitate better stress transfer between the phenolic matrix to the carbon fiber [65].

However, in general, CNT/CNF addition to CFRPs results in enhanced thermal conductivity which may result in enhanced back face temperature of ablative grade CFRPs. This restricts the thermal insulation ability of ablative grade CFRPs [66]. Besides CNTs/CNFs, other nanomaterials like nanosilica, nanoclay were also extensively studied as additive to the C-Phenolic composites [67,68]. The main aim of opting for ceramic additives is lowering the thermal conductivity of the C-phenolic composites. However, ceramic additives are known to bring down the mechanical properties like ILSS, flexural strength of C-phenolic composites.

2.7. Gaps identified in the literature

i)   Systematic studies on how does crosslink density of the epoxy will be effected by CNTs and in turn how this property is altering the toughness of two phase and mechanical properties of three phase nanocomposites is not explored.

ii)   No studies are reported so far, on how does matrix volume fraction and fiber volume fractions in the three phase composites influence the reinforcement role of CNFs.

iii)   No studies are reported so far, on how to exploit the combined benefits of the CNTs addition as well as the ceramic materials addition to CFRPs in realizing CFRPs with high mechanical properties as well as low thermal conductivity.

2.8. Aims of this work: Based on the literature survey following objectives are identified which are addressed in the present work.

i)   Understanding how MWCNTs influence the toughness of epoxy matrix and to study the relation between the mechanical property improvements of MWCNT-CFRPs (C-epoxy) with the toughness of MWCNTs –epoxy.

ii)   Understanding how strengthening mechanisms of carbon nanofiber in CFRPs changes as the fiber volume fraction of the CFRP changes

iii)   To understand how MWCNTs affects the inter laminar shear strength, flexural strength thermal conductivity, ablation performance of CFRPs. CNTs addition to CFRPs invariably increases the thermal conductivity. Hence, it is aimed to reduce the thermal conductivity of CFRPs by employing ceramic additives like zirconia.

To study the above aspects, availability of high pure MWCNTs are essential. Hence, purification of MWCNTs up to ultra high purity (99.99%) levels by high temperature heat treatment method and studying the structural changes to MWCNTs during high temperature heat treatment is included as part of the study.

2.9: Outline of the thesis: This section gives brief outline of the subsequent chapters. This includes a overview of the experimental work carried out, results obtained.

Chapter II deals with a brief overview of the principles of various characterization and testing methods used in the present work. Various characterization methods like Scanning Electron Microscope (SEM), Transmission Electron Microscope (TEM), Raman spectroscopy, Thermo Gravimetric Analysis (TGA), Differential Scanning Calorimeter (DSC), Fourier Transform Infrared Spectroscopy (FT-IR), X-ray Photo Electron Spectroscopy (XPS), X-ray Diffraction (XRD) were summarized. After summarizing the above characterization methods various testing methods used to test the CNT/CNF reinforced composites are summarized. The tests that were summarized are fiber

volume fraction, fracture toughness (K_{IC}), flexural strength, tensile strength, inter laminar shear strength, thermal conductivity test.

Chapter III deals with the purification and functionalization of MWCNTs. In general conventional methods of purification demand strong acids to remove the metallic impurities. In the preset work, high temperature (2600°C) heat treatment based purification of MWCNTs is employed. The objective of the experimental work is to understand the effect of duration of high temperature heat treatment on the purity and structural changes for MWCNTs. As part of experimental work, raw MWCNTs (MWCNTs having metallic impurities) were exposed to $2600^{o}C$ in nitrogen atmosphere for 60mins and 120mins. Thermo Gravimetric Analysis (TGA), X-ray Diffraction (XRD), Raman spectroscopy, Transmission Electron Microscopy (TEM) methods were used to analyze the affect of heat treatment duration on the purity and structural changes of MWCNTs. Typical results indicated that the high temperature heat treatment can be used to purify MWCNTs with proper optimization of the treatment time. It was observed that, while 60mins heat treatment can impart high purity and structural perfection to MWCNTs, 120mins heat treatment has resulted in structural degradation of MWCNTs with collapse of the innermost shells. Studies indicated that, metal impurities acts as moderator in controlling the degradation of MWCNTs up to a certain duration. Once the metal impurities are removed completely, further heat treatment degrades the structure of MWCNTs.

This chapter also deals with functionalization of MWCNTs. Functionalization is an essential step to use MWCNTs as reinforcements in polymer matrix composites. Amino functionalization of MWCNTs is reported as the suitable functionalization method to reinforce them with the epoxy matrix. Hence, in the present study, MWCNTs that were purified by high temperature heat treatment methods were subsequently amino functionalized by a three step functionalization process which involves carboxylation, acylation and amination. FT-IR and XPS were used to ascertain the presence of amino functional groups on the surface of MWCNTs.

Chapter IV is devoted to understand the effect of MWCNTs on the fracture toughness of two phase nano composites (CNT-epoxy) and also to study how toughness variations of matrix due to MWCNTs can influence the mechanical properties of the three phase composites (CNT-C-epoxy or CNT-CFRPs). Experimental work includes, fabrication of MWCNT reinforced epoxy nanocomposites (two phase), and MWCNTs-carbon-epoxy nanocomposites (three phase).   Two

phase and three phase composites were made by using both purified multiwalled carbon nanotubes (p-MWCNTs) as well as with amino functionalized MWCNTs (Af-MWCNTs) at 0.25wt%, 0.5wt%, 1.0wt% loadings and the mechanical properties were compared. DSC studies have indicated that, MWCNTs without any functional groups on their surface decrease the overall degree of cure, while the amino functionalised MWCNTs enhance the overall degree of cure of the epoxy matrix. Toughness of the two phase composites were studied following ASTM-D5045. It was observed that, up to an optimum crosslink density improvement, toughness of epoxy matrix increases, and beyond this the toughness of epoxy matrix decreases. Tensile, flexural and ILSS properties of the three phase composites were studied using a UTM. Observed variations in the mechanical properties of three phase composites due to p-MWCNTs and A_f -MWCNTs were seen in the light of the toughness changes to the matrix. It was observed that, the mechanical property improvements to CFRPs due to A_f-MWCNTs is directly related to the ability of A_f -MWCNTs to toughen the matrix/fiber-matrix interface. It was also observed that the addition of higher amount of A_f -MWCNTs cannot ensure better mechanical properties to CFRPs, primarily because higher amount of A_f -MWCNTs at the interface of C-fiber to matrix are embrittling the interface.

In Chapter V, the mechanical property evaluation of C-epoxy composites reinforced with amino functionalized carbon nanofibers were studied. Extenstive literature is available on CNF ability to improve the mechanical properties CFRPs. Many parameters like the length of these nanomaterials, type of functionalization and dispersion methods were studied by different research groups which could affect the mechanical properties of CFFRs. However, so far no systematic study was reported on how variation in the fiber/matrix volume fraction in CFRPs can influence the reinforcement ability of the CNFs. Hence, this chapter is devoted to understand, how CFRPs having different fiber volume fractions behave differently in terms of degree of mechanical property improvements when reinforced with same quantity of CNFs. To study this aspect, carbon–epoxy (C-epoxy) laminated composites with varying percentage of fiber volume fraction (V_f) namely 40, 50, 60, 70 were fabricated with and without addition of 1.0wt% of amino functionalized carbon nanofibers (Af-CNF). Flexural strength, inter laminar shear strength (ILSS) and tensile strength of Af-CNF reinforced C-epoxy composites were evaluated and compared with their corresponding blank composites having same V_f (without CNFs). It is observed that, the ability of A_f -CNFs to enhance the mechanical properties of C-epoxy composites diminished significantly on increasing the V_f of the composite from 40 to 60% and beyond this V_f, addition of A_f -CNFs (to C-epoxy having $70V_f$)

decreased the mechanical properties. Ability of A_f -CNFs to resist cracks propagating along the interface and their ability to increase the inter filament bonding are the main mechanisms responsible for the improved mechanical properties of A_f -CNFs reinforced CFRPs. Changes in the strengthening mechanisms with the change in the volume fraction of CFRPs is discussed in detail in this chapter.

In Chapter VI mechanical, thermal and ablative properties of CNT, zirconia modified carbon – phenolic composites were discussed. CNT reinforcement to CFRPs is known to give improved ILSS and flexural strength. However, thermal conductivity also increases with CNT addition, which is not intended for ablative grade CFRPs used in aerospace applications. Even though ceramic additives are known to decrease the thermal conductivity of CFRPs, they impart lower ILSS and flexural strength. Hence, this chapter is devoted to develop functionally graded CFRPs having CNT reinforcement up to certain thickness followed by zirconia reinforcement in the remaining thickness. The aim of making such a composite is to realize the ablative CFRP with higher mechanical property as well as low thermal conductivity. C-Ph composites containing MWCNTs at different wt% (0, 0.5wt%, 1.0wt% and 1.5wt %) were made. Thermal conductivity, ILSS and flexural strength were measured for the prepared composites. It was observed that, ILSS, flexural strength improvements due to CNT addition saturated at 0.5wt% addition, whereas, thermal conductivity was increasing with the increased loading of CNTs. On the other hand, a different set of composites were made with zirconia addition at 0 wt% (Blank), 3.5wt%, 6.5wt% and 9.5wt% to C-phenolic composites (Zr-C-Ph). Zirconia introduction on carbon fabric was done by developing zirconium oxide (Zirconia) coating on carbon fabric (C-fabric) using zirconia sol using sol-gel method. A functionally graded carbon – phenolic composite (FG-C-Ph) having CNT-C-Ph composition up to certain thickness followed by Zr-C-Ph composition for the remaining thickness was made based on the ILSS, flexural strength and thermal conductivity data obtained for Zr-C-Ph composites. Thermal insulation and ablative properties for blank C-Ph, Zr-C-Ph, FG-C-Ph were studied using plasma arc jet test which was carried out at a heat flux of 4.0 MW/m^2 for 30 seconds. Ablation mechanisms were proposed based on the microstructure and XRD studies of the ablated surfaces. Results from the plasma arc jet test shows the possibility of developing a CNT-CFRP structure with ceramic additives.

References

[1] A.K.Subramaniyan, C.T.Sun. Enhancing compressive strength of unidirectional polymeric composites using nanoclay. Composites: Part:A.37 (2006) 2257-2268

[2] Y.Rachmadini. V.B.C.Tan, T.E.Tay, Enhancement of mechanical properties of composites through incorporation of CNT in VARTM - A Review. Journal of Reinforced Plastics and Composites.29 (2010) 2782-2807

[3] Yutaka Iwahori, Shin Ishiwata, TomojiSumizawa, Takashi Ishikawa. Mechanical properties improvements in two - phase and three – phase composites using CNF dispersed resin. Composites: PartA.36 (2005) 1430 – 1439.

[4] Y.X.Zhou, F.Pervin,V.K. Rangari,S.Jeelani. Fabrication and evaluation of carbon nanofiber filled Cabron/epoxy composites. Mater.Sci. Engg. A. 426 (2006) 221-228.

[5] J.Cho. J.Y .Chen, I.M .Daniel. Mechanical enhancement of carbon fiber/epoxy composites by graphite nanoplatelet reinforcement. Scripta Materilia. 56 (2007) 685-688.

[6] J.M. Park, Z.J.Wang,D.J.Kwon, G.Y.Gu,W.I.Lee, J.K.Park, Interfacial properties and self sensing of single carbon fiber reinforced CNT-Phenolic nanocomposites using electro-micro mechanical and wettability tests. Composites: Part B. 43 (2012) 1171-1177.

[7] I.Srikanth, Alex Daniel, Suresh Kumar, N.Padmavathi, Vajinder Singh, P.Ghosal, Anil Kumar, G.Rohini Devi. Nanosilica modified carbon – phenolic composites for enhanced ablation resistance. Scripta.Materialia 63 (2010) 200-203.

[8] Yaxi Chen, Ping Chen, Changqing Hong, Baoxi Zhang, David Hui. Improved ablation resistance of carbon–phenolic composites by introducing zirconium diboride particles. Composites: Part B.47 (2013) 320–325

[9] W.Callister.Jr. Fundamentals of Materials Science and Engineering. 5th edition. John Wiley & Sons.2001.

[10] Ijima, Helical microtubes of graphitic carbon. Nature.354 (1991) 56-58

[11] M.F.Yu, O.Louire, M.J.Dyer, K.Moloni, T.F.Kelly, R.S.Ruoff. Strength and breaking mechanism of multiwalled Carbon nanotubes under tensile load. Science.287 (2000) 637-640.

[12]J.P.Salvetat,T.M.Bond,N.H.Thomson,A.J.Kulik,L.Forro,W.Bendit,L.Z.Uppiroli.App.PhySci.A.69 (1999) 255-260.

[13]TanilOzkan, Mohammad Naraghi, Ioannis Chasiotis. Mechanical properties of vapor grown Carbon nanofibers, Carbon.48 (2010) 239-244.

[14] N.J.Covlle, S.D.M.Langa, E.N. Nxumalo, A.A.Shaikjee. Review of shaped carbon nanomaterials. S.Afr.J.Sci. 107 (2011).Art .415.1-15. DOI: 10.4102/ sajs.v107i3/4.418

[15] Peng – Xiang Hou, Chang Liu, Hui – Ming Cheng. Purification of Carbon Nanotubes .Cabron 46 (2008) 2003-2025

[16] A.P.Yu, E.Bekyarova, M.E.Itkis, D.Fakhrutdinov, R.Webster, R.C.Haddon. Application of centrifugation to the large-scale purification of electric arc-produced single-walled carbon nanotubes. J Am Chem Soc .126 (2006) 9902–9908.

[17] Y.Kim,D.E. Luzzi. Purification of pulsed laser synthesized single wall carbon nanotubes by magnetic filtration. J Phys ChemB . 109 (2005) 16636–16643.

[18] W.Huang, Y.Wang, G.H.Luo, F.Wei. 99.9% purity multi-walled carbon nanotubes by vacuum high-temperature annealing. Carbon.41 (2003) 2585–2590.

[19] Park TJ, Banerjee S, Hemaraj-Benny T, Wong SS. Purification strategies and purity visualization techniques for singlewalled carbon nanotubes. J Mater Chem.16 (2006) 141–154.

[20] A.G.Osorio, I.C.L. Silveira, V.L. Bueno, C.P. Bergmann. H2SO4/HNO3/HCl— Functionalisation and its effect on dispersion of carbon nanotubes in aqueous media. Appl. Surf. Sci. 255 (2008) 2485–2489

[21] Kai Yang, MingyuanGu, YipingGuo, Xifeng Pan, Guohong Mu. Effects of Carbon nanotube functionalisation on the mechanical and thermal properties of epoxy composites. Carbon.47 (2009) 1723-1737.

[22] F.H. Gojny, J.Nastalczyk, Z.Roslanied, K.Schutle. Surface modified multi – walled carbon nanotubes in CNT/epoxy composites. Chem.Phys.Lett 370 (2003) 820-824.

[23] M.Nadler, J.Werner, T.Mahrholz, U.Riedel, W.Hufenbach. Effect of CNT surface functionalisation on the mechanical properties of multi-walled Carbon nanotube/epoxy-composites. Composites: Part A .40 (2009) 932–937.

[24] JianfengShen, Wishi Huang, Liping Wu, Yizhe Hu, Mingxin Ye. The reinforcement role of different amino-functionalized multi-walled Carbon nanotubes in epoxy nanocomposites Compos. Sci. Technol . 67 (2007) 3041–3050

[25] R.J. Chen, S.Bangsaruntip. K.A. Drouvalakis, N.W.S. Kam, M.Shim, Y. Li, W. Kim, P. J. Utz,H. Dai. Non covalent functionaliastion of carbon nanotubes for highly specific electronicbiosensors.Proc.Nat.Acad.Sce.USA.100(2003).4984-4989.doi:10.1073/pnas. 0837064100

[26] Peng – Cheng Ma, Naveed A. Siddiqui, Gad Marom, Jang – Kyo Kim. Dispersion and functionalisation of Carbon nanotubes for polymer – based nanocomposites: A review. Composites: Part A. 41(2010) 1345-1367.

[27] Priya V Lakshminarayanan, HosseinToghiani, Charles U Pittman Jr. Nitric acid oxidation of vapor grown Carbon nanofibers. Carbon 42 (2004) 2433-2442

[28] S.G. Prolong, M.Buron, M.R.Gude, R.Chaos, MCampo, A.Urena. Effect of dispersion techniques on the thermo physical properties of epoxy nanocomposites. Compos. Sci. .Technol. 68 (2008) 2722-2730.

[29] John Kathi, Kyong - Yop Rhee, JhoongHee Lee. Effect of chemical functionalisation of multi-walled Carbon nanotubes with 3-aminopropyltriethoxysilane on mechanical and morphological properties of epoxy nanocomposites. Compos: Part A 40 (2009) 800 – 809.

[30] Peng He, Yong Gao, JieLian, Lumin Wang, Dong Quan, JianZhaw,Wie Wang, Mark   J.Schulz, Xing Ping Zhou, Donglu Shi. Surface modification and ultra sonication effect on the mechanical properties of Carbon nanofiber/poly Carbonate composites. Compos: Part A 37 (2006)1270-1275

[31] Kin – tat Lau, Mei Lu, Chun – kiLan, Hoi Yan Cheung, Fen – Lin Sheng, Hun-Lin Li. Thermal and mechanical properties of SWCNT bundle reinforced epoxy nanocomposites: The role of solvent for nanotube dispersion. Compos. Sci. Technol. 65 (2005) 719-725

[32] Florian.H.Gojny, MalteH.G.Wichmann, Bodo Fielder, Karl Schulte. Influence of different CNTs on mechanical properties of epoxy matrix composites-A comparative study. Compos. Sci. Technol.65 (2005) 2300-2313.

[33] ZhengYaping, Zhang Aibo, Chen Quinghua, Zhang Jiaoxia, NingRongchang. Functionalized effect on Carbon nanotubes/epoxy nano-composites. Mater. Sci. Engg A. 435-436 (2006) 145–149.

[34] RichaRastogi, Rahul Kaushal, S.K. Tripathi, Amit L. Sharma , InderPreet Kaur, LalitM.Bharadwaj. Comparative Study of Carbon nanotube dispersion using surfactants. J. of Colloid. Interface Sci. 328 (2008) 421-428.

[35] Ian A Kinloch, Simon A Roberts, Alan H Windle, A Rheological study of concentrated aqueous nanotube dispersion. Polymer.43 (2002) 7483-7491.

 [36] Daniel.C.Davis, Justin.W. Wilkenson, Jiang Zhu, Viktor G.Hadjiev. A strategy for improving mechanical properties of a fiber reinforced composite using functionalised CNTs. Compos. Sci. Technol71 (2011) 1089-1097..

[37] Si Hwan Kim, Woo I Lee, Joung Man Park. Assessment of dispersion in Carbon nanotube reinforced composites using differential scanning calorimetry. Carbon 47 (2009) 2699-2703.

[39] Lijie Ci, Ji Bo Bai. The reinforcement role of Carbon nanotubes in epoxy composites with different matrix stiffness. Compos. Sci. Technol.66 (2006) 599 – 603.

[40] Luqi Liu , H. Daniel Wagner. Rubbery and glassy epoxy resins reinforced with carbon nanotubes. Composites Science and Technology. 65 (2005) 1861-1868.

[41] J.Cho , I.M. Daniel, D.A. Dikin. Effects of block copolymer dispersant and nanotube length on reinforcement of carbon / epoxy composites. Composites: Part A. 39 (2008) 1844-1850.

[42] Peng Cheng Ma, Jang – Kyo Kim, Ben Zhong Tang. Effects of silane functionalisation on the properties of Carbon nanotubes/epoxy nanocomposites. Compos.Sci.Technol. 67 (2007) 2965-2972.

[43] NoaLachman, H. Daniel Wanger. Correlation between interfacial molecular structure and mechanics in CNT/epoxy nano-composites. Composites: Part A . 41 (2010) 1093-1098.

[44] YanGeng, Ming Yang Liu, Jing Li, Xiao Mei Shi, Jang Kyo Kim. Effects of surfactant treatment on the mechanical and electrical properties of cnt/epoxy nanocomposites. Composites:Part A 39 (2008) 1876-1883.

[45] Y.L. Chen, B.Liu, X.Q. He, Y. Huang, K.C.Hwang. Failure analysis and optimal toughness design of Carbon nanotube – reinforced composites. Compos.Sci. Technol 70(2010)1360 – 1367.

[46] A.Allaoui, N.ElBounia. How carbon nanotubes affect the cure kinetics and glass tansition temperature of their epoxy composites . A review. eXPRESS Polymer Letters.3 (2009) 588-594.

[47] Enrique J.Garcia, Brian L. Wardle, A. John Hart. Joining and prepeg composite interfaces with aligned Carbon nanotubes. Composites: Part A . 39(2008) 1065 – 1070.

[48] TomohinoYokozeki, YukataIwahori, Shin Ishiwata, Kiyoshi Enomoto, Mechanical properties of CFRP laminates manufactured from unidirectional prepegs using CSCNT-dispersed epoxy, Composites: PartA.38 (2007) 2121-2130.

[49] S.Tsantzalis, P.Karapappas, A.Vavouliotis, P.Kostopoulos, T. Tanimoto, K.Friedrich, On the improvement of toughness of CFRPs with resin doped with CNF and PZT particles, Composites: Part. 38 (2007)1159-1162.

[50] M.T.Kim, K.Y.Rhee, J.H.Lee, D. Hui, Alan K.T. Lau. Property enhancement of Carbon fiber /epoxy composite by using Carbon nanotubes. Compsites:Part:B. 42 (2011) 1257-1261.

[51] K.H.Hung, W.S. Kuo, T.H.Ko, S.S.Tzeng, C.F.Yan. Processing and tensile characterization of composites composed of carbon nanotube grown carbon fibers. Composites : Part A. 40 (2009) 1299-1304

[52] A.Godara, L.Mezzo, F.Luizi, A.Warrier, S.V. Lomov, A.W. Van Vuure, L.Gorbatikh, P.Moldenaers, I.Verpoest. Influence of carbon nanotube reinforcement on the processing and the mechanical behavior of carbon fiber/epoxy composites. Carbon 47(2009) 2414-2423.

[53] F.H. Gojny, M.H.G.Wichmann, U.Kopke, B.Fiedler, K.Schulte. Carbon nanotubes – reinforced composites- enhanced stiffness and fracture toughness at low nanotubes contents. Compos. Sci. Technol.64(2004) 2363-2371

[54] Zhihang Fan, Michael H.Santare, Suresh G.Advani. Inter laminar shear strength of glass fiber reinforced epoxy composites enhanced with multi-walled Carbon Nanotubes. Composites: PartA. 39 (2008) 540-554

[55] Marcio Rodrigo Loos, Luiz Antonio Ferreira Coelho, Sergio Henrique Pezzin, Sandro Campos Amic. Effect of Carbon Nanotubes Addition on the Mechanical and Thermal Properties of Epoxy Matrices. Materials Research, 11 (2008) 347-352.

[56] SohelRana, RamsamyAlagirusamy, Mangala Joshi. Development of carbon nanofibre incorporated three phase carbon/epoxy composites with enhanced mechanical, electrical and thermal properties. Composites:Part A 42 (2011) 439-445.

[57] Zhou.Y.PervinF.Pervin, S.Jeelani.S,P.K.Mallick. Improvement in the mechanical properties of carbon fabric-epoxy composites using carbon nanofibers. J.Mater.Proc. Technol 198(2008) 445-453.

[58] Keith J.Green, Derrick R.Dean, Uday.K.Vaidya, Elijah Nyairo. Multiscale fiber reinforced composites based on a cabronnanofiber/epoxy nanophased polymer matrix: Synthesis,mechanical, and thermo mechanical bahavior. Composites:Part A 40 (2009)1470-1475

[59] S.S.Wicks, Roberto Guzmande Villoria and Brian L.Wardle. Inter laminar and intra laminar reinforcement of composite laminates with aligned carbon nanotubes. Compos.sci. Technol. 70 (2010) 20-28.

[60] Meisam Omidi, D.T.Hossein Rokni. Abbas.S.Milani, Rudolf J.Seethler, R. Arasteh. Prediction of the mechanical characteristics of multiwalled CNT/epoxy composites using new rule of mixtures. Carbon.48 (2010) 3218-3228.

[61] M.K.Yeh, N.H.Tai, Y.Jyun Li, Mechanical properties of phenolic based nanocomposites reinforced by multi-walled carbon nanotubes and carbon fiber. Composites:PartA 39(2008) 667-684

[62] R.D.Patton,C.U.Pittman,L.Wang.Jr,J.R.Hill.A.Day, Ablation, mechanical and thermal conductivity properties of vapor grown carbon fiber/ phenolic matrix composites. Composites: Part:A 33 (2002) 243-251.

[63] M.Natali, M.Monti, D.Puglia, M.Kenny, L.Torre. Ablative properties of carbon black and MWCNT/phenolic composites: A comparative study. Composites:Part A:43 (2012)174-17182

[64] R.B.Mathur, SouravChatterji,B.P.Singh, Growth of carbon nanotubes on carbon fibre substrate to produce hybrid/phenolic composites with improved mechanical properties. Compos. Sci. Technol 68 (2008)1608-1615

[65] Y.A.Kim, S.Kamio, T.Tajiri, T. Hayashi, S.M.Song, M.Endo, M.Terrones,M.S. Dresselhaus. Enhanced thermal conductivity of carbon fiber/phenolic resin composites by the introduction of carbon nanotubes.App. Phys. Lett. 90 (2007) 1-8.

[66] Namiko Yamamoto, , Roberto Guzman de Villoria, Brian L. Wardle. Electrical and thermal property enhancement of fiber-reinforced polymer laminate composites through controlled implementation of multi-walled carbon nanotubes. Compos. Sci. Technol 72 (2012) 2009–2015.

[67] M.Natali, M.Monti, J.Kenny, LTorre. Synthesis and thermal characterization of phenolic resin/silica nanocomposites prepared with high shear rate mixing technique J.of App. Polym. Sci 120 (2011) 2632-2640

[68] M.Natali, M.Moti, J.M.Kenny.L.Torre. A nanostructured ablative bulk molding compound: Development and characterisation. Composite: Part A 42 (2011):1197-1204.

Chapter: II

Experimental and Testing Methods

Experimental and Testing Methods

Various characterization and testing methods used for evaluating the CNT/CNF reinforced CFRPs are summarized in this chapter. Different characterization methods that are summarized are scanning electron microscope, transmission electron microscope, Raman spectroscopy, thermo gravimetric analyser, differential scanning calorimeter, Fourier transform infrared spectroscope, X-ray photo electron spectroscope and X-Ray diffraction (XRD). Various tests that were carried out for the fabricated composites like fiber volume fraction, fracture toughness, tensile strength, flexural strength, inter laminar shear strength and thermal conductivity tests are also summarized. Discussion is restricted to the principle of each instrumental method/testing method, purpose of using the concerned testing method for the present work and various inferences that are taken from each of these methods.

1. Experimental methods: Major portion of the experimental work in the present study, involves fabrication and testing of two phase (CNT-epoxy) and three phase (CNT-C-epoxy/CNF-C-epoxy) composites, besides purification and functionalisation of CNTs. Various fabrication methods used for the realising composites, and the methods used for purification and functionalisation of CNTs are discussed in the respective chapters subsequently.

2. Testing methods: Various testing methods used in the present work are summarized briefly.

2.1. Scanning electron microscope (SEM): It involves focusing electron beam passing through an evacuated column on to the specimen using electro magnetic lenses. Two kinds of images can be obtained from the SEM study of the sample. They are secondary electron image and back scattered electron image. The former mode of imaging gives topographic information of the material while the later mode of imaging gives information on the compositional distribution of various elements within the material. Previous versions of scanning electron microscopes (SEMs) were used to operate with electrons generated from the thermionic sources like heated tungsten filament. They suffer from low magnification (up to one lakh) and low resolution which limits their use to study nanomaterials and their composites. Advanced versions of electron microscopes have emerged, where electrons are generated through field emission effect and these SEMs are called as field emission scanning electron microscope (FESEM). They can give magnifications up to 10 lakhs with resolution up to 2 nanometers. FESEMs are widely used by various research groups to study CNTs/CNFs and their reinforcing effect in FRPs. By using SEM/FESEM**,** one can get information on the homogeneity of

CNTs/CNFs distribution, role of CNTs/CNFs at interface etc. To study low conducting polymer composites (ex: CNTs in epoxy matrix) environmental scanning electron microscope (ESEM) which is operated at low vacuum should be employed. SEM, FESEM with ESEM and low vacuum modes have been widely used in the present study to analyse the fracture surfaces of the two phase and three phase nanocomposites.

2.2. Transmission electron microscope (TEM): Filament of Lanthanum hexaboride acts as electron emission gun in TEM. High voltage (100-300KV) is applied to the gun which emits a beam of high energy electrons which are collimated by electromagnetic lenses and passed through a thin specimen. Electrons that got transmitted through the specimen forms image on the fluorescent screen below the specimen giving a bright field image, which is used to analyse the sample under study. In the present work, TEM is used to study the microstructure, diameter of CNTs/CNFs, structural changes to CNTs during high temperature based purification process and dispersion of CNTs in epoxy.

2.3. Raman spectroscope: It works on the principle that, when a monochromatic radiation is scattered by vibrating molecules, a small fraction of the scattered radiation is observed to have a different frequency from that of incident radiation. As shift in the frequency (Raman shift) is characteristic, it can be used to identify the nature of the chemical bonds in the molecule. In the present work, Raman spectroscopy is used for the following applications.

- To identify the type of carbon nanomaterial under study from first order bands arising from SP^2 vibration modes (G band at 1582 cm^{-1}, D band at 1350 cm^{-1} for MWCNTs)
- Intensity ratios between G band to D band to study the crystalline perfection of the carbon nanomaterial under study.

2.4. Thermo gravimetric analyser (TGA): This involves studying the change in the weight of the material as a function of temperature. This is used to ascertain the purity of the CNTs/CNFs under study.

2.5. Differential scanning calorimeter (DSC): In this technique, sample and reference are subjected to a precisely programmed temperature change, and energy is either added to sample or reference in order to maintain same temperature between the both. The balancing
energy yields a direct calorimetric measurement of the transition energy (the energy absorbed or release in the endothermic or exothermic reaction respectively that are taking place in the

sample). It is widely used to study, how CNTs change cure characteristics of resins, glass transition temperatures of the polymer matrices etc. In the present context, DSC is used to study, how CNTs influence the curing/crosslinking reactions.

2.6. Fourier transform infrared spectroscope (FT-IR): This involves, scanning the sample under study with the IR frequencies (Generally from $400cm^{-1}$ to $4000cm^{-1}$) and identifying the bonds present in the sample from the frequencies that are strongly absorbed. Strong absorption of selective frequencies occurs when the oscillating dipole moment produced by the vibrating molecule, interacts with the electric field of the radiation having same frequency. In the present study, FT-IR is used to study the functional groups present on CNTs and CNFs.

2.7. X-ray photo electron spectroscope (XPS): This technique involves, bombarding the molecules under investigation with high energy X-rays, to cause a emission of inner level electrons. The kinetic energy of emitted electron (photo electrons) are measured which gives the binding energy of the emitted electrons. Binding energy unambiguously defines a specific atom and its chemical environment (other atoms with which it is bonded). Applicability of this method to elements like Carbon, Nitrogen and Oxygen makes this method as an important tool to study the organic molecules. Chemical shift associated with electron binding energies depending on the chemical environment of the atom under study, makes this tool more versatile to know the oxidation state/ electro negativity etc. XPS is widely used to study the surface functional groups present on the CNTs/CNFs. In the present study, XPS is used to study whether the amine functional groups have formed on the surface of CNTs after functionalisation process.

2.8. X-Ray diffraction (XRD): This technique involves hitting the sample with X-rays and studying the intensity of the diffracted X-ray as a function of

- Incident & scattered angle
- Wave length

X-ray diffraction is not widely used for the analysis of CNTs, as the X-ray patterns of graphite, MWCNTs resembles closely. Similarly, CNT/CNF reinforced CFRPs also can't be studied with X - ray diffraction as polymeric materials/ matrices are not amenable for XRD studies. In the present context, XRD is used to study the crystalline perfection/d-spacing value changes for MWCNTs

during high temperature heat treatment. Besides this, XRD is also used to study the ablation mechanisms of CFRPs in presence of ceramic additives.

2.9. Testing of composites: Various tests that were carried out for the composites are summarized below.

2.9.1. Fiber volume fraction (V_f): Mechanical properties of the composites are very sensitive to the volume fraction of fibers and their orientations. For studying the reinforcement effect of CNTs/CNFs in the three phase composites, one should ensure that volume fraction of the composites that are being compared remain the same. To find out the volume fraction of the CFRPs (epoxy or phenolic based) acid digestion test as per ASTM D 3171 is followed. The method involves taking a known weight of the composite samples (minimum 1 g) and dissolving the matrix part selectively by subjecting the sample to refluxing nitric acid. Carbon fibers can resist the acid attack and remain undigested. After dissolving the matrix portion of the composites, the remaining carbon fibers are washed, dried and weighed. From this weight fraction of the carbon fibers and the matrix were found out. These values were converted into volume fractions by using the densities of the fibers and matrix.

The following formula is used to calculate the fiber volume fraction.

$$V_f = \frac{W_f/\rho_f}{\frac{W_f}{\rho_f} + (1 - W_f)/\rho_m}$$

W_f= Weight of the fibre (obtained from the acid digestion test)

ρ_f = Density of the fibre

ρ_m = Density of the matrix

2.9.2. Fracture toughness (K_{IC}): Fracture toughness of the material indicates it's resistance to fracture in neutral environment in presence of a sharp crack whose tip is small compared to the crack size and specimen dimensions. K_{IC} value of a given specimen is function of testing speed and temperature. To measure the fracture toughness, samples having approximately 50mm x 8mm x 4

mm dimensions were cut from the composite. For each sample a straight notch of 4 mm (0.5 times of width) along its width was made. Initial notch up to a depth of 3mm was made with the isomet equipped with diamond coated cutting wheel having a thickness of 0.5mm. Depth of the notch was further increased to 4mm by using a razor blade to ensure that a sharp notch is present at the tip. Testing was carried out as per ASTM D 5045 on a universal testing machine (United 50KN) at a crosshead speed of 10 mm/min. Maximum load was recorded when specimen fractured, from which fracture toughness (K_{IC}) was calculated.

The following formula is used to calculate the fracture toughness (K_{IC})

$$K_{IC} = \frac{P_q f(x)}{BW^2}$$

P_q = Load obtained from the test

B = Specimen thickens

W = Specimen depth (width)

x = a/W

a = Crack length

$$f(x) = \frac{6x^{\frac{1}{2}} [1.99 - x(1-x)(2.15 - 3.93x + 2.7x^2)]}{(1+2x)(1-x^{\frac{3}{2}})}$$

2.9.3. Flexural strength: Flexural strength is a measure of the ultimate strength of a specified beam in bending. Flexural test methods are commonly used to determine the strength and deformation of monolithic ceramics, brittle polymers and CFRPs. Flexural behavior and strength of a CFRPs are dependent on, its inherent resistance to fracture, the presence of fracture sources, any inclusions/ additives which are resisting the interfacial cracks or combination of these in CFRPs. CFRP material tested in flexural may fail in a variety of fracture modes, depending on the interaction of the non-uniform stress fields in the flexural specimen and the local mechanical properties at the interface between the fiber and matrix. The specimen may fail in tension, shear, or in a mix of these modes. The geometry of the specimen must be chosen so that shear stresses are kept low relative to tension. This is done by maintaining a high ratio between the support span (L) to thickness (d) of the specimen. This L/d ratio is generally kept at values of > 16 for 3point bending test. Typical dimensions of the CFRPs tested for flexural strength in the present study are 60 mm x 10 mm x 2

mm and typical rate of loading(crosshead speed) is 2 mm/min. In the present study, flexural strength test for CFRPs was carried out as per ASTM D 790.

Flexural strength was calculated using the following equation

$$\text{Flexural strength} = \frac{3PL}{bd^2}$$

P = maximum load on load-deflection curve, L = support span,

b = width of beam tested, d = depth of the tested beam,

2.9.4. Tensile strength: Most common mechanical stress–strain test is the tensile test performed by applying tensile forces to the test specimen. Although flexural testing of the samples by three point bending is easier to test for CFRPs, the non uniform stress distribution of the flexural specimen in addition to ambiguity in mode of failure like shear/ compressive/ tension etc-- lead to more preference for tensile data in the design. In this test, a specimen is deformed, usually to fracture, with a gradually increasing tensile load that is applied uni-axially along the length of the specimen. Flat samples are used for tensile testing of the CFRPs. In uni axial tensile, material is uniformly stressed which is required to effectively evaluate the mechanical property of the CFRP composite. The final failure of the sample under tension could be due to any of the damage processes like matrix cracking, matrix/fibre debonding, fibre fracture, delamination etc. In the present study, tensile testing of CFRPs was carried out as per ASTM D 3039. Ultimate tensile strength is calculated from the following equation.

$$\text{Tensile strength} = \frac{P_{max}}{A}$$

P$_{max}$ = maximum force before failure,

A = average cross sectional area,

2.9.5. Inter laminar shear strength (ILSS): This test method is also used as a quality control and as a comparative study of the various composite materials under study.   Testing involves 3-point bending of the composite. However to ensure shear failure, the span length to the thickness ratio should be lower than six. Shear strength tests gives an indication of the bonding strength of the fiber to the matrix and inter-filament bond strength. It is a matrix dominated property. However ultimate strength value measured is not a direct measure of the matrix strength, but a combination of the strength of matrix and bonding between the matrix and reinforcement. In the present study, CFRPs were tested, for ILSS following ASTM D 2344.

ILSS was calculated using the following equation

ILSS$= \dfrac{3P}{4bd}$

P = maximum load on the load-deflection curve,

L = support span, b = width of beam tested, d = depth of beam tested

2.9.6. Thermal conductivity: It is the property of material to conduct heat. It can be defined as the heat energy transferred in unit time across unit area between the surfaces which differ in their temperature by a unit degree. Thermal conductivity for CFRPs is an important parameter when they need to be deployed for high temperature/ablation applications. Generally thermal conductivity for CFRPs is measured by hot guard method, which involves measuring the temperature drop across the sample when a known heat input is transferred from the top surface to the bottom surface by sandwiching the sample between two reference cylinders. In the present study, silica cylinders were used as the reference. Thermal conductivity of ablative CFRPs was measured as per ASTM E 1225 in the through thickness direction at 300^0C under steady-state conditions. Typical sample sizes used for measuring the thermal conductivity are 25 mm (dia) x 5 mm (height).

Chapter: III

Purification and

Functionalisation of

Multiwalled Carbon nanotubes

Purification and Functionalisation of MWCNTs

Raw MWCNTs having metallic impurities needs to be purified before using them as reinforcements to CFRPs. Hence, they were purified by high temperature heat treatment (2600^0C) process to ultra high purity levels (99.9%). Structural changes that are taking place to MWCNTs during high temperature heat treatment process were studied with TGA, Raman spectroscopy, TEM and XRD methods. Suitable mechanisms are proposed for the observed microstructural changes to MWCNTs which were exposed to high temperatures. Present study indicates that, high temperature heat treatment for controlled durations can enhance structural perfection to MWCNTs. These purified MWCNTs were subsequently amino functionalised through carboxylation, acylation and amination processes. FT-IR and XPS were used to ascertain the presence of functional groups on the surface of MWCNTs.

1. Introduction: Large scale synthesis of MWCNTs is generally carried out by chemical vapor deposition (CVD) process. This method involves, decomposition of hydrocarbons at a prescribed temperature and pressure under controlled quantities of catalysts [1]. In general, either transition metals (d-block elements like Iron, Nickel etc--) or organo metallic complexes (ex: ferrocene) are decomposed to generate the metal catalyst. Though catalyst helps in generation of carbon nanotubes (CNTs) with controlled diameter, they remain in the final product as an impurity. As a result of it, as synthesized MWCNTs contain metal catalysts as impurities. Besides, the metal catalysts, MWCNTs are also known to contain other carbonaceous impurities such as amorphous carbon. Removal of impurities is the essential step to use CNTs for any of the applications. In the context of composite applications, impurities acts as flaws or stress concentration zones, which can initiate failure of the composite. Hence purification process is an essential prerequisite to use MWCNTs as reinforcements to composites.

In general, purification of MWCNTs is carried out by a two step process [2]. In the first step selective oxidation is carried out to remove the amorphous carbon. This involves exposing the raw MWCNTs (containing metal impurities along with the amorphous carbon) to an approximate temperature of 450^0C in air. During this process, amorphous carbon will be selectively oxidized and removed. This is because amorphous carbon is more reactive as compared to MWCNTs. In the second step, MWCNTs having metallic impurities are refluxed in strong acids. During this process, metallic impurities are removed by dissolution in strong acids. However, the above method of

purification, involving refluxing the MWNCTs in strong acids, suffers from the major drawback of creating defects on MWCNTs as exposing to strong acids is known to cause structural degradation to MWCNTs [3,4].

To overcome the problem of structural damage to the CNTs by the above purification method, alternate purification methods were tried by different research groups. Some of them are magnetic method, centrifugation method, high temperature heat treatment method etc-[2.]. These methods rely on the differences in the physical size, gravity, magnetic properties or thermal stability of the MWCNTs as compared to the impurities. As these methods do not involve oxidative treatments and acid exposure of MWCNTs for purification, they do not impart any structural damage to the MWCNTs. However, most of these methods are less effective in terms of final degree of purity of MWCNTs. various purification methods reported for MWCNTs, along with their advantages and limitations was reviewed by Peng et al and Sato et al. [2, 5]. Among various purification methods that were summarized, high temperature heat treatment (above $2500^{0}C$) in inert atmosphere is identified as one of the best methods which removes metallic impurities by evaporating them. This method is suitable for purification of large quantities of MWCNTs. The advantage of this method is besides giving highly pure MWCNTs, MWCNTs with enhanced structural perfection can be obtained [6-10].

Though it is widely reported that, high temperature heat treatment, gives improved structural perfection to MWCNTs, more understanding on the mechanism involved in the structural changes taking place during the high temperature treatment is necessary. This is because, some unwanted changes to the CNT structure during high temperature heat treatment like transformation of single walled carbon nanotubes (SWCNTs) to MWCNTs, disappearance of the inner walls of the MWCNTs and their transformation to double walled carbon nanotubes (DWCNTs) were reported [11,12]. On the other hand, formation of carbonaceous material deposit on MWCNTs surfaces at high temperatures was also reported [13]. Hence, mechanism involved in high temperature purifications of CNTs needs thorough understanding to obtain CNTs with high purity and also with enhanced structural perfection.

Purification by high temperature heat treatment method, involves a two step process. In the first step amorphous carbon and other carbonaceous impurities will be removed by heating the MWCNTs at

around 450^0C in air. In the second step, MWCNTs will be heat treated up to approximately 2600^0C in inert atmosphere to remove all the metallic impurities which will get eliminated by evaporation. The objective of this work is to study, the effect of duration (60 minutes and 120 minutes) of high temperature heat treatment (at 2600^0C) under nitrogen atmosphere on purity and structural changes to MWCNTs.

2. Raw materials: MWCNTs synthesized by chemical vapor deposition method were procured from M/s Chemapol Industries Ltd, Mumbai. MWCNTs in the pristine conditions (as procured) had following features.

1. Metallic impurities : 36 weight percent (wt %)
2. Diameter : 20 - 30nm
3. Length : 2 - 4microns

SEM images of the raw MWCNTs are shown in Fig.3.1

3. Experimental work: MWCNTs (of approximately 100g in a batch) were loaded in to a graphite crucible having a volume of 1000ml. Graphite crucible was kept inside the high temperature furnace and heated to $2600^°$C under the nitrogen atmosphere at atmospheric pressure. Typical heating cycle involved heating the furnace up to $1200^°$C at a heating rate of 2ºC/min, and then raising the temperature from $1200^°$C to $2600^°$C at a heating rate of $1.5^°$C/min. Once the furnace temperature reached 2600ºC, then soaking (holding the furnace temperature) was carried out. One batch of MWCNTs were soaked for 60 minutes (here after referred as 60 min heat treated MWCNTs) and the other batch of MWCNTs were soaked for 120 minutes (here after referred as 120 min heat treated MWCNTs). After furnace was cooled to room temperature, MWCNTs sample was collected and the purity of MWCNTs was measured with thermo gravimetric analysis (TGA). TGA was carried out at a heating rate of $10^°$C/min from room temperature to 850^0C under compressed air flow (50ml/min). Microstructural changes associated with the heat treatment processes were determined by X-ray diffraction (XRD, Philips PWD, Model No.1830, Netherlands), Raman spectroscopy (Jobin Yuan, Model: 64,000X), scanning electron microscopy (ESEM, FEI, Quanta 400, The Netherlands) and transmission electron microscopy (TEM, Tecnai 20, FEI, The Netherlands).
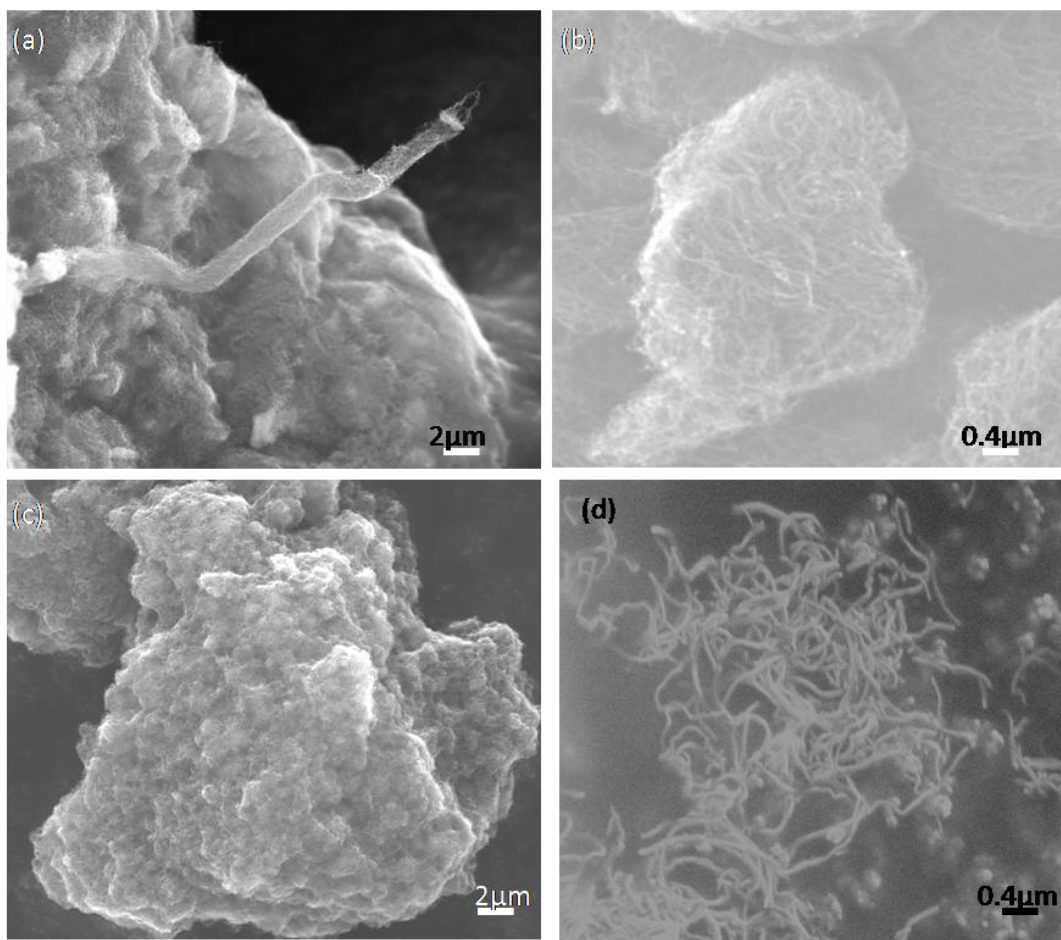
Figure.3.1: SEM images of the raw MWCNTs (a),(b) & (c) showing highly entangled bundle of MWCNTs (d) Unbundled (de-agglomerated) MWCNTs after sonication in acetone solvent.

4. Results and Discussion: Thermo gravimetric analysis results of the MWCNTs (raw), MWCNTs heat treated for 60 min (purified MWCNTs) are shown in Fig.3.2. During TGA studies, in presence of oxygen and high temperature, carbon nanotubes and other carbonaceous impurities burnout leaving behind the metallic impurities. When the carbonaceous materials start to oxidize, it results in a rapid weight loss which can be observed from approximately 550°C for the raw MWCNTs. The weight loss continued to increase until it reached a stable plateau region near approximately 650^0C.
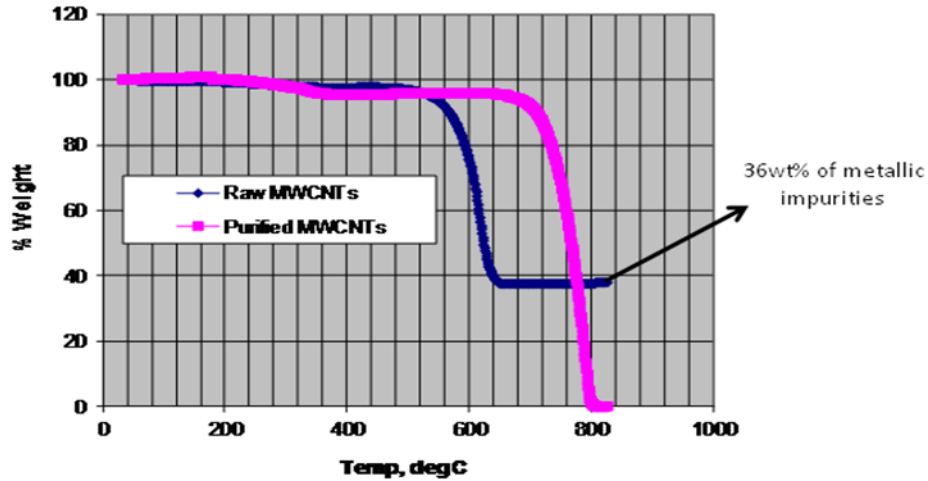
Figure.3.2: TGA patterns of the raw and 60 min heat treated MWCNTs

The residual weight of approximately 36% indicates the weight percentage of metallic impurities present in the raw MWCNTs. From the TGA pattern of 60 min heat treated (purified) MWCNTs it can be seen that the residual weight drops to base value. This indicates absence of any metallic impurities. It can be seen from the TGA curves (Fig 3.2) that, 60 min heat treated MWCNTs are stable to up to 700°C where as raw MWCNTs were oxidized at 550^0C itself. This indicates enhanced thermal stability for the 60 min heat treated MWCNTs which could be assigned to the following reasons.

     i) There are no metallic impurities which can catalyse the oxidative decomposition of   the MWCNTs.

     ii) High temperature heat treatment can remove the microstructural defects of

     MWCNTs. This resulted in more thermal stability to MWCNTs.[8]

The TGA curve of the 120 min heat treated MWCNTs is shown in Fig 3.3. The TGA graph also has shown the trend similar to 60 min heat treated MWCNTs in terms of purity and thermal stability of MWCNTs.
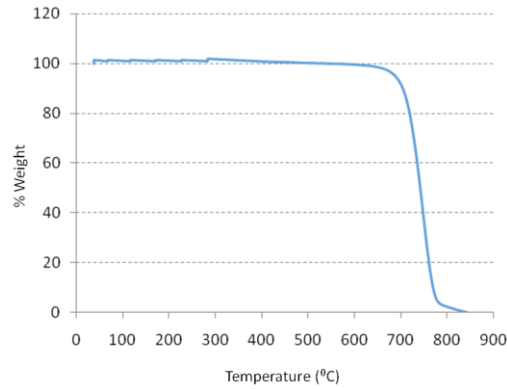
Figure.3.3: TGA of 120 min heat treated MWCNT

XRD patterns of the raw, 60 min heat treated and 120 min heat treated MWCNTs are shown in Fig 3.4. Peaks observed near 2θ of 26 degrees corresponds to (002) plane while the peak that was observed near 2θ of 42 degrees corresponds to (100) plane. Position and the intensity of the (002) indicates the inter planar spacing while the (100) plane indicates the in plane graphitic structure [8].
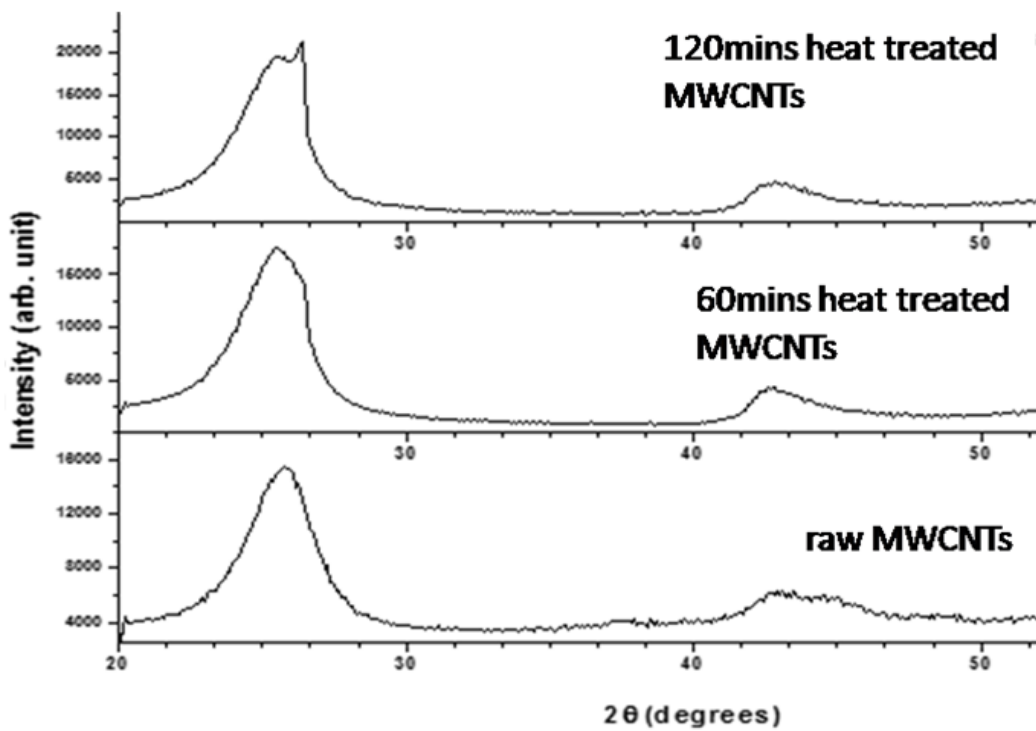
Figure.3.4: XRD patterns of the raw, high temperature heat treated MWCNTs

Ideal graphite has got an inter layer spacing of 0.3348 nm, while the turbo static graphite shows an inter layer spacing of 0.344 nm. Smaller (002) inter layer spacing, smaller full width half maxima (FWHM) of (002) and higher (002) intensities, indicate a highly developed graphitic structure. By

42

using the Bragg's law inter layer spacing was calculated for raw, 60 min heat treated and 120 min heat treated MWCNTs which are shown in Table.3.1

It can be seen that, the inter layer spacing of the raw MWCNTs is much deviated from the ideal graphitic structure. This is because, MWCNTs are generally synthesized through CVD method, where the synthesis temperatures are generally in the range of 1000°C. As the MWCNTs were not exposed to graphitization temperatures during synthesis, they would not show ideal graphitic structure. Besides this, during the formation of MWCNTs in CVD chamber, different precipitation rates of the carbon atoms through catalyst are possible which gives high degree of disorder. This could result in more deviation in interlayer spacing as compared to ideal graphitic structure for the raw MWCNTs [13].

Table.3.1: Inter layer spacing, full width half maxima (FWHM) of MWCNTs

MWCNTs	$2\theta_{(002)}$	$d_{(002)}$ (nm)	FWHM $_{(002)}$ (^{o})
Raw	25.83	0.344	1.92
60 min heat treated	26.56	0.3493	1.34
		0.3353	0.28
120 min heat treated	25.51	0.34690	1.34
	26.37	0.33572	0.28

TEM images of the MWCNTs are shown in Fig.3.5. Raw MWCNTs have shown metallic impurities (Fig.3.5.a). High temperature heat treatment can improve the structural perfection of MWCNTs besides removing metallic impurities by evaporation. This is because, high temperature heat treatment, can give required thermal energy for the diffusion of the atoms, and thus reorient the structure close to the ideal graphitic structure [13]. This can be evidenced, from the TEM images of the 60 min heat treated MWCNTs, which have shown linear, stiff graphene layers along the tube axis (Fig.3.5.b). The inter layer spacing values obtained from the XRD (Table.3.1) for the 60 min heat treated MWCNTs have shown generation of layers with graphitic d-spacing (0.3352 nm) near to ideal graphitic structure (0.3348 nm). This indicates that, even if the MWCNTs were grown with turbostatic structure at low temperatures, near graphitic structure can be obtained with high temperature heat treatment [14]. Small difference between the interlayer spacing of the 60 min heat treated MWCNTs as compared with the ideal graphite inter layer spacing could be due to the restriction in the graphene sheet spacing inherent to the curved sheet form present in the MWCNTs.
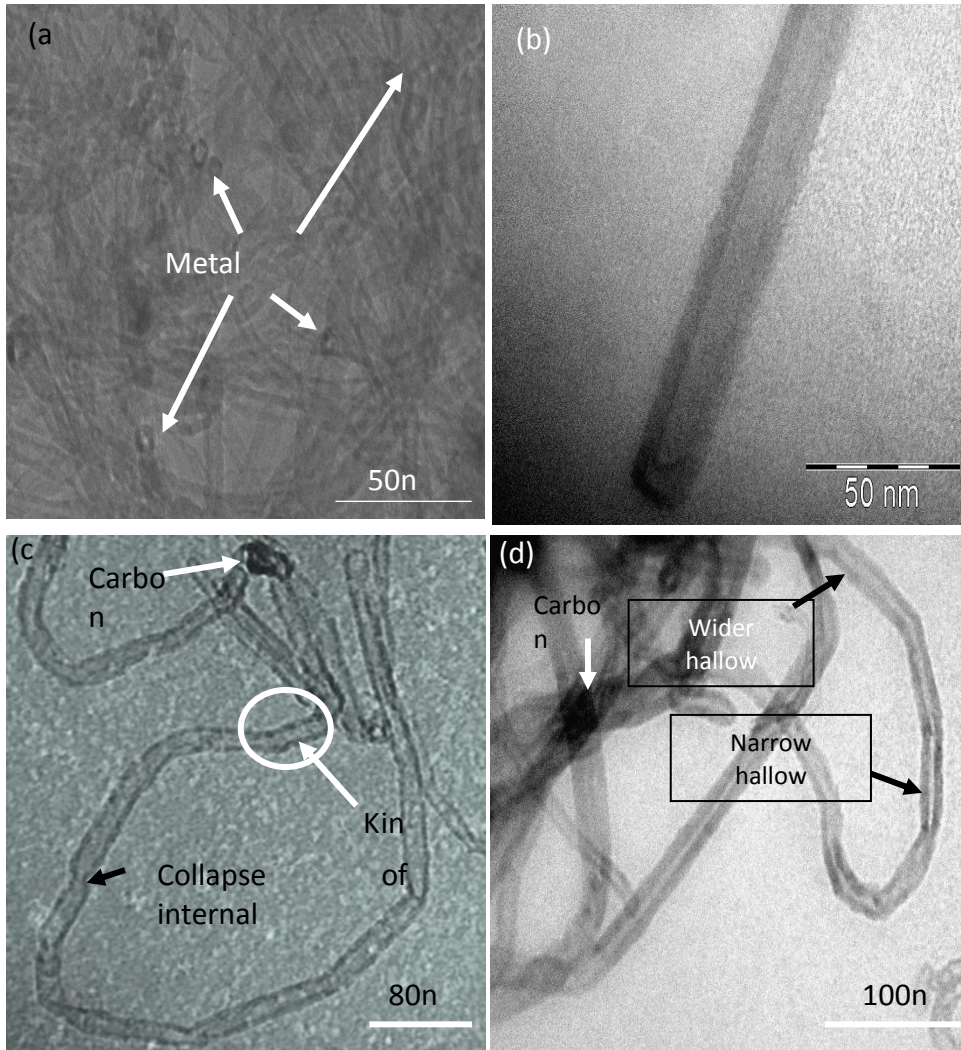
Figure.3.5: TEM of MWCNTs (a) Raw MWCNTs with metal impurities (b) 60 min heat treated MWCNTs with stiff graphene planes (c) 120 min heat treated MWCNTs with kinks, collapsed internal walls, deposited carbon soot (d) 120 min heat treated MWCNTs with varying internal hollow core diameter.

Continued heat treatment up to 120 min could not further refine the inter layer spacing towards ideal graphite, rather it resulted in the inter layer distortions with more turbostatic nature and collapsed internal layers (Fig.3.5.c). Though the graphitic peak is raising in prominence, there is huge distortion in the innermost layers [6]. This can be attributed to the fact that, as the annealing is a thermally activated process, during the prolonged annealing, different layers having different diameters experiences a varying degree of internal stresses. The innermost layers which are having lowest diameter, will have more stress and will collapse ahead of other inner layers during their

44

continuous shrinkage due to thermal annealing [11]. On the other hand, outermost layers may not experience significant stresses and thus can retain near graphitic structure. Inner most layers, which collapses due to thermally induced stresses, generates carbon species. These carbonaceous species diffuse out and form carbon coating on MWCNTs surface [Fig.3.5.c]. Enhanced diameter of the hollow core of 120 min heat treated MWCNTs reinforces this mechanism (Fig.3.5.d) [13]. As the internal layers collapse continues, crack-like voids, kinks can develop along the tube axis. (Fig.3.5.c)

Limited or no degradation of the innermost layers of the MWCNTs when heat treated for 60 mins could be due to the fact that, metal catalyst that is present in the raw MWCNTs may be acting as a moderating source to prevent the collapse of the inner layers. As and when, carbon atoms breaks away from the ordered structure, metal catalyst present as the impurity reacts with the carbon and forms the metal carbide. This metal carbide decomposes to precipitates out the carbon atoms which gets integrated in to ordered graphitic structure mimicking the CNTs growth mechanism. This kind of second growth of CNTs during high temperature annealing were reported earlier by Kim et al. [13]. However, once the metal particles evaporated completely during prolonged heating, no such reverse integration of the carbon atoms that are diffusing out of the graphitic structure is possible which leads to complete collapse of the inner most walls. This mechanism is reinforced by the observation, that, when the heat treatment was continued for 120 min, MWCNTs were observed to show significant amount of carbon soot on their surfaces [Fig.3.5.c].

Thus it is inferred that, high temperature heat treatment for limited duration (60 mins in present study) is helping in improving the graphitic nature of the MWCNTs while prolonged (120 min in present study) heating is resulting in significant structural distortions.

The above structural changes due to high temperature heat treatment was also confirmed by Raman spectroscopy studies. D band of the Raman spectrum arises out of defects present in the MWCNTs while the G band arises from the graphitic planes of the MWCNTs. Ratio of the intensities of the D band (I_D) to G band (I_G) i.e. I_D/I_G (R value) is used to evaluate the crystal planar domain size of graphite. Lower the R value, better is the structural perfection of the MWCNTs [15]. Raman spectra shows an increased intensity for G band and reduction in the intensity of the D band with 60 min treatment as shown in Fig.3.6 & Table 3.2.

It can be seen that, with 60 min heat treatment of MWCNTs, R value has come down significantly indicating that, defects are healed and the size of in-plane graphitic structure of MWCNTs is becoming larger. This observation is in consistence with the XRD and TEM studies. However, when the high temperature heat treatment was continued for 120 min, structural degradation of the MWCNTs was observed as inferred from the R value which started to increase (Table.3.2).
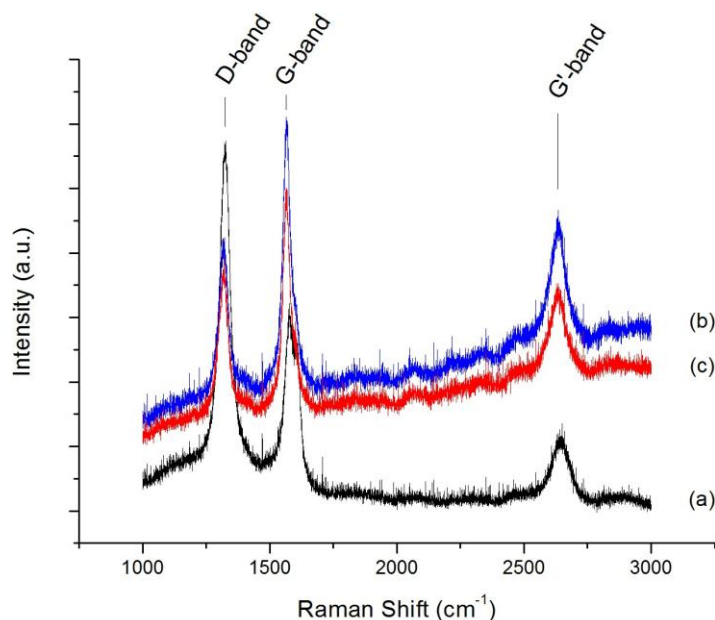
Figure 3.6: Raman Spectra of MWCNT samples (a) Pristine MWNT (b) 60 mins heat treated MWCNT (c) 120 min heat treated MWCNTs

Increased R-value for 120 min heat treatment of MWCNTs indicates generation of structural defects and disorder during prolonged heat treatment.

Table.3.2: Raman data for raw and heat treated (HT) MWCNTs

Sample	D-band (cm⁻¹)	G-band (cm⁻¹)	I_D/I_G (R)
Raw MWCNT	1324	1579	1.775
60 min HT MWCNT	1321	1564	0.692
120 min HT MWCNT	1321	1568	0.793

5. Functionalisation of MWCNTs: Raw or purified MWCNTs don't contain reactive functional groups. This restricts their wettability with the polymer matrices. To make the purified MWCNTs

compatible with the epoxy matrix, amino functionalisation is carried out. Amino functionalisation process of MWCNTs involves, three important steps. They are carboxylation, acylation and amination. Experimental methods involved in each of these steps are briefly described below.

5.1. Carboxylation: Purified MWCNTs, were carboxylated using concentrated HNO_3 . This process involves, adding MWCNTs (approximately 6g) to 400 ml of 69% HNO_3 taken in a two-neck round bottomed glass flask. The reaction flask containing the mixture of MWCNTs in HNO_3 was equipped with reflux condenser, magnetic stirrer and thermometer. The mixture was heated in an oil bath at 70-80 ^oC (+/- 3^0C) for 24 hours. After cooling the mixture to room temperature, MWCNTs were filtered through PTFE membrane (10μm pore size, 47mm diameter), and washed several times with double distilled water till the pH of the filtrate reached close to 7. This process generates the carboxylic groups on the surface of the MWCNT as shown in the reaction (1). MWCNT sample was dried and labeled as carboxylated MWCNTs/ CNT-COOH.

$$CNT+HNO_3 \xrightarrow{\text{70-80}^0C \text{ for 24Hrs}} CNT\text{-}COOH \qquad \text{----------} \quad (1)$$
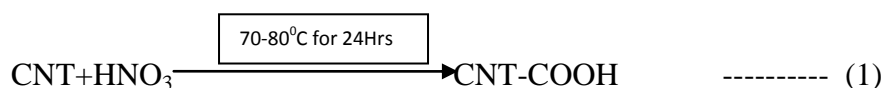
5.2. Acylation: Carboxylated MWCNTs were refluxed with a mixture of $SOCl_2$ and DMF (300mL, 20:1 v/v) at 70^oC(+/-3^0C) for 24 hours. This process converts the carboxylic groups that were grafted to CNTs in to carbonyl chloride groups as shown in the reaction (2).

$$CNT\text{ -}COOH \ + \ SOCl_2 \xrightarrow{\text{70}^0C \text{ for 24hrs}} CNT\text{-}COCl +HCl \quad \text{----------} \quad (2)$$

After acyl-chlorination, the MWNTs were filtered and washed with anhydrous THF for five times. The remaining solid was dried under vacuum at room temperature. These were labeled as acylated MWCNTs.

5.3.Amination: The acyl-chlorinated MWCNTs were reacted with 200 mL of ethylene diamine (EDA) solution at 100∘C (+/- 3∘C) for 48 hours until no HCl gas existed (checked with pH indicator paper). After cooling to room temperature, the MCWNTs were washed with ethanol for five times to remove excess EDA. The sample was dried at room temperature overnight. This process adds the amine groups to the MWCNTs as shown in the reaction (3).

$$CNT\text{ -}COCl + H_2N\text{-}CH_2\text{-}CH_2\text{-}NH_2 \xrightarrow{\text{100}^0C \text{ for 48hrs}} CNT\text{-}CO\text{-}HN\text{-}CH_2\text{-}CH_2\text{-}NH_2 +HCl \text{ ------} \quad (3)$$
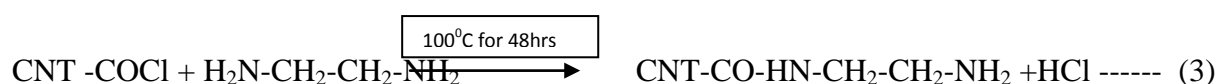
FTIR and XPS studies were performed to analyse the chemical state and the presence of functional groups on the surface of carbon nanotubes.

5.4. Results: FT-IR spectroscopy pattern of the purified MWCNTs (before functionalisation) is shown below. Peaks observed at 1567cm^{-1} indicates the C=C graphene back bone of the MWCNTs, whereas, an intense peak observed at 3432cm^{-1} is associated with the physically absorbed water [17]. On the other hand the FT-IR spectrum of the amino functionalised MWCNTs (Fig.3.8) have shown new peaks indicating incorporation of amine groups on their surfaces. Peak intensity at the 3434cm^{-1} decreased significantly (in comparison to other peaks), indicating dehydration and reduction of O-H. Still the peak at 3434cm^{-1} is intense and overlaps with the peak position of the amine making it difficult to recognise the amine groups through FT-IR.
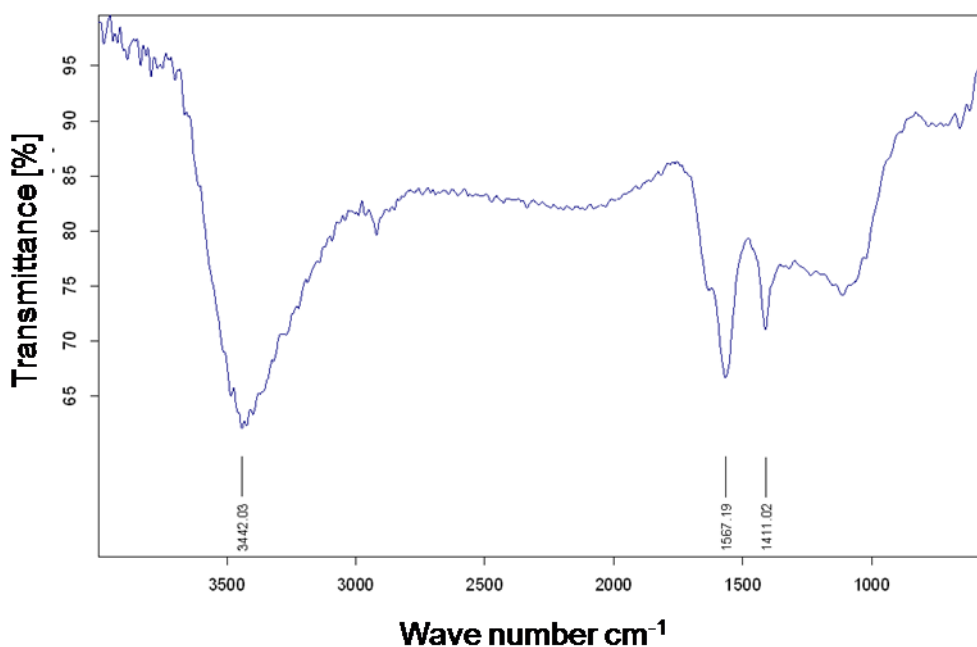
Figure.3.7: FT-IR pattern of the purified MWCNTs (60 min heat treatment)

Though the band at 3434cm^{-1} remained, change in the shape of the peak (symmetric peak) with much lower peak intensity may be attributed to the N-H stretching of the amine group.
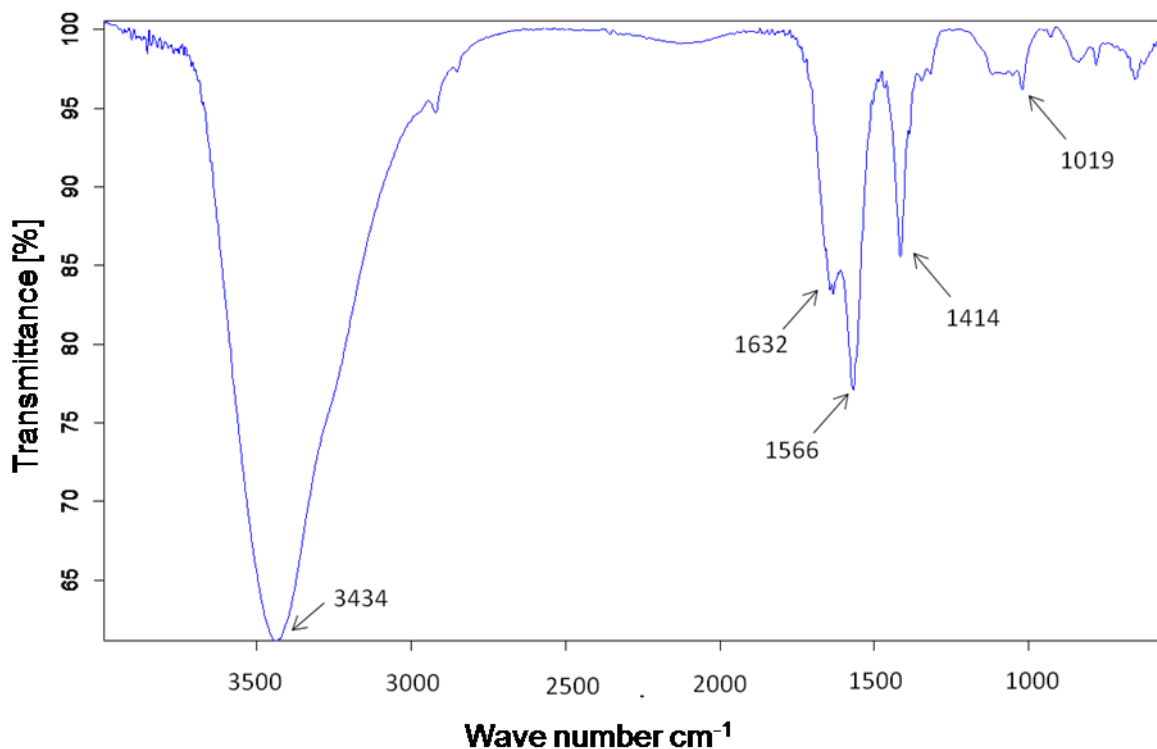
Figure.3.8: FT-IR pattern of the amino functionalised MWCNTs.

On the other hand, N-H in-plane stretching should appear at $1580cm^{-1}$ which again overlaps with the intense C=C stretching frequency observed at $1566cm^{-1}$ (graphitic back bone of MWCNTs), making it difficult to infer presence of N-H groups [18]. However, appearance of peak at $1020cm^{-1}$ corresponding to C-N bond and increased intensity of the peak at $1630cm^{-1}$ corresponding to C=O bond, indicates successful introduction of the nitrogen/amine groups through reaction 2, and reaction 3 [17]. As it can be seen from the Fig.3.7 and Fig.3.8 which have got close resemblance, it is inferred that FT-IR alone can't give a concluding evidence on introduction of amino groups on the surface of MWCNTs. Hence, XPS studies were carried out to get more evidence on the successful introduction of amino groups on the surface of MWCNTs.

XPS spectrum of the purified MWCNTs has shown intense peak at 285ev corresponding to SP^2 hybridised 'C' atoms (Fig.3.9.a) Absence of any measurable peaks at 399-400ev indicates absence of C-N bonds. On other hand, amino functionalised MWCNTs have shown new peak at 399.5ev indicating introduction of C-N bond. (Fig.3.9.b)

49
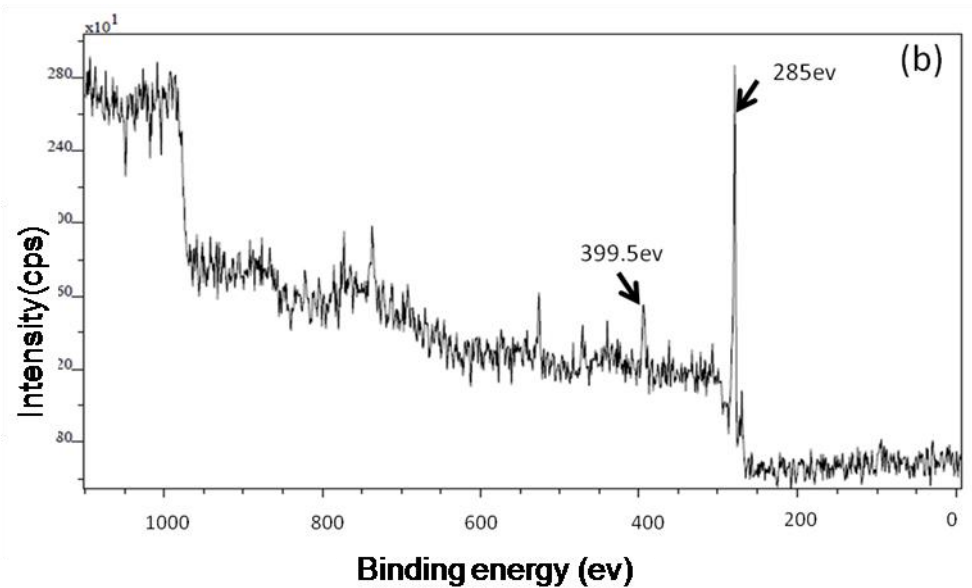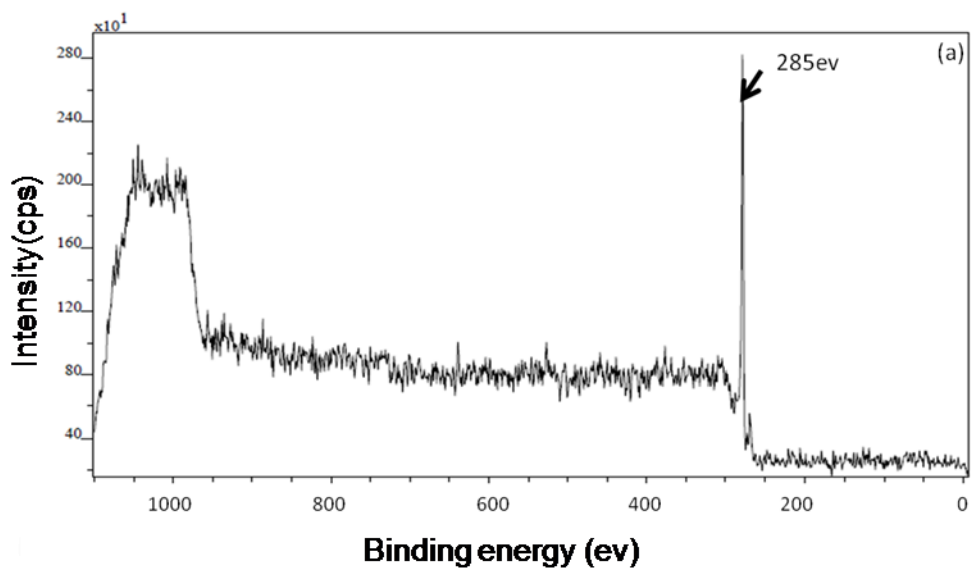
Figure 3.9: XPS pattern of (a) Pure MWCNTs (b) Amino functionalised MWCNTs

The peak that was observed for purified MWCNTs (without functionalisation) around 285ev is deconvoluted which shows the peak pattern as shown in Fig.3.10
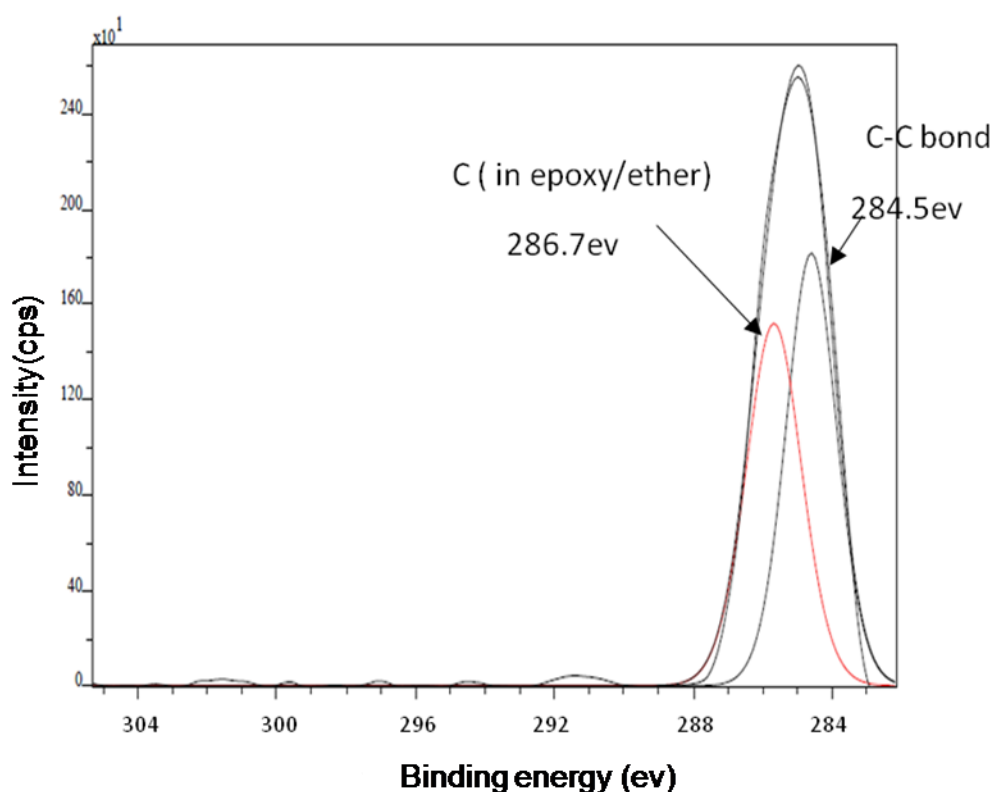
Figure.3.10: Deconvoluted peak of pure MWCNTs observed at 285ev.

For the pure MWCNTs appearance of oxygen related peak in the form of C-O at 286.7ev indicates the presence of surface oxygen either in the form of epoxy/ether groups or the surface absorbed moisture. On the other hand the peak that was observed for amino functionalised MWCNTs at 285ev is deconvoluted which shows the peak pattern as shown in Fig.3.11. Peaks at 285.9ev and 287ev in Fig.3.11. are indicating the presence of C-N and C=O groups respectively on the surface of the MWCNTs. Formation of the C=O and C-N bonds can be ascribed to the reaction (2) and reaction (3) respectively. Disappearance of the peaks that were observed for the pure MWCNTs at 286.7ev indicates decrease of oxygen concentration which is present in the forms of either epoxy/ether or absorbed moisture before the CNTs were functionalised. This infers incorporation of the amine groups on the surface of MWCNTs.

51
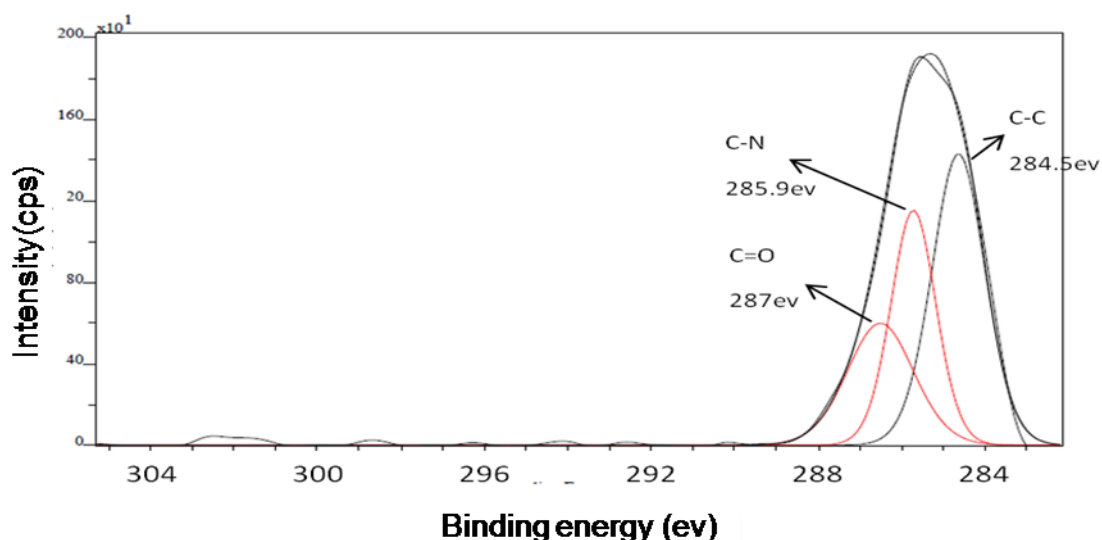
Figure.3.11: Deconvoluted peak of amino functionalised MWCNTs observed at 285ev.

Additional peak that was observed for amino functionalised MWCNTs at around 399.5 ev is deconvoluted and shown in Fig.3.12.
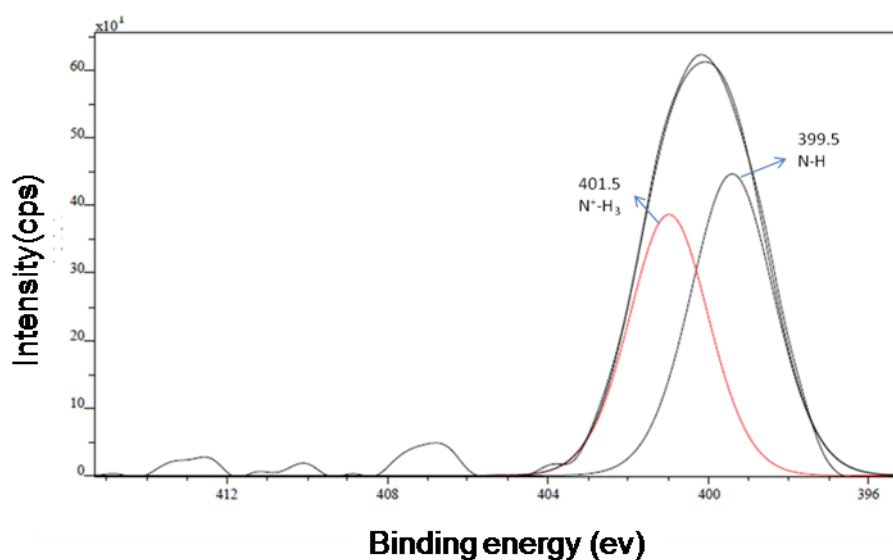
Figure.3.12: Deconvoluted peaks of amino functionalised MWCNTs observed at 399.5ev.

Figure.3.12, shows two peaks at 399.5eV and 401.5 eV. The standard binding energy of free amine groups falls in the region of 399-401ev and that of protonated amine groups shifts to higher side by approximately 1.5 -2eV. Thus peaks at 399.5 ev and 401.5 can be attributed to the nitrogen atoms in the form of -NH and NH_3^+ respectively. This confirms the generation of amino groups on the surface of MWCNTs [19].

For the subsequent experimental work i.e. fabrication of CNT reinforced CFRPs, amino functionalised MWCNTs which were functionalised by the methods described so far are used.

6. Conclusions:

i) High temperature heat treatment at 2600^0C in inert atmosphere for controlled durations (60 min in present study) can give ultra high pure MWCNTs having enhanced structural perfection.

ii) Metal impurities present in the MWCNTs act as a moderating source in arresting the structural collapse of MWCNTs.

iii) Continued heat treatment of MWCNTs, even after all metal impurities are eliminated, can cause structural damage to MWCNTs by collapse of internal walls and inter layer distortions of graphitic layers.

iv) By following the methods mentioned in this chapter, amino functionalisation of MWCNTs can be carried out successfully.

References

[1] M.Endo, R.Saito, MSDresselhaus, G.Dresselhaus. In: T.W.Ebbesen, editor, Carbon nanotubes: preparation and properties, CRC Press, 1997.

[2] Peng-Xiang Hou, Chang Liu, Hui - Ming Cheng. Purification of carbon nanotubes. Carbon 46 (2008) 2003-2025.

[3] M.T.Martinez,M.A.Callejas, A.M.Benito, M.Cochet, T.Seeger, A.Anso´n. Sensitivity of single wall carbon nanotubes to oxidative processing: structural modification, intercalation and functionalisation, Carbon 41(2003) 2247–2256.

[4] Y.Xing, L.Li, C.C.Chusuei, R.V.Hull. Sono-chemical oxidation of multiwalled carbon nanotubes, Langmuir 21 (2005) 4185–4190.

[5] Y.Sato, T.Ogawa, K.Motomiya, Purification of MWCNTs combining wet grinding, hydrothermal treatment, and oxidation. J. Physical Chem B 105 (2001): 3387-3392.

[6] Katayama T, Araki H, Yoshino K. Multiwalled carbon nanotubes with bamboo-like structure and effects of heat treatment. J. App. Phys. 91 (2002) 6675-6678.

[7] Wei Huang, Yao Wang, Ghohua Luo, Fei Wei. 99.9% purity multi - walled carbon nanotubes by vacuum high-temperature annealing. Carbon 41 (2003) 2585-2590.

[8] R. Andrews, D. Jacques, D. Qian, E. C. Dicky. Purification and structural annealing of multiwaled carbon nanotubes at graphitization temperatures. Carbon, 39 (2001) 1681-1687.

[9] H.Zhang. C.H.Sun, F.Li., H.X.Li, H.M.Cheng. Purification of carbon nanotubes by annealing and extraction based on difference in vander walls potential. J. Phys Chem B 110 (2006) 9477-9481.

[10] Yao Wang, Jun Wu and Fei Wei. A Treatment method to give separated multi-walled carbon nanotubes with high purity, high crystallization and a large aspect ratio. Carbon, 41 (2003) 2939-2948.

[11] A.Koshio, M.Yudasaka, S.Ijima. Disappearance of inner tubes and generation of double wan carbon nanotubes from highly dense multiwall carbon nanotubes by heat treatment. J. Phy Chem C, 111 (2007) 10-12.

[12] M.Yadusaka. T. Ichihashi, D. Kasuya, H. Katura, S. Ijima. Structure changes of single wall carbon nanotubes and single wall carbon nanohorns caused by heat treatment, Carbon, 41 (2003) 1273-1280.

[13] Y. A. Kim, T. Hayashi, K.Osawa, M. S.Dresselhasu, M. Endo. Annealing effect on disordered multi-wall carbon nanotubes. Chemical Physics Letters, 380 (2003) 319-324.

[14] M.Endo, K.Nishimura, Y.A.Kim, K.Hakamada, T.Matushita, M.S.Dresselhaus, G.Dresselhaus. J.Mater Res. 14 (1999) 4474-4477

[15] C.A.Cooper, R.J.Young. Investigation of structure/ property relationships in particulate composites through the use of Raman spectroscopy. Journal of Raman Spectroscopy, 30 (1999) 929-938.

[16] Sebastian Osswald, Mickael Havel, Yury Gogotsi. Monitoring oxidation of multiwalled carbon nanotubes by Raman spectroscopy. Journal of Raman Spectroscopy. 38 (2007) 728-736.

[17] L.Lai, L.Chen, Dazhan, L.Sun, J.Liu, S.H.Lim.C.K.Poh.Z.Shen.J.Lin.. One-step synthesis of NH2-graphene from insitu graphene - oxide reduction and its improved electrochemical properties. Carbon 49 (2011) 3250-3257

[18] J.Li, M.J.Vergne, E.D.Mowles, W.H.Zhong, D.M.Hercules, Charles.M.Lukehart. Surface functionalisation and characterization of graphitic carbon nanofibers (GCNFs) . Carbon 43 (2005) 2883-2893.

[19] Lei Zhang, Jian Liu, Jie Yang, Qihua Yang, Can Li. Direct synthesis of highly ordered amine-functionalised mesoporous ethane - silicas. Microporous and Mesoporous Materials.109 (2008) 172-183.

Chapter: IV

MWCNT Reinforced Carbon – Epoxy Composites

MWCNT Reinforced Carbon – Epoxy Composites

Present study is aimed to understand how the addition of p-MWCNTs and A_f-MWCNTs to epoxy resin can change its cure characteristics and the crosslink density. It was observed that, A_f-MWCNTs can increase the crosslink density of epoxy as well as toughness. Mechanical property improvements of A_f-MWCNTs - CFRPs are observed to be primarily due to the ability of A_f-MWCNTs to increase the interface toughness of CFRPs by increasing the interface crosslinking. Beyond optimum loading of A_f-MWCNTs to CFRPs, mechanical properties of CFRPs tends to comedown as higher crosslink densities triggered by the high loading of A_f-MWCNTs embrittles the interface. This study infers that, even with good dispersion of A_f-MWCNTs in CFRPs, mechanical properties may not increase beyond certain optimum loading.

1.Introduction: Excellent mechanical, thermal and electrical properties of MWCNTs have attracted composite fraternity to explore the possibility of using them as an additional reinforcement in carbon fiber reinforced epoxy (C-epoxy) composites [1-2]. Possibility of realizing composites with enhanced mechanical properties at a very low loading of nano materials is the main point of attraction which triggered extensive research world over on these materials. Functionalisation of CNTs with suitable reactive groups and their dispersion in polymeric resin systems were widely studied by various research groups as these aspects are identified as the main challenges to realize the potential of CNTs as reinforcements [3]. Significant efforts were not made to understand, how the CNTs addition could affect the curing behavior of the epoxy resin systems. This aspect cannot be ignored as there is a close relation between the curing behavior / degree of crosslinking and its mechanical properties [4,5]. In general the curing process of the epoxy resin is divided in two stages [6]. In the first stage, the crosslinking reaction is chemically controlled in which hydrogen bearing electron donor molecules (curing agent) breaks the epoxy ring and sets in the reaction with the formation of hydroxyl groups. Along with the progress of the crosslinking reaction, the viscosity of the resin system increases. When the viscosity reaches to a critical value, curing reaction becomes diffusion controlled which is considered as the second stage of curing reaction. When there are heterogeneous materials (like CNTs) present in the resin system, they can influence the rate and degree of curing. In general it is reported that, when CNTs are

added in their pristine form (without purification and surface functionalisation), they tend to accelerate the curing in the initial stages (first stage) due to catalytic effects of the metallic impurities that they possess [6]. However as the crosslinking reaction proceeds, and when the viscosity of the system increases significantly, presence of CNTs makes the mobility of the polymer chains more difficult [7,8]. This may bring down the overall degree of curing. However, when MWCNTs are having reactive functional groups like amine groups on their surfaces, they should increase the degree of crosslinking because of the extra amino groups offered by the MWCNTs in addition to the amino groups of the crosslinking agent.

On the other hand, It was reported that functionalised MWCNTs in epoxy can enhance the fracture toughness of the matrix [9,10]. Daniel R.Bortz et al. made a detailed compilation of various possible mechanisms which can contribute to enhanced toughness observed due to amino functionalised MWCNTs (A_f-MWCNTs) / CNFs in epoxy [11]. Most of these mechanisms were based on the ability of strongly bonded A_f-MWCNTs to deflect or bridge the propagating cracks. However, there are no systematic studies reported so far on the changes in the degree of crosslinking due to A_f-MWCNTs in epoxy and its effect on toughness.

Understanding additional toughening mechanisms is essential to interpret the mechanical property enhancements in C-epoxy composites. In general it is observed that, the mechanical property enhancements due to A_f-MWCNTs in C-epoxy are coinciding with the enhancement in the interface toughness of the C-fiber to the matrix [12, 13]. Hence, there should be a relation between, toughened interfaces of three phase composites to their improved mechanical properties, which is not studied systematically so far. Hence, this aspect is extensively studied in the present work. In general, the strength improvements in the carbon fiber reinforced plastics (CFRPs) added with the CNTs are interpreted in the following way.

When the composite is subjected to external load, it undergoes elongation/deformation before failure. However, the strains displayed by the fiber and matrix are not same, due to the difference in their stiffness. These differential strains, generates interfacial sliding/shearing before fibers pulls out of the matrix and breaks [14]. When CNTs are present in the CFRPs, they act as anchoring sites between the fiber and matrix and resist the sliding of the fiber from the matrix and thus offers

more hindrance for fiber pulling [15]. It is reported that, CNTs takes load during this process and needs to be broken before fibers can be pulled out of matrix [16]. As breaking of CNTs consumes more energy, this results in enhanced mechanical properties for CFRP made of CNTs. The reason for saturation / reduction in mechanical properties beyond certain weight percentage addition of CNTs to CFRPs is generally assigned to poor dispersion of CNTs [17]. If this concept were true, as long as good dispersion of CNTs is ensured in CFRPs, there should be continuous increase in the mechanical properties with increased loading of CNTs. To validate above concept, in the present work, studies were carried out to see, whether good dispersion of A_f-MWCNTs in CFRPs continue to give improvement in the mechanical properties.

In the present study, MWCNTs without any functional groups (p-MWCNTs) and A_f- MWCNTs were used in the same proportions to fabricate two phase (MWCNT-epoxy) and three phase (MWCNTs-C-epoxy) composites. This is to study, how MWCNTs without functional groups effects various properties of two phase and three phase composites in comparison to A_f-MWCNTs. DSC was used to study the changes in the degree of crosslinking of epoxy resin system in presence of p-MWCNTs and A_f-MWCNTs.

2. Raw Materials: In the present work, epoxy resin with hardener, carbon fibers and carbon nanotubes were used as raw materials. Various technical details of the raw materials are given below.

Epoxy resin: Epoxy resin and hardener were procured from M/s Fine Finish Organics Pvt.Ltd, Mumbai. Technical specifications of resin and hardener are given below.

1. Chemical formula	:	Diglycydyl ether of bisphenol −A	
2. Viscoscity	:	10,000cP at 30°C	
3. Density	:	1.2 g/cc	
4. Acid Value	:	85-120	
5. Commercial name	:	LY-556	

Hardener:

1. Chemical formula	:	Diethyl toluene diamine	
2. Viscosity	:	200 cP at 25°C	
3. Density	:	1.0 g/cc	
4. Commercial name	:	HY5200	

Carbon fiber specifications: PAN (Poly acrylo nitrile) based carbon fibers (M/s Toray, Japan) with the following specifications were used in the present study.

    1. Tow type   :   12k (12,000 filaments in a tow)

    2. Density   :   1.75 g/cc

    3. Tensile strength   :   4.8 GPa

    4. Tensile modulus   :   240 GPa

    5. Commercial name   :   T-700 grade

Carbon nanotubes: CVD synthesized MWCNTs were procured from M/s Chemapol Industries, Mumbai (India). They were purified in our laboratory by high temperature heat treatment method as discussed in chapter.III. Specifications of the MWCNTs used in the present study are given below.

    1. Purity   :   99.9% (after purification)

    2. Metallic impurities   :   less than 0.1wt%

    3. Diameter   :   20-30 nm

    4. Length   :   2-4 μm

Amino functionalisation of MWCNTs was carried out following the procedures elaborated in Chapter.III (Section.5). MWCNTs which were not functionalised are referred as p-MWCNTs and amino functionalised MWCNTs are referred as Af-MWCNTs.

3. Experimental Work: The following section gives a brief overview of experimental work.

3.1. Composite fabrication: Initially, MWCNT dispersed epoxy resin system was made. This involves, adding required weight percentage (wt %) of MWCNTs to epoxy resin at room temperature followed by sonication (Mesonix-3000, USA) for 30 minutes and ball milling (Insmart Systems, India) at a speed of 250 rpm for 120 minutes. Required quantity of hardener (4:1 weight ratio) was added to the MWCNT-resin mixture and continued the ball milling. Completion of the dispersion was ensured from differential scanning calorimetric (DSC) (TGA/DSC -1, Mettler–Toledo) studies. This was done by taking approximately 20 mg of resin-CNT mixture and subjecting it to DSC studies between 30^0C to 260^0C at 5^0 C/min heating rate. DSC data gives evolved heat during curing. Ball milling was continued till heat evolution (of DSC run) reaches to a saturation value which indicates completion of the dispersion. Similar procedure was followed for both p-MWCNT-epoxy and A$_f$-MWCNT-epoxy compositions. These MWCNT - epoxy mixtures were used to fabricate two phase and three phase composites as described below.

3.1.1. Two phase composites: To realize two phase composites, MWCNT-epoxy mixture was poured into a die and cured for two hours at 120ºC followed by three hours curing at 180ºC, which is the peak cure temperature of the compositions under study. Thus, seven different two phase nanocomposites were made by mixing different weight percentages of MWCNTs which are shown in the Table.4.1.

Table.4.1: Different types of two phase composites fabricated

Weight percentage of MWCNTs (wt %)	Types of two phase composite	
	p-MWCNTs	A_f-MWCNTs
0	Blank	
0.25	0.25wt% p-MWCNT-epoxy	0.25wt% A_f-MWCNT-epoxy
0.50	0.5wt% p-MWCNT-epoxy	0.5wt% A_f -MWCNT-epoxy
1.0	1.0wt% p-MWCNT-epoxy	1.0wt% A_f -MWCNT-epoxy

Typical two phase composites along with the dies are shown in Fig.4.1
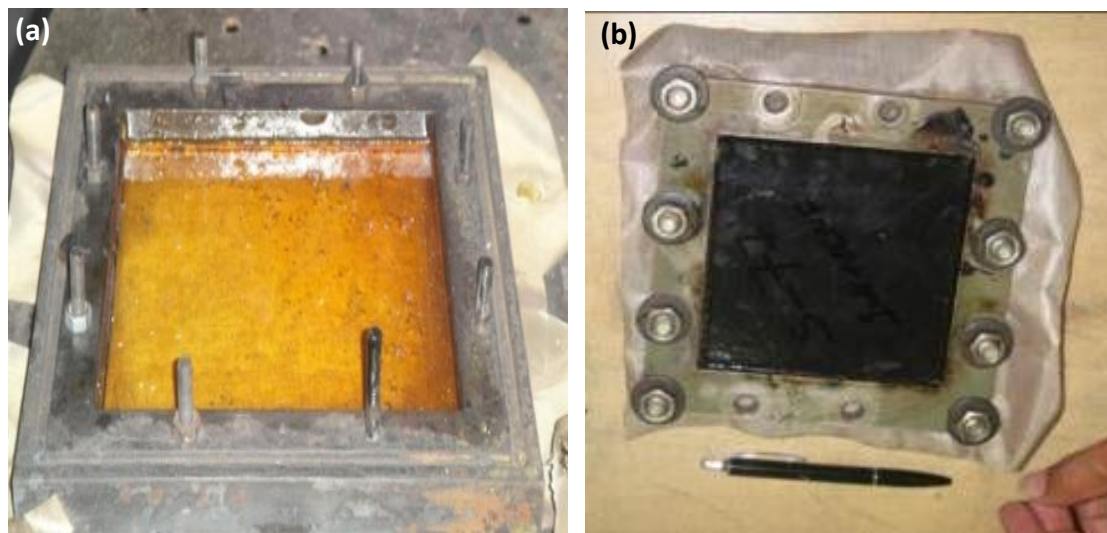
Figure.4.1: Two phase epoxy composites (a) Blank Epoxy (b) MWCNT-epoxy

3.1.2.Three phase composites: MWCNT - C-epoxy three phase composites were made by filament winding process using continuous carbon fibers and MWCNT dispersed epoxy resin mixture. Continuous carbon fibers dipped in the MWCNT - epoxy resin mixture was wound on to a flat plate at a band gap of 1.9mm. After winding required number of cycles of C-fibers on to the flat plate, the wound fiber-resin was compressed to required thickness by sandwiching it between flat plates. This step squeezes out the extra resin. This gives precise control on the fiber volume fraction of the composite. Thus, by controlling the number of cycles of the winding and the thickness, volume fraction of three phase composites was controlled at 60% (+/- 1%). Same cure cycle that was employed for two phase composites (section 4.1.1) was used for curing three phase composites. Different types of three phase composites that were made are shown in the Table.4.2.

Table.4.2: Different types of three phase composites fabricated.

Weight percentage of MWCNTs (wt %)	Type of three phase composite	
	p-MWCNTs	A_f-MWCNTs
0	Blank	
0.25	0.25 wt% p-MWCNT-C-epoxy	0.25 wt% A_f-MWCNT-C-epoxy
0.50	0.5 wt% p-MWCNT-C-epoxy	0.5 wt% A_f -MWCNT-C-epoxy
1.0	1.0 wt% p-MWCNT-C-epoxy	1.0 wt% A_f -MWCNT-C-epoxy

Experimental work that is discussed so far (section4.1.1 and 4.1.2) for fabrication of two phase and three phase composites is shown as flow diagram. Flow diagram also includes various tests that were carried out for each of the composite.

Flow diagram: Schematic flow of experimental work

Mixing MWCNTs in to epoxy resin

⬇

Dispersion by sonication and ball milling

Addition of curing agent and ball milling

Filament winding around the plate using CNT dispersed resin mixture

Casting epoxy resin –CNT mixture (Two-Phase composite)

Curing in the oven (120ºC two hours and 180ºC three hours)

Cutting the samples to required sizes for testing tensile strength, flexural strength, ILSS

Curing in the oven (120ºC two hours and 180ºC three hours)

Sample preparation for fracture toughness test

Two-phase composites ready for testing

Three – phase composites ready for testing

Various raw materials and tools used for the fabrication of three phase composites and typical composites after fabrication are shown in Fig.4.2.
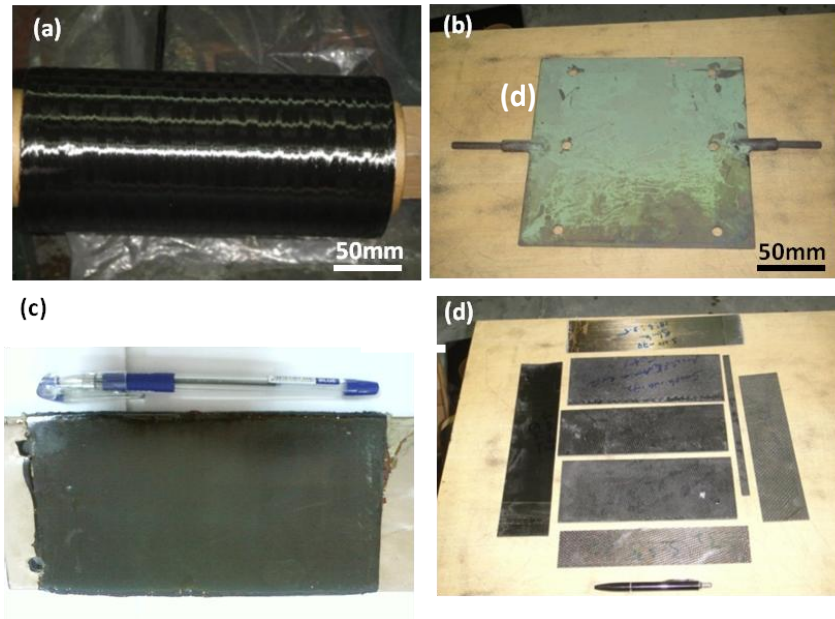
Figure.4.2: (a) Carbon fiber spool (b) Metal plate used for filament winding of carbon fiber (c) MWCNT-C-epoxy composite made for ILSS test (d) MWCNT-C-epoxy composite made for tensile strength and flexural strength tests.

3.2. Composite testing: Two phase composites were tested for fracture toughness (K_{IC}) value. Five samples of dimensions 50 mm x 8 mm x 4 mm were collected from each of the fabricated two phase composites. A notch was made at the center of the specimen using isomet. The edge of the crack was sharpened with a sharp edged blade. These samples were tested as per ASTM D 5045 on a universal testing machine (United 50KN) at a crosshead speed of 10 mm/min. Three phase composites were tested for their mechanical properties. To measure the mechanical properties samples having dimensions of 250mm x 10mm x1.6mm, (for tensile strength test) 60 mm x 10 mm x 2 mm (for flexural strength test) and 30mm x10mm x 2mm (for ILSS test) were collected. Tensile strength was measured as per ASTM D 3039 while flexural strength and ILSS were measured as per ASTM D 790, ASTM D 2344 respectively on a universal testing machine (United 50 KN). Fractured surfaces of two phase and three phase composites were analyzed with environmental scanning electron microscope (ESEM, model FEI-Quanta 400). Dispersion of A_f-MWCNTs in two phase composites was analyzed by transmission electron microscope (TEM, Tecnai 20, FEI, The Netherlands) studies of the A_f-MWCNT – epoxy sample which is thinned down to electron transparency level by using precision ion polishing system (PIPS, make Gatan). Fracture surfaces of three phase composites were studied using field emission scanning electron microscope (FESEM, model Zeiss-Neon 40) to see the dispersion of A_f-MWCNTs and p-MWCNTs.

4. Results and discussion:

4.1. Crosslink density of two phase composites: Observed heat evolution patterns from DSC studies for each loading of p-MWCNT to epoxy resin system are shown in Fig.4.3. Magnitude of heat evolved, was measured from the area under the peak.

Figure.4.3: DSC curves showing the heat evolution patterns of the epoxy with different   weight fractions of p-MWCNTs.

From the DSC results, it is observed that, as the p-MWCNTs concentration increased, heat evolution during curing is coming down [Table.4.3]. This indicates that, higher the amount of p-MWCNTs, more is the hindrance for the crosslinking reaction and thus less is the degree of cure. This could be due to two possible reasons.

i)   As p-MWCNTs don not contain reactive functional groups, they cannot participate in crosslinking reaction and thus cannot contribute to evolved heat during curing.

ii)   FESEM image with improper dispersion of p-MWCNTs in epoxy is shown below in Fig 4.4. It is known that, p-MWCNTs tend to agglomerate easily due to van der waals   forces   of attraction between the individual tubes [18]. Viscosity levels of the resin raises significantly due to agglomeration of CNTs. As the diffusion of epoxy molecules through viscous resin will be hindered due to

65

drag as well as due to entangled CNTs, degree of crosslinking will be abnormally low. More is loading of p-MWCNTs, more will be reduction in the degree of crosslinking [Table.4.3].
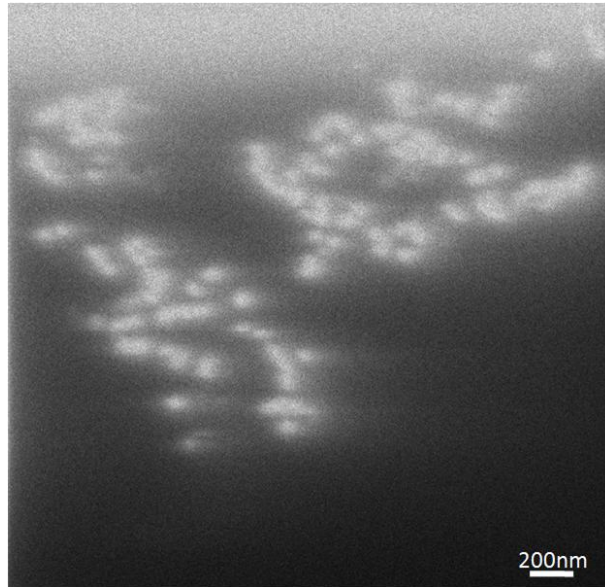
Fig.4.4: FESEM image showing some zones rich with agglomerated p-MWCNTs (bright zones) and other zones without p-MWCNTs (dark zones) indicating poor dispersion

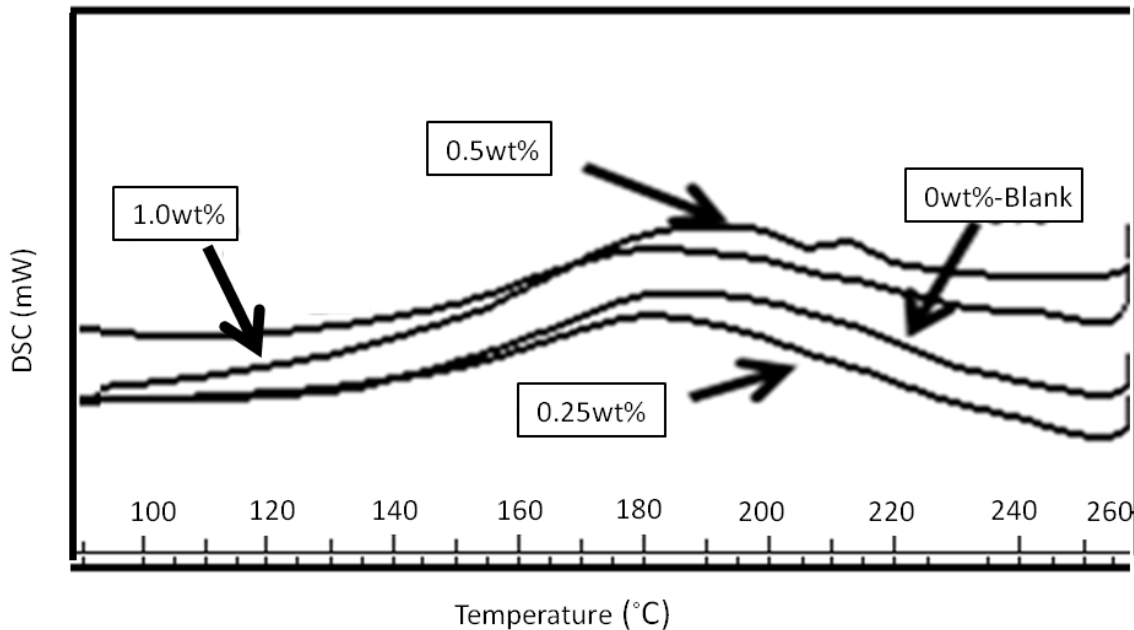Observed heat evolution patterns from DSC studies for each loading of A_f-MWCNT to epoxy resin system are shown inFig.4. 5.
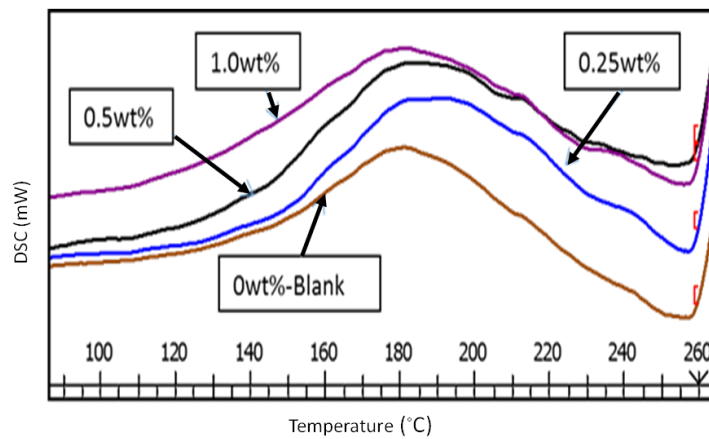
Figure.4.5: DSC curves showing the heat evolution patterns of epoxy with different

weight fractions of A_f-MWCNTs.

It can be seen from Fig.4.5 that, as we keep on increasing the loading of A_f-MWCNT in epoxy, heat raised significantly up to 0.5wt%. It was reported that, functionalized CNTs can covalently integrate with the epoxy network through exothermic reactions [8]. In the present case, additional heat evolutions can be attributed to extra crosslink reactions occurred due to additional amino groups available on the A_f-MWCNTs. Amino groups present on the A_f-MWNTs are known to form strong covalent bonds with the epoxy matrix [20]. Beyond 0.5wt% loading there is only a marginal increase in the evolved heat (Table.4.3). This could be either due to the exhaustion of the epoxy sites that can avail the additional amino groups present on the A_f-MWCNT or due to improper dispersion at higher loading. However, SEM/TEM micrographs are showing good dispersion even at 1.0wt% loading of A_f-MWCNT (Fig.4.6). This indicates that, for the DGEBA epoxy resin having DETDA curing agent in the ratios of 4:1 weight percentage, saturation in accommodating A_f-MWCNT will occur somewhere between 0.5wt% to 1.0wt% loadings. This is because, amino groups present on the A_f-MWCNT compete with the amino groups of hardener/curing agent in crosslinking with the epoxy groups. As the loading of A_f-MWCNT increases, more and more amino groups will be available while the epoxy groups are not increasing proportionately.

Hence, at some loading of A_f-MWCNT, a situation arises, where, though amino groups are present for crosslinking, there will be no more epoxy groups available, making further crosslinking impossible. Relative percentage (%) improvements/change in the crosslink density (%CD) due to A_f-MWCNT over the blank is measured using following formula and the obtained results are summarized in Table.4.3.

$$\%CD = \frac{\Delta H \ (MWCNT \ epoxy) - \Delta H \ (Blank \ epoxy)}{\Delta H \ (Blank \ epoxy)} \times 100$$

Table.4.3: Heat evolution during crosslinking, percentage (%) change in the crosslink density (%CD) and fracture toughness for two phase composites

Wt% of MWCNTs in epoxy	ΔH (j/g)	%CD	Fracture toughness (MPa.m$^{1/2}$)
0% MWCNT (Blank)	165	-	0.96± 0.05
0.25% p-MWCNT	154	-7	0.90 ±0.10
0.5% p-MWCNT	147	-11	0.88±0.13
1.0% p-MWCNT	128	-22	0.75± 0.07
0.25% A_f-MWCNT	202	22	1.07 ± 0.04
0.5% A_f-MWCNT	242	46	1.28 ±0.03
1.0% A_f-MWCNT	268	62	1.21 ±0.05

FESEM/TEM images showing good dispersion of A_f-MWCNT in epoxy are shown in Fig.4.6
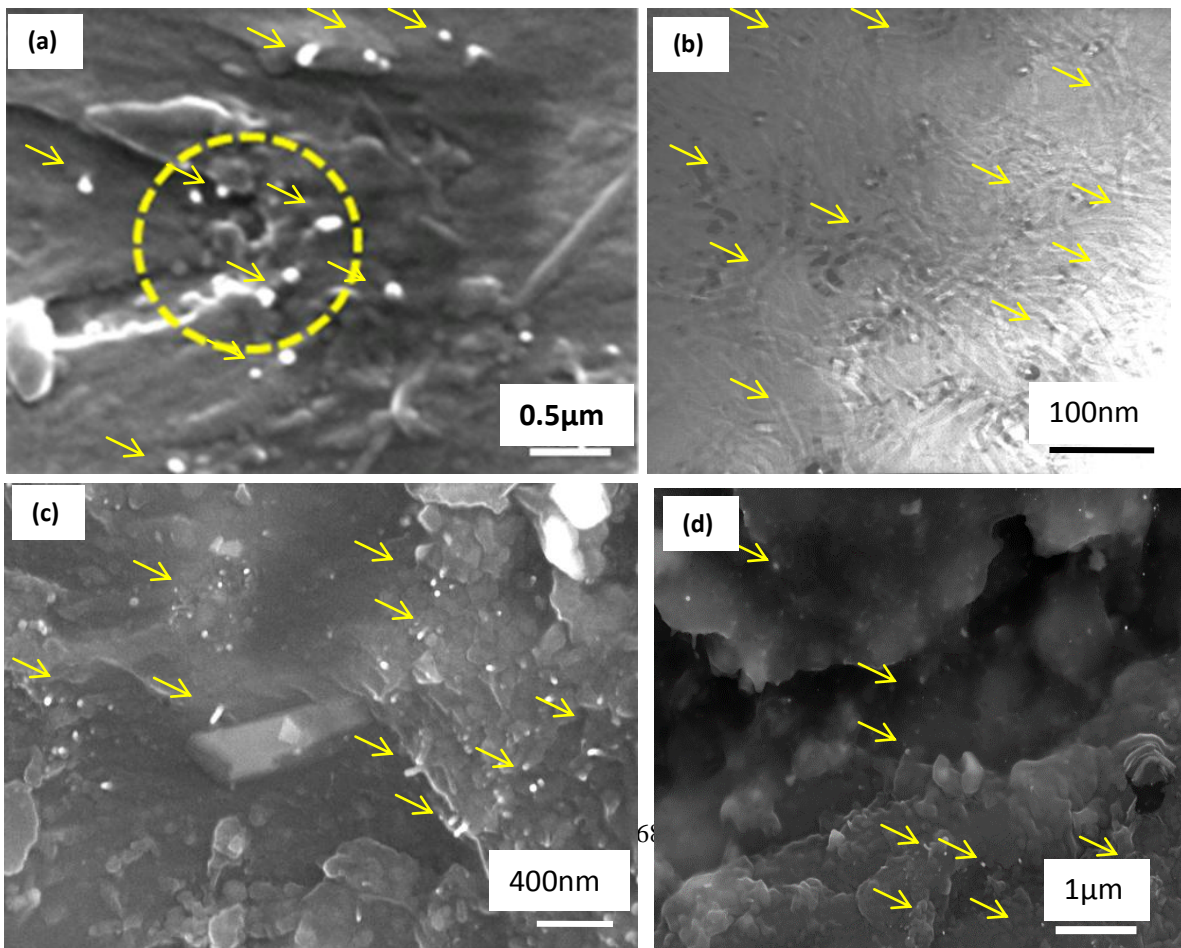
Figure.4.6: Electron microscope images of two phase composites (a) SEM image of 1.0wt% A_f-MWCNT-epoxy failed under fracture toughness test showing crack deflection (encircled zone) by A_f-MWCNT (shown by arrows) (b) TEM images of 1.0wt% A_f-MWCNT-epoxy showing good dispersion of A_f-MWCNT (shown by arrows) (c) & (d) FESEM images of 0.5wt% A_f-MWCNT -epoxy showing good dispersion of A_f-MWCNT (Shown by arrows)

4.2. Fracture toughness of two phase composites: In case of two phase composites, fracture toughness is found to decrease with the increasing loading of p-MWCNTs. On the other hand, it increased with increased loading of A_f-MWCNTs up to 0.5wt% [Fig.4.7].
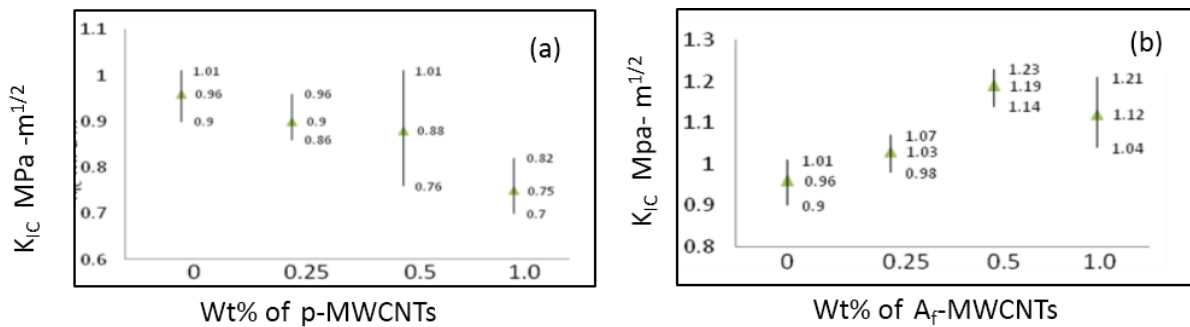
Fig.4.7: Fracture toughness of MWCNT-epoxy two phase composites as a function of weight percentage of MWCNTs (b) p-MWCNTs-epoxy (b) A_f- MWCNTs - epoxy

Reduction in toughness for epoxy with the addition of p-MWCNTs can be attributed to agglomeration of later [Fig.4.4]. In the agglomerated form, p-MWCNTs cannot offer resistance to propagating cracks effectively. This is because, resin infiltration in to agglomerated MWNCTs will be poor and hence they act as defect zones. Hence, crack propagation becomes easier as defect zones do not offer resistance to propagating cracks. This is inferred from the microstructure of the fracture surfaces of the p-MWCNT-epoxy composites which are observed to show glassy surface without crack deflections as shown in Fig.4.8. This resulted in reduced fracture toughness for p-MWCNT-epoxy two phase composites.
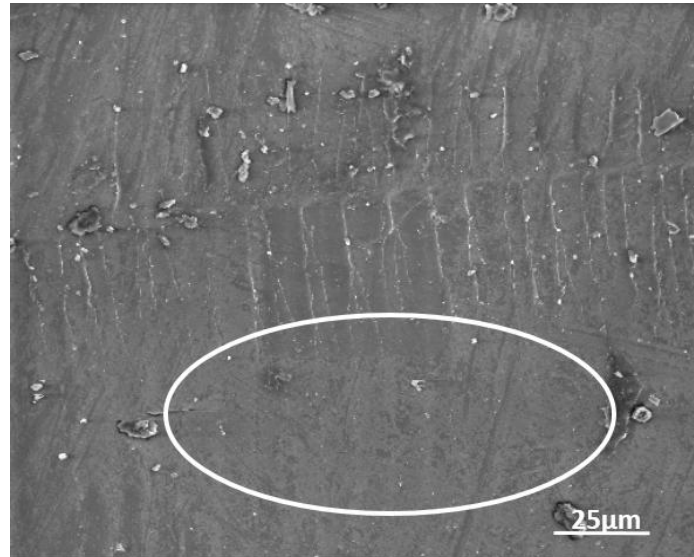
Figure.4.8: SEM image of the fracture surface of p-MWCNT-epoxy showing glassy surface without crack deflections (encircled zone)

A_f-MWCNTs are observed to enhance the toughness of epoxy matrix (Table.4.3). This can be understood due to two reasons. The first one being, the ability of the strongly bonded A_f-MWCNTs to deflect the cracks originated in the matrix as shown in Fig.4.6.a. which forces the advancing crack front to follow torturous paths leading to generation of rough surface having more surface area. As generation of more surface area during fracture, absorbs more energy it resulted in enhanced toughness [21,22]. Rough surfaces generated for A_f-MWCNT -epoxy two phase composites as compared to the blank epoxy can be seen in the following Fig.4.9.
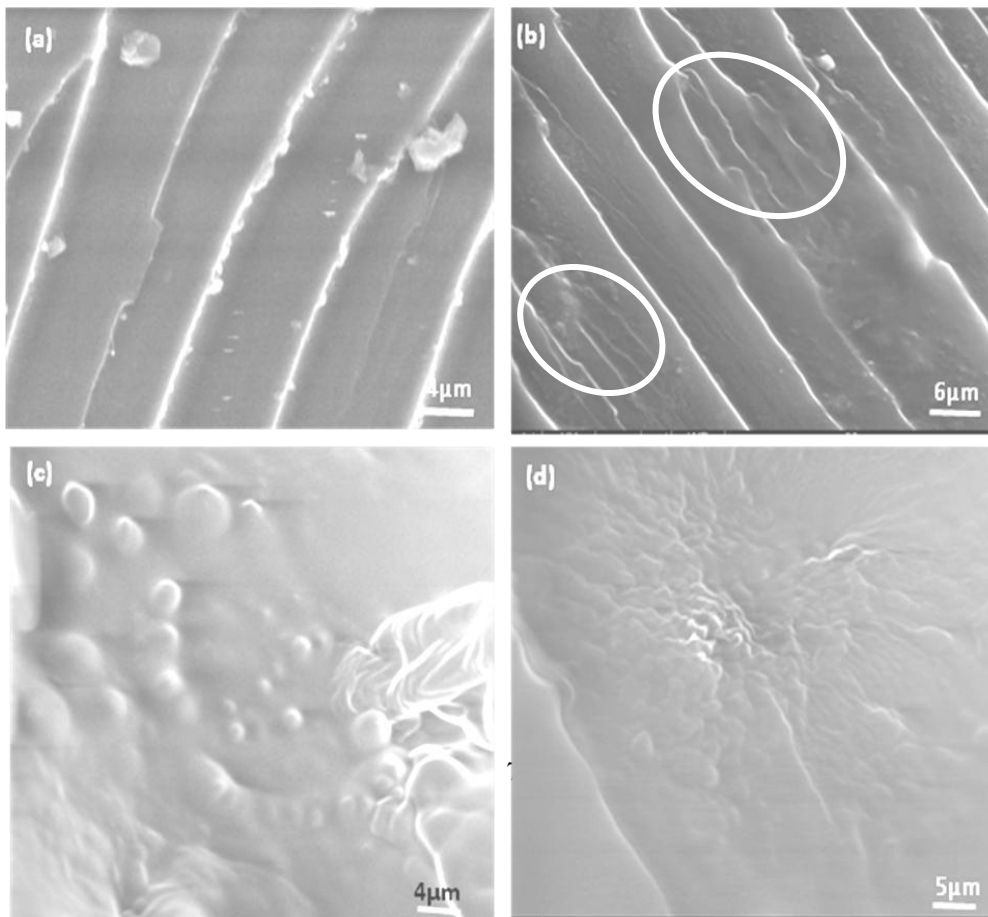
Figure.4.9: SEM images of the fracture surfaces of two phase composites. (a) Blank epoxy showing fracture planes with insignificant crack deflections (b) 1wt% A_f-MWCNT-epoxy two phase composite showing crack deflection along the fracture planes (encircled zone). (c) & (d) High magnification view of the 1wt% A_f-MWCNT-epoxy two phase composite showing rough fracture surfaces in different regions.

The other reason for enhanced toughness can be understood due to enhanced crosslink density of epoxy matrix in presence of A_f-MWCNTs. This aspect is elaborated in detail in the following section.

4.2.1. Effect of crosslink density changes on toughness of epoxy: Crack deflection by CNTs is generally believed as the primary mechanism contributing to the toughness improvements of the two phase composites. However, if it were the primary mechanism effecting the toughness, then it should have increased further at 1.0wt% loading of A_f-MWCNTs compared to 0.5wt% of loading. As observed from the results (Table.4.3), for 1.0wt% loading of A_f-MWCNTs average fracture toughness value decreased by about 6% as compared to the toughness value observed at 0.5wt% loading. Dispersion problem of A_f-MWCNTs cannot be attributed for this as good dispersion was observed even up to 1.0wt% loading as shown in Fig.4.6. This concludes that, the toughness variations in epoxy matrix are due to additional reasons other than crack deflections and bridging. Additional reason for toughness variations can be attributed to the enhanced crosslinking of epoxy in presence of A_f-MWCNT. The negative trend observed for toughness beyond 0.5wt% loading of A_f-MWCNTs indicates that, crosslink density improvements beyond an optimum value will bring down the toughness of the matrix.

Two phase composites discussed so far acts as matrix in three phase composites. Hence three phase composites, are expected to get influenced by the properties of the two phase composites. The following sections discusses, the mechanical properties of the three phase composites in the light of toughness variations of the two phase composites.

4.3. Mechanical properties of three phase composites:

4.3.1. Mechanical properties of p-MWCNT-C-epoxy: All the mechanical properties were observed to be coming down with the addition of p-MWCNTs to C-epoxy composites (Table.4.4). There is no precise trend in the mechanical property reduction due to p-MWCNTs addition. For instance, 0.5wt%-p-MWCNT-C-epoxy has shown higher flexural strength but lower tensile and very low ILSS properties as compared to the blank C-epoxy. 1.0wt% p-MWCNTs have shown poor tensile and flexural properties compared to any other composition, but slightly better ILSS than 0.5wt% p-MWCNT-C-epoxy. In general it can be stated that,

reduction in mechanical properties are found to be more with increased loading of p-MWCNTs. Reasons for the observed reduction in the mechanical properties can be understood as following

MWCNTs in non-functionalised form are generally highly entangled. Highly entangled p-MWCNTs needs very high shear forces to unbundle. Hence, uniform dispersion of p-MWCNTs in the resin systems is very difficult as compared to the functionalised MWCNTs. It can be seen from the Fig.4.10.a, that there are undispersed bundles of p-MWCNTs which are not infiltrated well with the resin system. These, resin deficient zones are acting as defects in the C-epoxy composites which initiates early failure of the composite under applied loads. However, wherever there is good dispersion of p-MWCNTs, they are able to enhance the interface strength of C-fibre with the matrix (Fig.10.b).

Poor and non-uniform dispersion and resultant non-uniformity in the interfacial bond strength, can be evidenced from the microstructure of the fractured samples with some zones showing good interfacial bonding (Fig10.c &d) and other zones showing poor bonding.

Table.4.4: Mechanical properties of p- MWCNT-C-epoxy three phase composites at different wt% of MWCNTs

Property (MPa)	Blank (0% MWCNT)	0.25wt% p-MWCNT	0.5 wt% p-MWCNT	1 .0wt% p-MWCNT
Tensile strength	2220(180)	2119(189)	2150(113)	1763(101)
Flexural strength	1269(48)	1385(94)	1326(83)	1128(100)
ILSS	58(3)	62(2)	48(5)	49(6)

Values in the parentheses are standard deviations

Generally, samples having agglomerated MWCNTs may be showing poor strength and the samples collected from the well dispersed zones may be showing good mechanical properties. This could be the reason for unpredictable trend in the mechanical properties of the p-MWCNTs.
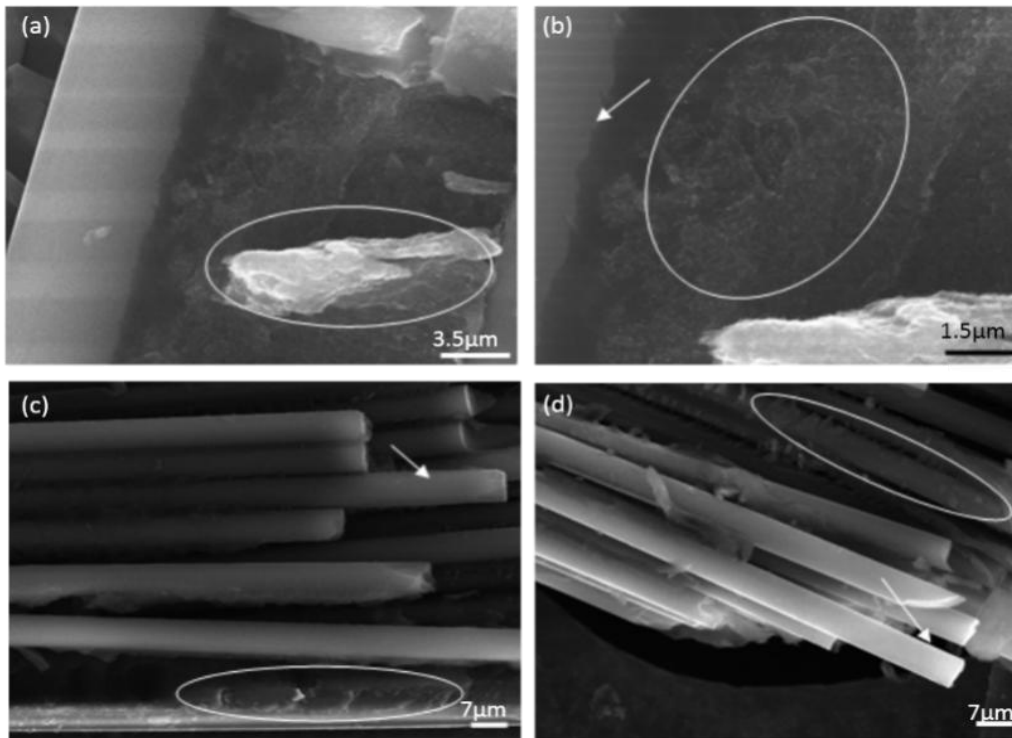
Figure.4.10: SEM images of 1.0wt% p-MWCNT-C-epoxy composites. (a) Bundles of MWCNTs with poor dispersion (encircled) (b) Showing good adhesion of matrix to the fiber (shown with arrows) in the zones where p-MWCNTs are well dispersed (encircled zone) (c) & (d) Fracture surfaces showing good adhesion of matrix to some filaments (encircled zone) and poor matrix adhesion to most of the other filaments (shown with arrow) .

4.3.2. Mechanical properties of A_f-MWCNT-C-epoxy: Similar to fracture toughness of two phase composites, tensile and flexural strengths of the three phase composites also increased with increased loading of A_f-MWCNTs up to 0.5wt% beyond which, these properties started to show a downward trend (Table.4.5).

Table.4.5: Mechanical properties of Af-MWCNTs -C-epoxy three phase composites at different wt% of MWCNTs

Property (MPa)	Blank (0wt% MWCNTs)	0.25wt% A_f-MWCNTs	0.5 wt% A_f-MWCNTs	1.0wt% A_f-MWCNTs
Tensile strength	2220(180)	2356(96)	2450(57)	2430(178)
Flexural strength	1269(48)	1353(104)	1463(80)	1401(110)
ILSS	58(3)	63(4)	66(2)	68(6)

Values in the parentheses are standard deviations

73

Strength improvement due to addition of A_f-MWCNTs could be attributed to the strengthened fiber matrix interface which is evident from the significant change in the failure modes of the blank C-epoxy composites as compared to the failure modes of the A_f-MWCNTs-C-epoxy composites. SEM micrographs of the fracture surfaces of the tensile specimen of blank C-epoxy samples are showing more fiber matrix debonding and inter filament debonding indicating less interface toughness (Fig.4.11). Failure of the blank C-epoxy composite with more inter filament debonding can be understood as below.

Fiber-matrix interface zone is the weakest zone in the composite. This is due to the fact that, fiber and matrix are two distinct phases joined at the interface. Hence, across the interface zone, there is sudden change in the mechanical properties like tensile strength, stiffness. Under the applied tensile loads, initially both fiber and matrix elongate uniformly up to some critical strain. However, as the stiffness of the fiber and matrix are not same, there will be mismatch in the strain of the fiber to the matrix which keeps on increasing with the increasing applied load. This results in generation of micro cracks at interface. Once the micro cracks are generated at the interface, stress concentration buildsup at the cracked zones which results in easy propagation of initially formed cracks. This leads to immature failure of the blank C-epoxy composites with more inter filament debonding as shown in Fig.4.11.

On the other hand, 0.5wt% A_f-MWCNT reinforced C-epoxy composites are found to display distinct failure modes with less inter filament debonding as compared to the blank C-epoxy composites as shown in Fig.4.12. The distinct failure modes with less inter filament debonding observed for 0.5wt% A_f-MWCNT-C-epoxy could be explained by the fact that, the A_f-MWCNTs present at the interface, anchor the C-fiber to the matrix strongly thus strengthening the interface and ensuring uniform stress buildup along the length of the C-fiber –matrix interface under the applied load [23].

It is evident from the micro structure of the fractured surfaces of 0.5wt% A_f-MWCNT-C-epoxy that, A_f-MWCNTs are strengthening the fiber-matrix interface by resisting the generation of the micro-cracks. Even after the generation of matrix micro-cracks at the interface, A_f-MWCNTs can offer more resistance for the propagation of interface cracks through crack deflection and also by crack bridging. Strengthened interface ensures uniform load distribution across the sample and thus the maximum mechanical property of the every filament present in the C-fibers tows is realized.
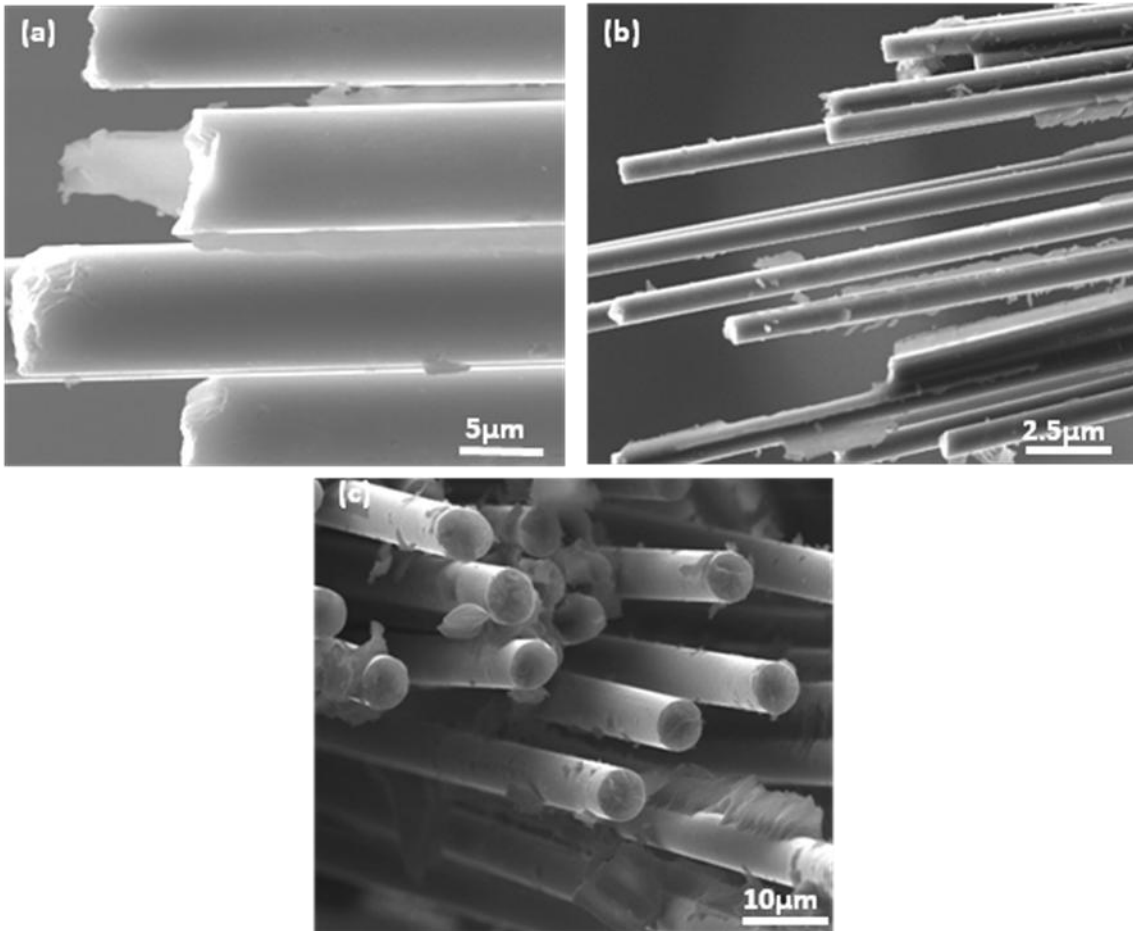
Figure.4.11: SEM images of the fracture surface of blank C-epoxy composites (a) Fully debonded individual filaments (b) & (c) Filaments with little or no resin attached to their surfaces.

In essence, prior to the failure of the composite carbon filaments/fibers slides past the matrix. If the composite is having A_f-MWCNT as additional reinforcements, they act as anchoring sites between the fiber to the matrix. Hence during the sliding of the fibers more energy will be consumed. This is because of A_f-MWCNTs also needs to be pulled out of the matrix. Thus 0.5wt% A_f-MWCNT-C-epoxy has shown higher tensile and flexural properties [15].

The macro images of the fractured samples under tensile loads also support the observations made with SEM. It can be observed from the Fig.4.13 (a-c) that, when A_f-MWCNTs are present in C-epoxy, tensile failure of the composite is by explosive failure (XGM mode of failure as per ASTM D 3039) with individual filaments opening up and breaking at once and forming a broomstick kind of structure by the fractured specimen. Failure of the, A_f-MWCNT-C-epoxy composites predominantly by explosive mode of failure indicates strong interaction between individual filaments which are responding uniformly to the applied load, across the area

of the composite that is subjected to the tensile loads. Hence, they all failed at once. This ensured maximum utilization of the mechanical properties of the all the filaments which resulted in improved tensile strength for the A_f-MWCNT-C-epoxy composites.
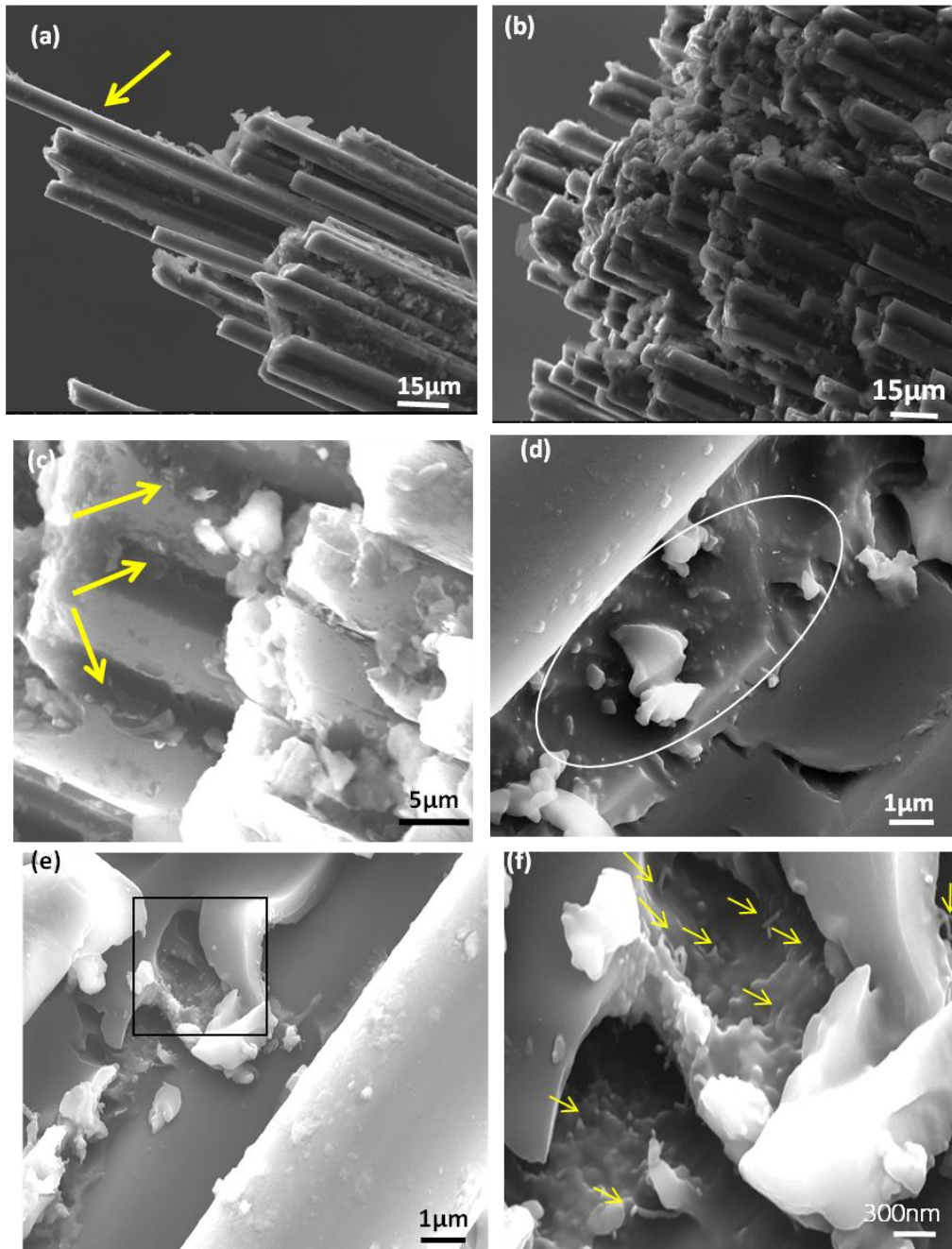
Figure.4.12: SEM images of 0.5wt%A_f-MWCNT-C-epoxy after tensile failure (a) Showing very less inter filament debonding (debonded filament shown with arrow). (b) & (c) Showing good inter-filament bonding (indicated by arrows) (d) FESEM image showing good dispersion of A_f-MWCNTs (encircled zone) (e) FESEM image showing matrix deformed zones at fracture surface where A_f-MWCNTs are visible (encircled zone) (f) Magnified view of encircled zone of image 'e' showing well dispersed A_f-MWCNTs .
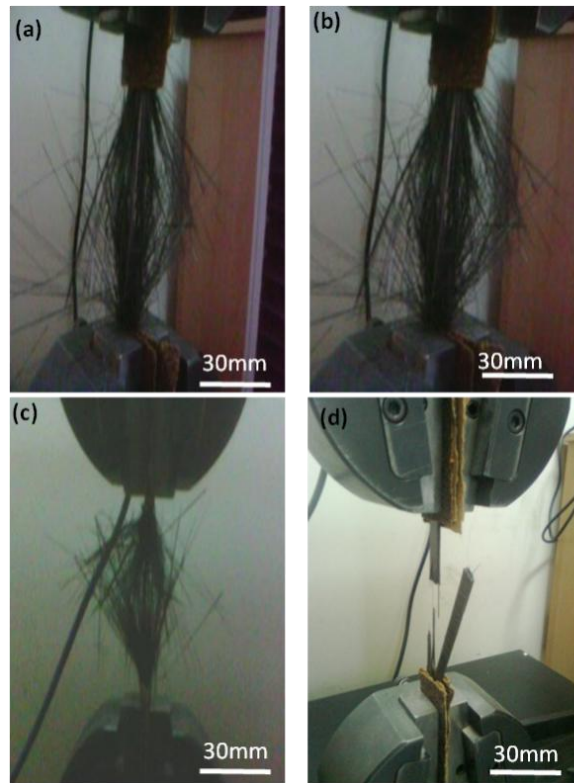
Figure.4.13: Macro images of the fractured specimens under tensile loads (a) 0.25wt%A_f-MWCNT-C-epoxy (b) 0.5wt% A_f-MWCNT-C-epoxy (c) 1.0wt% A_f-MWCNT-C-epoxy (d) Blank-C-epoxy

However, if the primary reason of strength improvement for CFRPs is due to A_f-MWCNTs, then the mechanical properties should have increased more at 1.0wt% addition of A_f-MWCNTs than 0.5wt% addition of A_f-MWCNTs. This is because at 1.0wt% addition of A_f-MWCNTs, more amount of A_f-MWCNTs should have offered more number of anchoring sites across the interface. However, results show a remarkable improvement in the tensile, flexural strength only up to 0.5wt% loading of A_f-MWCNTs. Beyond this, at 1.0wt% loading of A_f-MWCNTs there is a saturation in the tensile and flexural strength with indications of slight reduction in the properties. Saturation in mechanical properties at 0.5wt% loading of A_f-MWCNTs and slight reduction in mechanical properties at 1.0wt% A_f-MWCNTs loading is similar to the trend that was observed for fracture toughness of the two phase composites (A_f-MWCNTs-epoxy) which is acting as the matrix in the three phase composite (A_f-MWCNTs-C-epoxy). Hence, the following section is oriented to visualize mechanisms of strength improvements for A_f-MWCNTs- C-epoxy in terms of toughness changes to matrix/ matrix present at the interface.

4.3.2.1. Effect of matrix toughness on tensile strength, flexural strength: At the interface of A_f-MWCNTs-C-epoxy, additional crosslinking reactions will occur between the A_f-MWCNTs & epoxy and between A_f-MWCNTs and the epoxy sizing on the C-fibers [9]. This additional crosslinking not only increases the interfacial strength but also interfacial toughness as it is observed that, increased crosslinking is

found to increase the matrix toughness up to some optimum value (Fig.4.7.b) which is 0.5wt% loading in the present case. Enhanced interface toughness due to functionalized MWCNTs up to optimum loading, and it's saturation beyond optimum interface crosslink density was earlier reported by some research groups [24]. In the present case, at 0.5wt% loading of A_f-MWCNTs, toughness reaches optimum value at C-fiber and epoxy matrix interface. Hence up to this loading, inter filament bonding is intact with very less or no signs of micro-cracks. (Fig.4.12. b &4.12. c).

As the A_f-MWCNTs loading increased to 1.0wt%, interface toughness has come down which is inferred from the, observed micro-cracks at the C-fiber-matrix interfaces for 1.0wt% A-MWCNT-C-epoxy (Fig.4.14.a). This can be attributed to the fact that, higher crosslinking at the C-fiber-matrix due to higher loading (1.0wt %) of A_f-MWCNTs reduced the toughness of the interface. This is validated by the fact that, cracks are observed to be originating from the zones where A_f-MWCNTs are present at the interface (Fig.4.14.b &4.14.c). This indicates that, even with good dispersion of A_f-MWCNTs (as inferred from Fig.4.14.b-f) at higher loading, A_f-MWCNT's ability to anchor the C-fiber to the matrix is overshadowed by the reduced interface toughness due to higher crosslinking.

As micro cracks propagation increases at the interface, mechanical properties starts to come down as interface cannot act as effective load transfer medium between the matrix to fiber or fiber to fiber. This implies that, the interface toughness of C-epoxy which is altered by A_f-MWCNTs is playing a significant role in influencing tensile and flexural properties of the three phase composites. In essence, at their optimum loading (0.5wt% in the present study) A_f-MWCNTs are assisting in deriving the maximum mechanical properties of carbon fibers by minimizing the interface cracks. This can be further evidenced from the load Vs deflection curves of the samples failed under tensile loads (Fig.4.15).
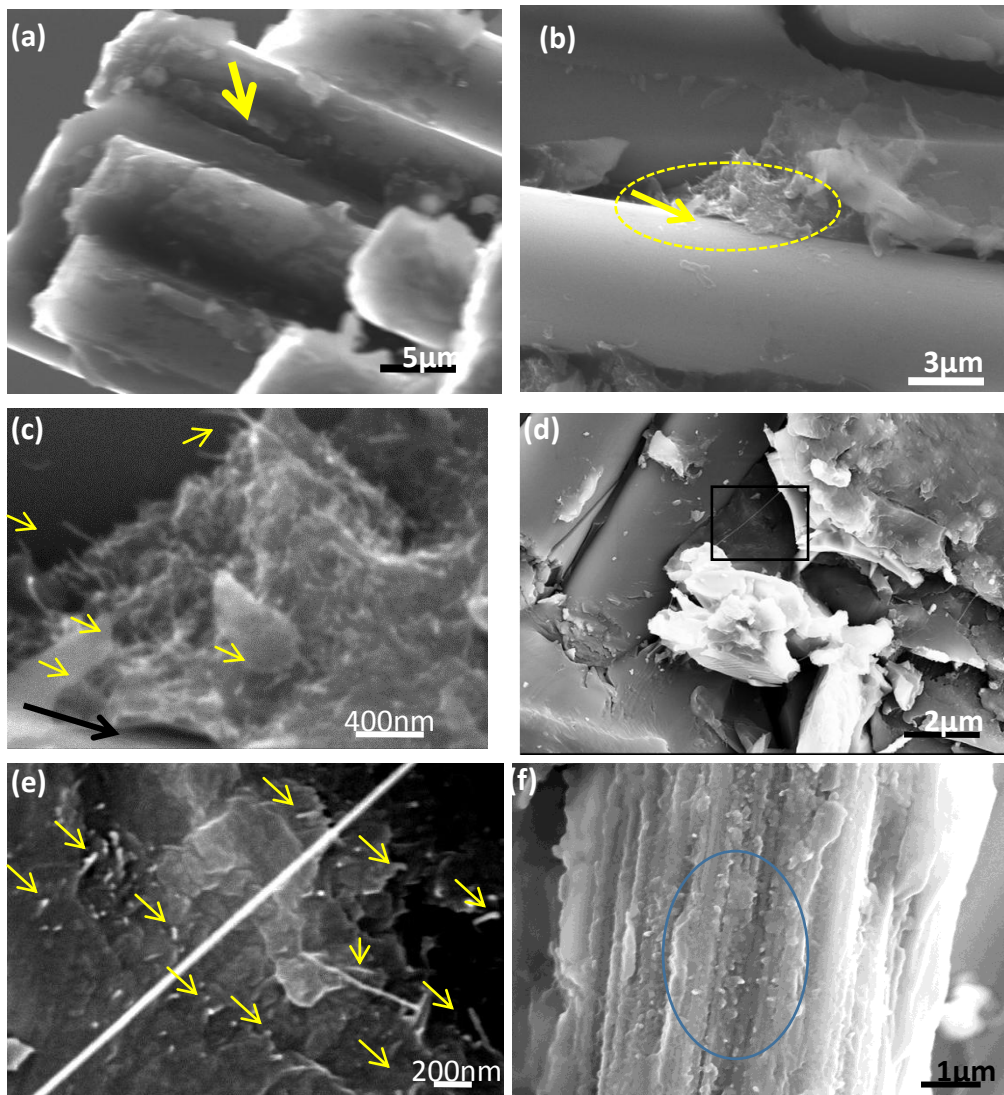
Figure.4.14: SEM/FESEM images of the 1.0wt%A_f-MWCNT-C-epoxy samples after fracture (a) Showing micro-cracks at the interface (shown by arrow) (b) Encircled zone showing initiation of debonding at C-fiber matrix interface (c) Close view of the encircled zone in fig.b, showing initiation of matrix debonding at interface where well dispersed A_f-MWCNTs are present at higher loading (1.0wt% loading of A_f-MWCNTs) (d) Fractured sample where A_f-MWCNTs are located (encircled zone) (e) Magnified view of the encircled zone in image 'd' showing well dispersed A_f-MWCNTs (f) Well dispersed A_f-MWCNTs on the surface of the C-fiber (encircled zone).
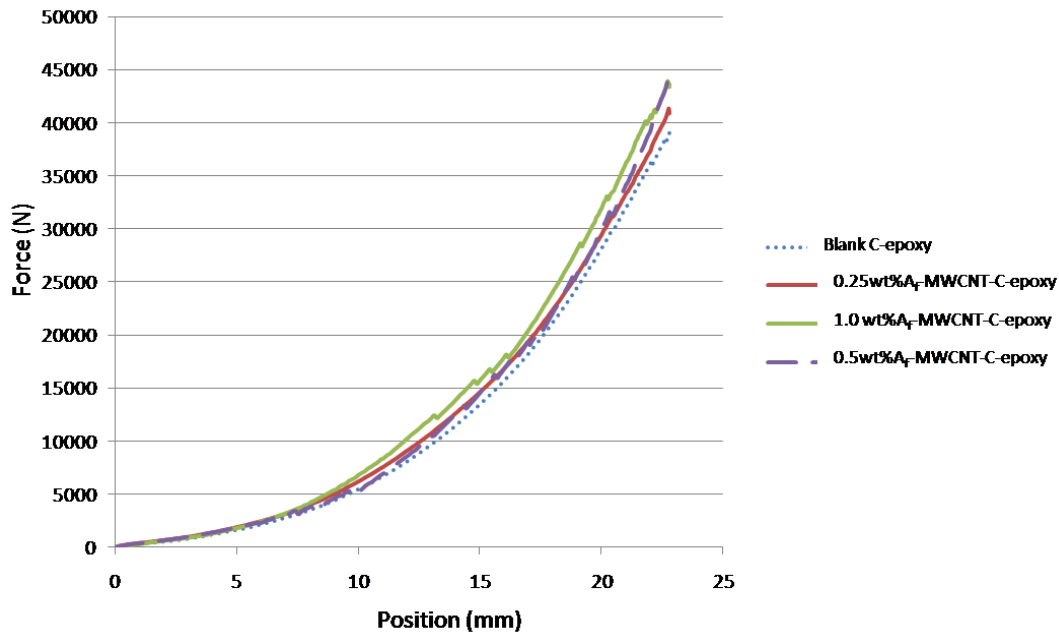
Figure.4.15: Force Vs deflection of curves of C-epoxy/A_f-MWCNT-C-epoxy composites subjected to tensile testing.

It can be seen from the Fig.4.15, that the maximum deflection at which carbon fibers are failing has not changed. But the maximum load the composite can experience before it strained to its maximum capacity has increased. It indicates that, in case of blank C-epoxy, due to generation of micro cracks at the interface, stress concentration has increased at selective zones resulting in the premature failure of the composite. On the other hand, when optimum loading of Af-MWCNTs are present at the interface, they are cushioning the interface micro-cracks and thus ensuring uniform load distribution to all the fibers across the sample area, there by deriving the maximum potential of the reinforced carbon fibers. Beyond optimum loading, as the interface embrittlement starts, again stress concentration zones increases leading reduction in mechanical properties.

Hence, even if good dispersion of A_f-MWCNTs is ensured in C-epoxy composites, mechanical properties namely tensile and flexural strengths will not increase beyond optimum loading of A_f-MWCNTs (0.5wt%A_f-MWCNTs in present study). This is due to the reduction in the interface toughness beyond a critical amount of loading of A_f-MWCNTs.

4.3.2.2. ILSS property of A_f-MWCNTs -C-epoxy: Inter laminar shear strength (ILSS) values increased up to 1.0wt% loading of A_f-MWCNTs in C-epoxy, though the matrix toughness was coming down beyond 0.5wt% loading of A_f-MWCNTs. This can be understood by the fact that, failure by ILSS involves more shearing and deformation at the fiber - matrix interface compared to the tensile and flexural failures. In such failures, more anchoring sites provided by higher loading of A_f-MWCNTs can strongly resist the interface shearing leading to higher ILSS [25]. This indicates that, interface bridging by the A_f-MWCNTs plays a predominant role in improving the ILSS property than the interface toughness.

5.Conclusions: i) Pure MWCNTs (without any functional groups)/ p-MWCNTs brings down the crosslink density of epoxy matrix while amino functionalised MWCNTs (A_f-MWCNTs) can increase the crosslink density of the epoxy matrix.

ii) p-MWCNTs are reducing the toughness of epoxy while A_f-MWCNTs are increasing toughness of epoxy up to a optimum loading. This is attained at a loading of 0.5wt% of A_f-MWCNTs to epoxy in present study

iii) p-MWCNTs are reducing the mechanical properties of C-epoxy composites due to their tendency of agglomeration.

iii) Toughness improvement (at C-fiber - matrix interface) due to A_f-MWCNTs is resulting in the tensile, flexural strength improvements in C-epoxy composites. These properties start to show a downward trend beyond optimum loading of A_f-MWCNTs, even when they are well dispersed. This is due to declining interface toughness beyond optimum loading of A_f-MWCNTs. Hence, even well dispersed A_f-MWCNTs cannot impart improved mechanical properties to C-epoxy composites beyond an optimum loading.

iv) ILSS property of the C-epoxy composites is found to increase with increased loading of A_f-MWCNTs which is not following the trend observed in the toughness of the matrix.

References

[1] G.Lubineau. A.Rahaman. A review of strategies for improving the degradation properties of laminated continuous fiber/epoxy composites with carbon based nano reinforcements. Carbon 50 (2012) 2377-2395.

[2] S.Bal, S.S.Samal, Carbon nanotube reinforced polymer composites – a state of the art. Bullet. Mater. Sci. 67 (2007)1-28.

[3] Peng – Cheng Ma, Naveed A. Siddiqui, Gad Marom, Jang – Kyo Kim. Dispersion and functionalisation of Carbon nanotubes for polymer – based nanocomposites: A review. Composites: Part A. 41(2010) 1345-1367.

[4] Hong Xuhui, Hua Youqing.The effects of curing cycles on properties of the epoxy system 3221/RH glass fabric composites. Polymer Composites. 29(2008)364–371,

[5] NuriErsoy, Tomasz Garstka, Kevin Potter, Michael R.Wisnom, David Porter, Martin Clegg, Graeme Stringer. Development of the properties of a carbon fiber reinforced thermo setting composite through cure. Composites: Part:A : 41.2010. 401-409

[6] A.Allaoui, N.ElBounia. How carbon nanotubes affect the cure kinetics and glass transition temperature of their epoxy composites? eXpress Polymer Letters 3 (2009) 588-594.

[7] Mohammad Reza Saeb, EhsanBakhshandeh,Hossein Ali Khonakdar,Edith Mader, Christina Scheffler,Gert Heinrich. Cure Kinetics of epoxy nanocomposites affected by MWCNTsfunctionalisation:Areview.2013(2013)http://dx.doi.org/10.1155/2013/703708

[8] D.Puglia.,L Valentini.,I Armentano.,J.M.Kenny. Effects of single-walled carbon nanotube incorporation on the cure reaction of epoxy resin and its detection by Raman spectroscopy. Diamond and RelatedMaterials.12 (2003) 827–832.

[9] F.H.Gojny, Malte H.G. Wichmann, Bodo Fiedler, Karl Schulte. Influence of carbon nanotubes on the mechanical properties of epoxy matrix composites-A comparative study. Compos. Sci. Technol. 65(2005) 2300-2315

[10] F.H.Gojny, M.H.G.Wichmann, U.Kopke, B.Fiedler, K.Schulte. Carbon nanotubes – reinforced composites- enhanced stiffness and fracture toughness at low nanotubes contents. Compos. Sci. Technol. 64 (2004) 2363-2371

[11] Daniel R.Bortz, Cesar Merino, Ignacio Marin –Gullon. Carbon nanofibers enhance the fracture toughness and fatigue performance of a structural epoxy system. Compos. Sci. Technol. 78(2011) 31-38.

[12] YokozekiTomohino, Y.Iwahori, S.Ishiwata, E.Kiyoshi. Mechanical properties of CFRP laminates macufactured from unidirectional prepets using CSNT - dispersed epoxy. Composites: Part A 38 (2007) 2121-2130.

[13] Daniel C.Davis, Justin W. Wilkerson, Jiang Zhu and Viktor G.Hadjev. A strategy for improving mechanical properties of a fiber reinforced epoxy composite using functionalised carbon nanotubes. Compos. Sci. Technol. 71 (2011) 1089-1097

[14] S.U.Khan, G.Y.Li, Naveed.A.Siddiqui,J.K.Kim.Vibration damping characteristics of carbon fiber-reinforced composites containing multi-walled carbon nanotubes. Composite.Sci and Technol 71(2001):1486-1494.

[15] K.H.Hung, W.S. Kuo, T.H.Ko, S.S.Tzeng, C.F.Yan. Processing and tensile characterization of composites composed of carbon nanotube grown carbon fibers. Composites: Part A. 40 (2009) 1299-1304

[16] A.Godara, L.Mezzo, F.Luizi, A.Warrier, S.V. Lomov, A.W. Van Vuure, L.Gorbatikh, P.Moldenaers, I.Verpoest. Influence of carbon nanotube reinforcement on the processing and the mechanical behavior of carbon fiber/epoxy composites. Carbon 47(2009) 2414-2423

[17] F.H.Gojny, M.H.G.Wichmann, B.Fiedler,W.Bauhofer,K.Schulte. Influence of nano-modifiation on the mechanical and electrical properties of conventional fiber - reinforced composites. Composites: Part A 36 (2005) 1525 - 1535.

[18] S.B.Jagtap, D.Ratna. Preparation and characterization of rubbery epoxy/multiwall carbon nanotubes composites using amino acid salt assisted dispersion technique. eXPRESS Polymer Letters. 7 (2013) 329-339.

[19] M.Nadler, J.Werner, T.Mahrholz, U.Riedel, W.Hufenbach. Effect of CNT surface functionalisation on the mechanical properties of multi-walled carbon nanotube/epoxy-composites. Composites: Part A 40 (2009) 932-937.

[20] JiafengShen, W. Huang, Liping Wu, Y.Hu, M. Ye. The reinforcement role of different amino-functionalised multi-walled carbon nanotubes in epoxy nanocomposites. Compos.Sci.Technol. 67(2007) 3041-3050.

[21] Peng Cheng Ma, Jan Kyo Kim, Benzhong Jang. Effects of silane functionalisation on the properties of carbon nanotube /epoxy nanocomposites. Compos. Sci. Technol. 67(2007) 2965–2972.

[22] Yuanxin Zhou. FarhanaPervin. Lance Lewis. Shaik Jeelani. Fabrication and characterization of carbon/epoxy composites mixed with multi-walled carbon nanotubes. Mater. Sci.Engg A (2007), doi: 10.1016/j.msea.2007.04.043

[23] Larissa Gorbatikh, StepanV.Lomov, IgnaasVerpoest. Nano-engineered composites: A multiscale approach for adding toughness to fiber reinforced composites. Procedia Engineering 10 (2011) 3252-3258

[24] Y.L. Chen, B. Liu, X.Q. He, Y. Huang, K.C. Hwang. Failure analysis and the optimal toughness design of carbon nanotube – reinforced composites. Compos. Sci. Technol.70 (2010) 1360 – 1367.

[25] J.Cho, I.MDaniel, D.A.Dakin, Effects of block copolymer dispersant and nanotube length on reinforcement of carbon/epoxy composites. Composites: PartA39 (2008) 1844-1850.

Chapter: V

CNF Reinforced Carbon -Epoxy Composites

CNF Reinforced Carbon – Epoxy Composites

The studies carried out so far have indicated that, amino functionalized carbon nanotubes are strengthening the fiber-matrix interface which is resulting in the enhanced mechanical properties for CFRPs. Matrix toughness/interface toughness improvements due to addition of A_f-MWCNT was found to be the main reason behind the mechanical property improvement of A_f-MWCNT- CFRPs. This infers that, CFRPs having more matrix content (lower fiber volume fractions) should get benefited more with the addition of A_f-MWCNT. Moreover, as it was observed that, CNTs are not acting as load bearing reinforcements in CFRPs rather acting as interface modifiers, it is expected that, similar results can be obtained with amino functionalized carbon nanofibers (A_f-CNFs) which are akin to MWCNTs. Since, A_f-CNFs are available at lower costs and easy to disperse in polymeric resins compared to A_f-MWCNT, it is essential to explore them as reinforcements to CFRPs. Hence, in this chapter, effect of A_f-CNFs addition to CFRPs having different fiber volume fractions is studied. It was observed that, A_f-CNFs can significantly increase the flexural strength and shear strength of CFRPs having lower fiber volume fractions. As the fiber volume fraction increases, their role as addition reinforcements are becoming insignificant.

1. Introduction

Carbon nanofibers (CNFs) are crude form of MWCNTs. Their surface contains thick pyrolitic graphite coating deposited on the core of MWCNTs. The graphitic planes of CNFs are also not oriented along the longitudinal axis of the tube, rather they are slightly canted with respect to the tube axis. These features makes them distinct from MWCNTs. However, they are also known to possess good mechanical properties, which makes them attractive materials to reinforce CFRPs. Besides this, CNFs are generally available at lower prices as compared to MWCNTs, which makes them economically viable for reinforcing large structures CFRPs. Hence, carbon nanofibers (CNF) were also widely explored as additional reinforcements to enhance the mechanical properties of the carbon fiber reinforced plastics (CFRPs) [1]. Studies on the functionalisation of CNFs and their homogeneous dispersion in polymer matrices were reported extensively by many research groups, which enables to realize the full potential of CNF as reinforcements in CFRPs [2-4]. It is reported that, amino functionalised CNF can react with epoxy matrix and thus form a covalent bond with the matrix [5]. Even after substantial understanding of functionalisation and dispersion of CNFs, still there are diverse reports on the degree of mechanical property improvements for CFRPs

due to the addition of CNFs. For instance, flexural strength improvements of fiber reinforced composite laminates due to the addition of CNF are reported up to as high as 22%, and also as low as 2.7% [6-7]. In general, improvement in the mechanical properties of CFRPs due to addition of functionalised CNFs is attributed to the strengthened fiber – matrix interface area [8]. In turn, interface area is dependent on the fiber volume fraction (V_f) of the composite. Hence, the extent of the mechanical property improvement due to the CNF addition in CFRPs depends on the V_f of the composite [9]. The significance of the V_f of CFRPs in to which CNFs are added could be one of the reasons for the large scatter observed in the reported mechanical properties of CNF reinforced CFRPs. So far, there are no systematic studies reported on, how CNFs addition influence the mechanical properties of the CFRPs/C-epoxy composite laminates having different fiber volume fractions. In this chapter an attempt was made to bridge this gap. V_f of the composite used in most of the practical applications generally lies in the range of 40-70%. Hence this range is considered in this study.

2. Raw materials: Epoxy resin, carbon fabric, and amino functionalised carbon nanofibers are the main raw materials in the present study. Brief specifications of the raw materials are given below.

Epoxy resin:

1. Chemical formula	:	Diglycydyl ether of bisphenol –A
2. Viscosity	:	10,000cP at 30°C
3. Density	:	1.2 g/cc
4. Acid Value	:	85-120
5. Commercial name	:	LY-556

Hardener:

1. Chemical formula	:	Diethyl toluene diamine
2. Viscosity	:	200 cP at 25°C
3. Density	:	1.0 g/cc
4. Commercial name	:	HY-5200

Carbon fiber specifications: Poly acrylo nitrile (PAN) based high strength carbon fabric woven with 3k fiber of T-300 grade were used to make laminated (2D) CNT-C-Epoxy composites. Brief specifications of carbon fibers are as given below.

1. Tow type	:	3k (3000 filaments in a tow)
2. Weaving pattern	:	8- H Satin

3.	Density of fiber	:	1.75 g/cc
4.	Areal density of fabric	:	380 g/ m^2
5.	Tensile strength (tow)	:	3.5 GPa
6.	Tensile modulus (tow)	:	180 GPa
7.	Commercial name	:	T-300 grade fabric

Carbon nanofibers (CNFs): CVD synthesized CNFs, which were subsequently purified and amino functionalised were procured from M/s Chemapol industries (Mumbai). Brief specifications of the amino functionalised CNFs (A$_f$-CNFs) are given below.

1. Purity	:	99.9wt%
2. Metallic impurities	:	less than 0.1wt%
3. Diameter	:	100-200 nm
4. Length	:	10-20 microns

Microstructure, FT-IR and TGA pattern of the amino functionalised CNFs in as received form are shown in Fig.5.1.

Microstructure shows approximately 150 nm-250 nm diameter for A$_f$-CNFs in as received form. Cupstacked structure of CNFs is visible from Fig.5.1.b. FT-IR shows a strong and symmetric peak at 3448 cm^{-1} as well as a shoulder at 1632cm^{-1} indicating presence of N-H bonds on the surface. TGA has not shown any residual weight indicating absence of any metallic impurities.
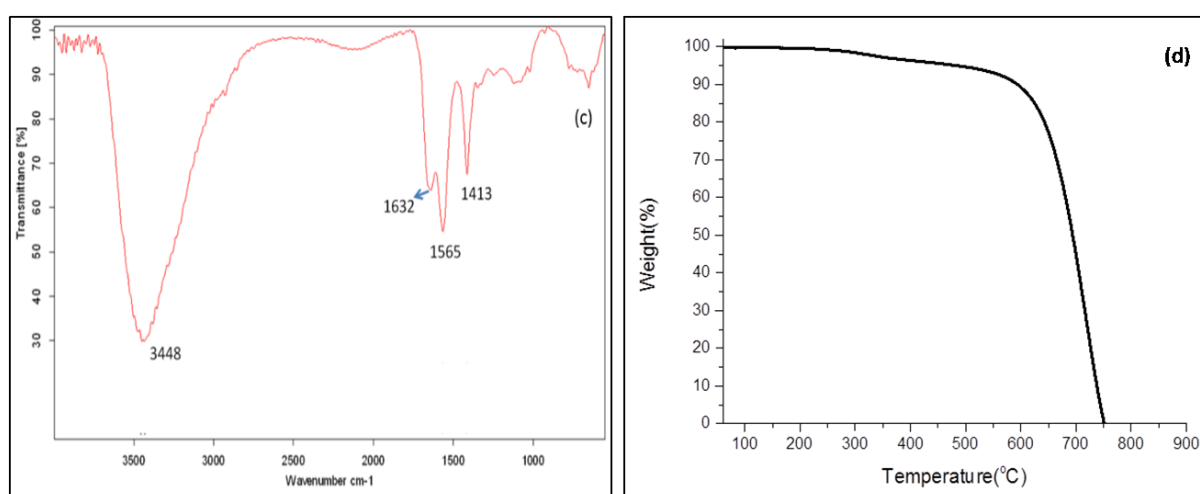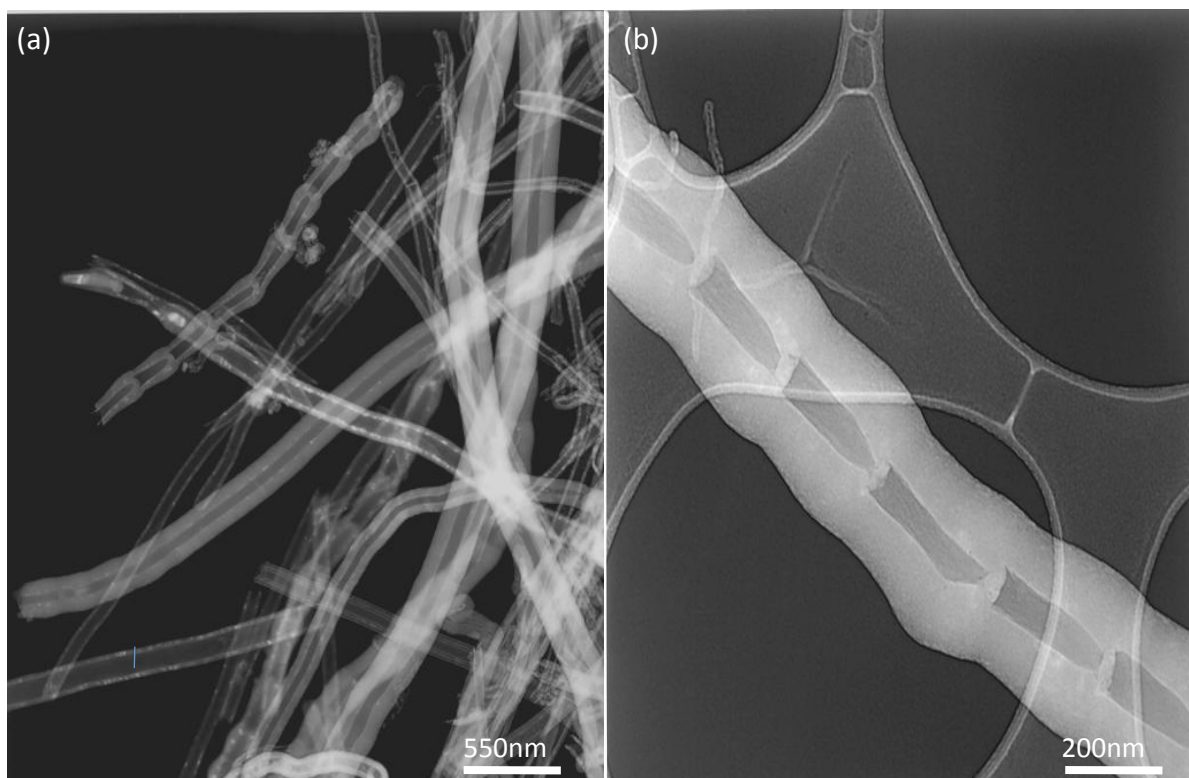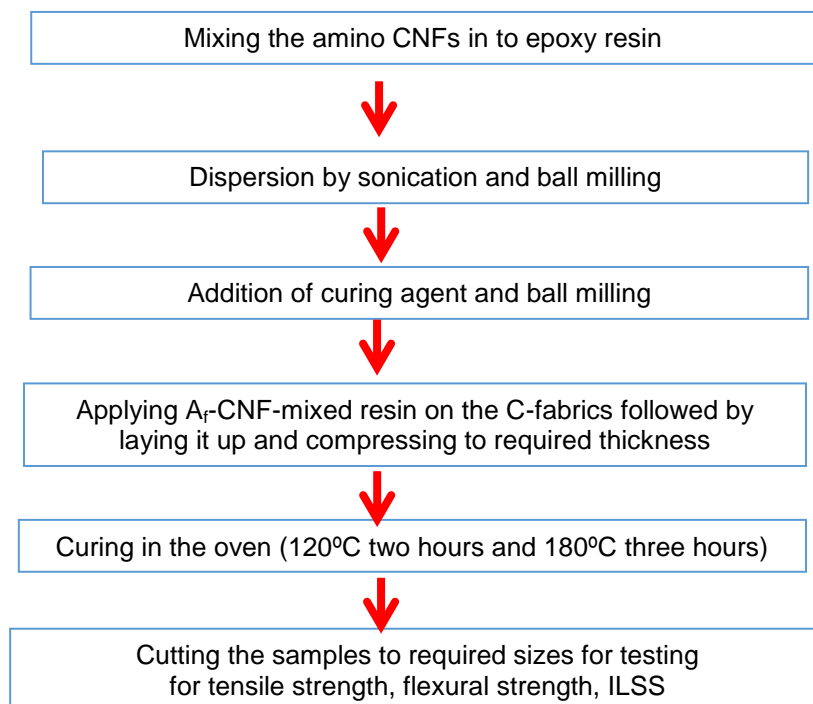
Figure 5.1: (a) & (b) Micro structure of as received A_f-CNFas observed under transmission electron microscope at different magnificaitons. (c) FT-IR pattern of the as received A_f-CNF(d) TGA pattern of the as received A_f-CNF .

3. Experimental work: The scheme of experimental work that is carried out is given breifly below.

3.1. Fabrication of composites: For fabricating the composite laminates, initially 1.0 weight percentage (wt%) of A_f-CNFs (1.0g of A-CNFs for 100g of epoxy) were dispersed in the epoxy resin using a probe type ultrasonicator (Mesonix-3000, USA) for 45 minutes followed by ball milling at 250 rpm for 120 minutes. Hardener was added to the A_f-CNF- epoxy mixture (24 parts of hardener to 100 parts of the epoxy resin by weight). This mixture was further ball milled at 250 rpm for 30min. Carbon fabric (C-fabric) was cut in to predecided specific dimensions and impregnated with A_f-CNF–epoxy-hardener mixture. Impregnated fabric layers were stacked and compressed in a suitable size metallic die. Curing of the stack in the compressed condition was carried out at 120ºC for 120minutes followed by180ºC for 180 minutes. V_f of the composite was controlled by varying the number of fabric layers in the given thickness (approximately 2.5mm). Various steps involved in composite fabrication procedure is shown in the following flow diagram.

Flow diagram: Schematic flow of experimental work

```
┌─────────────────────────────────────────────────────────┐
│         Mixing the amino CNFs in to epoxy resin          │
└─────────────────────────────────────────────────────────┘
                            ⬇
┌─────────────────────────────────────────────────────────┐
│        Dispersion by sonication and ball milling         │
└─────────────────────────────────────────────────────────┘
                            ⬇
┌─────────────────────────────────────────────────────────┐
│         Addition of curing agent and ball milling        │
└─────────────────────────────────────────────────────────┘
                            ⬇
┌─────────────────────────────────────────────────────────┐
│   Applying Af-CNF-mixed resin on the C-fabrics followed by │
│      laying it up and compressing to required thickness   │
└─────────────────────────────────────────────────────────┘
                            ⬇
┌─────────────────────────────────────────────────────────┐
│  Curing in the oven (120ºC two hours and 180ºC three hours) │
└─────────────────────────────────────────────────────────┘
                            ⬇
┌─────────────────────────────────────────────────────────┐
│          Cutting the samples to required sizes for testing │
│           for tensile strength, flexural strength, ILSS   │
└─────────────────────────────────────────────────────────┘
```

Various raw materials and tools used for fabrication of three phase composites and a typical laminated (2D) composite after fabrication are shown below in Fig.5.2.

Figure.5.2. (a) Carbon fabric roll from which fabric layers of required dimensions were collected (b) Die plates used to sandwich the stacked fabric layers (c) A_f- CNF- C-epoxy composite fabricated for mechanical property evaluation.

Different composite laminates that were made with varying V_f are shown in Table.5.1.

Table 5.1: Different types of A_f- CNF- C-epoxy composites fabricated

Sample description	Sample code	Wt% A_f-CNF	%Vf (+/-1%)
Blank C-epoxy	40BCE[a]	0	40
A_f-CNF -C-epoxy	40CCE[b]	1.0	40
Blank C-epoxy	50BCE	0	50
A_f-CNF -C-epoxy	50CCE	1.0	50
Blank-C-epoxy	60BCE	0	60
A_f-CNF-C-epoxy	60CCE	1.0	60
Blank –C-epoxy	70BCE	0	70
A_f-CNF -C-epoxy	70CCE	1.0	70

[a]BCE: Blank Carbon-epoxy composite, [b]CCE: A_f-CNF-C-epoxy composite.

Composite laminates made without A_f-CNF addition are, denoted as BCE (Blank–Carbon-Epoxy) while the composite laminates made with the addition of A_f-CNF are denoted as CCE (CNF reinforced Carbon–epoxy). The numbers prefixing the BCE/CCE indicates the fiber volume fraction. For example, 60CCE indicates A_f-CNF reinforced C-epoxy composite having $60V_f$. V_f of the composite laminates was determined with acid digestion test, using concentrated nitric acid following ASTM D3171. Flexural strength, interlaminar shear strength (ILSS) and tensile strength of the prepared composite laminates were determined as per ASTM D790 (three point bending test), ASTM D2344 and ASTM D 638 respectively on universal testing machine (United 50KN, USA). Minimum eight numbers of samples were tested from each laminate for each of the measured property and the results obtained is the average of the measurement (Table.5.2.). Microstructure and fracture modes of the tested samples were analyzed with environmental scanning electron microscopy (ESEM-FEI, Quanta 400, USA).

4. Results and discussion

4.1. Flexural strength: Flexural strength trend for A_f -CNF-CFRPs at lower and higher V_f was observed to be different which are discussed in the subsequent sections.

4.1.1. Flexural strength at $40V_f$-$60V_f$: A_f-CNF reinforced C-epoxy (CCE) composite laminates have shown higher flexural strength as compared to their corresponding blank (BCE) composite laminates having same V_f (Table.5.2).

Table.5.2: Summary of the mechanical properties of composites

V_f	[a]F.S (MPa) BCE CCE [e]	% imp[b]	ILSS (MPa) BCE CCE	% imp	[c]T.S (MPa) BCE CCE	% Imp
40	529(23) 682(41)	28.9	32 (1.2) 41 (1.1)	28.1	722 (42) 775(26)	7.3
50	601(39) 690(44)	14.8	35 (2.8) 40 (1.8)	14.2	756 (23) 777(7.4)	2.7
60	765 (38) 788(38)	3.0	47 (2.4) 48 (1.6)	2.1	855(18) 896(42)	4.7
70	921 (28) 869(27)	-5.6	47 (4.5) 45 (3.2)	-4.4	915(14) 854(39)	-6.6

[a]Flexural strength, [b] Percentage improvements, [c]Tensile Strength

 Note: Values in the parenthesis indicates standard deviations

It can be seen from the Table.5.2, that, as the V_f of the composite is increasing, there is a downward trend in the flexural strength improvements for CCE as compared to their corresponding BCE (having same V_f). For instance, flexural strength of 40CCE is 28.9% higher than 40BCE, while it is only 3% higher for 60CCE as compared to 60BCE. SEM studies of the fractured specimens have shown good dispersion of A_f-CNF at all V_f (40-70%) of the composite laminates (Fig.5.3).
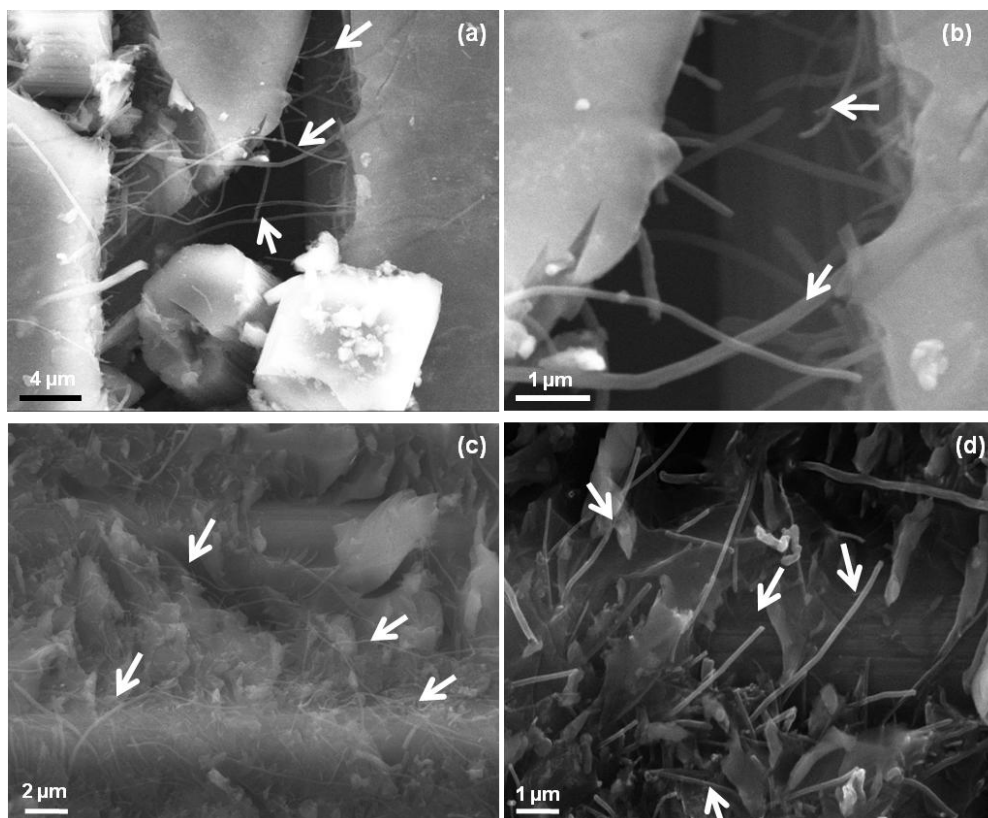
Figure.5.3: Fractured samples of C-epoxy composites failed under flexural/ tensile loads showing good dispersion of A_f-CNF(indicated by arrows) (a) 40CCE failed under flexural load (b) 50CCE failed under flexural load (c) 40CCE failed under tensile load (d) 60CCE failed under tensile load.

As the dispersion of A_f-CNFs was observed to be uniform, the observed variation in the flexural strength improvements may not be due to poor dispersion of A_f-CNFs. As all other experimental parameters were kept same, and only fiber volume fraction was varied, the systematic reduction in the degree of mechanical

property improvements with increasing V_f of CFRP can be attributed to the effects imposed by V_f only. Possible mechanisms for the observed trends are discussed based on the micro and macro images of the fractured samples. Mode of crack propagation during flexural failure and microstructure of the fractured samples are shown in Fig.5.4.
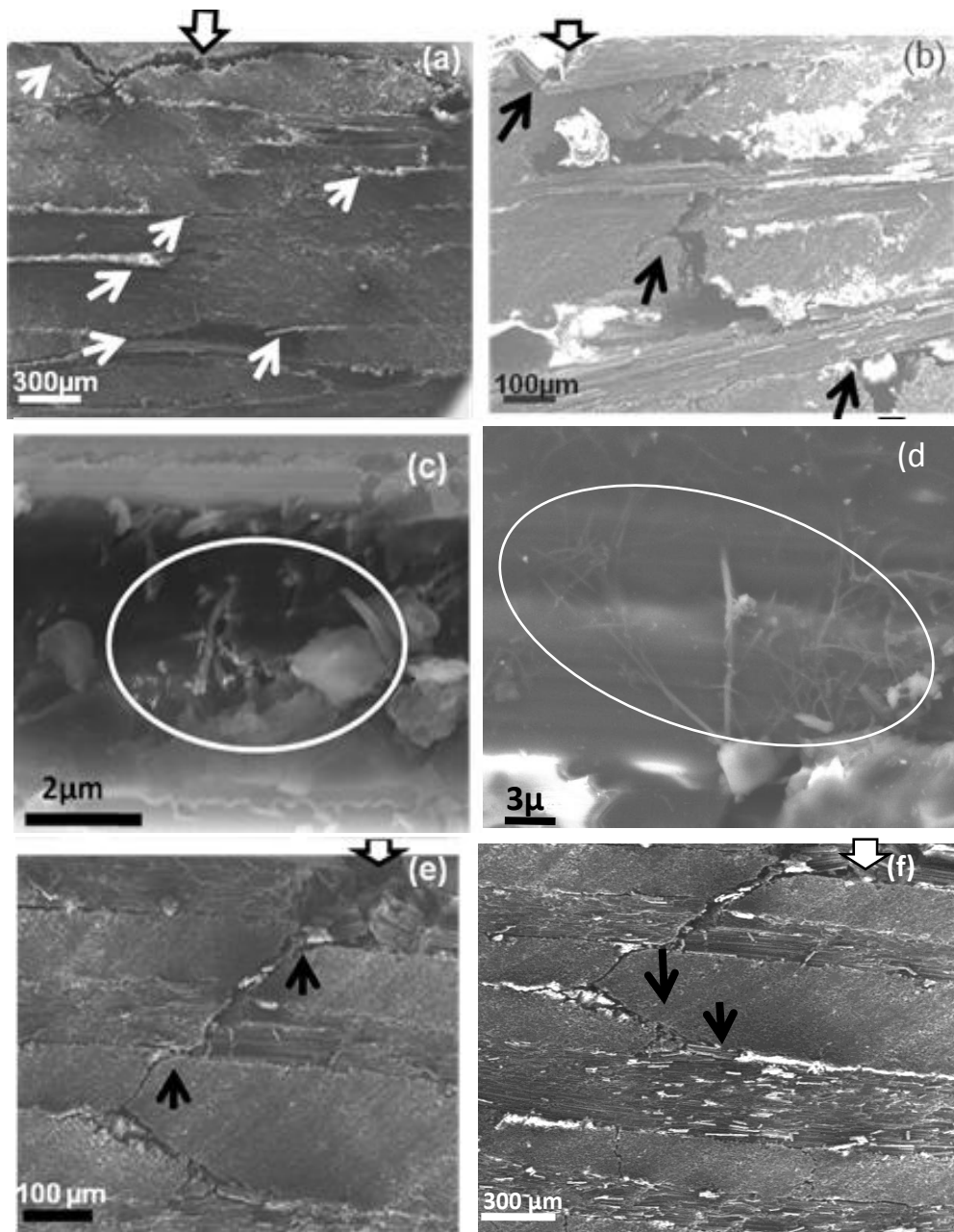
Figure 5.4: Showing C-epoxy samples failed under flexural loads. Broad arrows on top of each figure is indicating the loading point (a) 40BCE showing failure predominantly by interlaminar crack propagation(Indicated by arrows) (b) 40CCE showing predominant failure by rupture of C-fabrics (indicated by arrows) with no interlaminar crack propagation (c) SEM image of 40CCE showing interface strengthening by A_f CNF(encircled zone) (d) 40CCE showing interpenetrated A_f - CNF network joining many filaments (e)&(f) 60BCE showing failure by rupture of C-fabric layers with minimum interlaminar crack propagation.

Flexural failure of the CFRP is known to involve a combination of the failure by shearing of the fiber – matrix interface at the loading point and failure by rupture of fibers (in tensile mode) generally away from loading point. SEM images of the BCE & CCE samples failed under flexural loads, shows failure by combination of both interface shearing and rupture. However, it was observed that, the magnitude of the former and later modes of the failures varied significantly for BCE and CCE.

For instance, in case of 40BCE, failure initiated under the loading point in the flexural strength test, resulted in predominant formation of interlaminar cracks due to interface shearing (Fig.5.4.a). It is reported that, the crack propagation through the matrix rich interface zones encounters less resistance [9]. Hence, 40BCE failed at lower strength. On the other hand, in case of 40CCE, crack propagation was predominantly translaminar with the rupture of the C-fabric layers with minimum or no interface shearing (Fig.5.4.b). This mode of failure indicates that, A_f-CNF strengthened the interface due to their ability to interlock the fiber-matrix interface as shown in Fig.5.4.c & 5.4.d [10-11]. Hence crack is forced to propagate in translaminar (through thickness) direction with the rupture of the C-fabrics. As the C-fiber rupture consumes more energy, 40CCE which failed through the translaminar crack propagation with the rupture of C-fibers, has shown a significant improvement in the flexural strength. Besides this, the epoxy matrix, reinforced by the A_f-CNFs is known to exhibit enhanced stiffness, and this stiffened matrix can effectively restrain fiber bending which also contributed to the improved flexural strength of 40CCE [12-13].

Load Vs extension graphs of the samples failed under flexural loads are shown in Fig.5.5. It can be seen from the graphs that, at lower V_f, BCE are failing at lower load where as the failure loads for the CCE samples have increased significantly. This indicates that, more amount of C-fibers are involved in the failure of the CCE samples as compared to the BCE samples. More elongation of the composite before failure supports this view point.
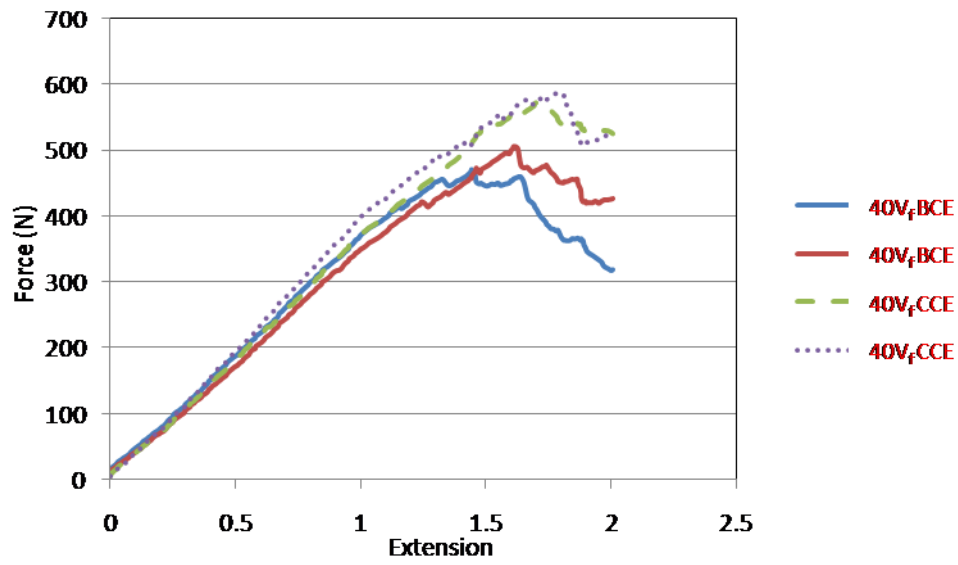
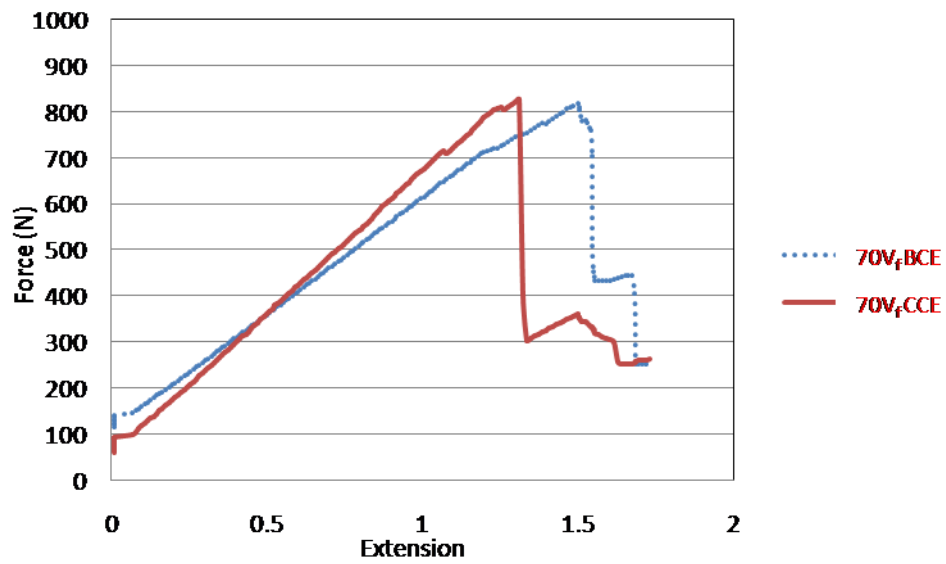Fig.5.5: (a) Force Vs extension patterns of the BCE and CCE samples having 40 V_f

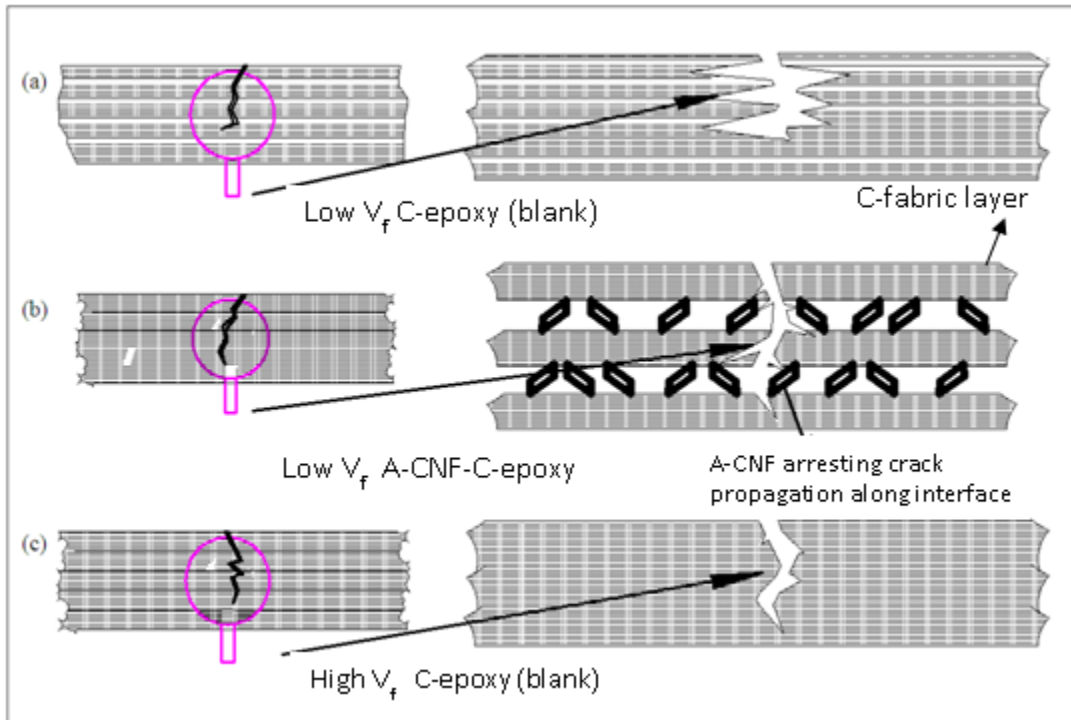Fig.5.5: (b) Force Vs extension patterns of the BCE and CCE samples having 70V_f.

Fig.5.6: Showing schematic flexural failure modes of C-epoxy/ A_f-CNF -C-epoxy at different V_f. (a) Low V_f C-epoxy showing horizontal spread of crack at each layer giving more interlaminar crack propagation. (b) Low V_f C-epoxy with A_f-CNF showing, A_f-CNF arresting the horizontal spread of crack and forcing the crack to propagate by rupturing C-fabric layers (c) High V_f C-epoxy showing highly compacted C-fabric layers and translaminar crack propagation

As the V_f of the composite laminates increased to $60V_f$, the fracture modes have changed significantly. Even in case of BCE crack propagation mode during flexural failure was observed to be predominantly translaminar (Fig.5.4.e & 5.4.f). Reduced interface shearing even for BCE at higher V_f can be attributed to the crimp of the woven fabrics. Crimp is a curvature or deformation arising out of weaving [14]. At higher V_f, when fabric layers are well compacted, crimp zones can interlock with adjacent fabric layer zones having complementary curvatures. These interlocks could resist interface shearing. Thus, at higher V_f of C-epoxy, crack propagation is proceeding with rupture of carbon fabric layers even for BCE samples. Hence, need of A_f-CNF to resist the interlaminar cracks would be limited for higher V_f C-epoxy composites. Schematic flexural failure modes of BCE and CCE at lower and higher V_f are shown in Fig.5.6(c).

As both, 60BCE and 60CCE failed in a similar mode, a significant improvement in the flexural strength due to the addition of A_f-CNF was not observed. However, A_f-CNF present in CCE, can still offer some

97

additional advantages as shown in the Fig.5.7. A_f-CNF reinforced C-epoxy composites failed under flexural loads are found to show formation of many subsidiary cracks (diffuse cracks) away from the main crack front in contrast to the limited number of diffuse cracks observed for the blank C-epoxy composites (Fig.5.7.a & 5.7.b).Formation of diffuse cracks can be attributed to the interconnected network of A_f-CNFs (Fig.5.4.d) which can transmit the load to long distances from the point of the bending load. As matrix is having well dispersed A_f-CNFs dispersed in it (Fig.5.7.c & 5.7.d), formation of diffuse cracks over a large area involves pulling out of A_f-CNFs from matrix in a larger area which consumes significant energy. This resulted in the improvement of the flexural strength.
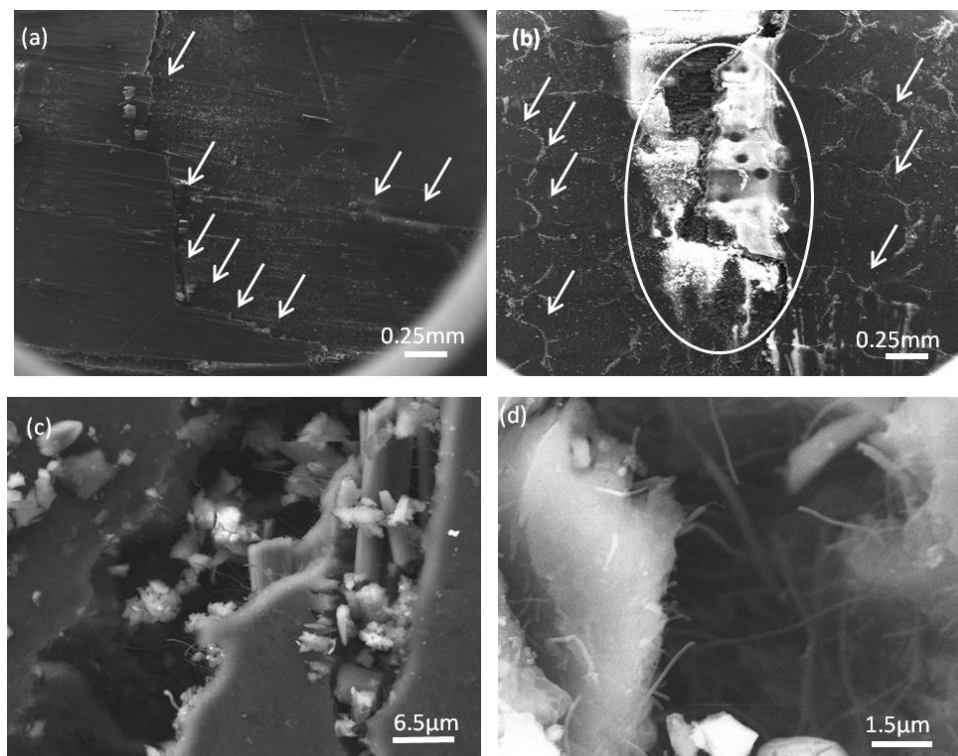
Figure.5.7: SEM images of the C-epoxy composites failed under flexural loads. (a) 60BCE showing one major crack front (path shown with arrows) with insignificant subsidiary/ diffuse cracks (b) 60CCE showing major crack (encircled zone) associated with many subsidiary cracks (shown with arrows) spread over a large area of the sample. (c) & (d) A_f-CNFs pulled out of the cracked surfaces of the matrix failed under flexural loads at different locations.

4.1.2. Flexural strength at 70V_f : Addition of A_f-CNFs to the C-epoxy laminates having 70Vf (70CCE) was found to reduce the flexural strength (Table.5.2) by 6.6% as compared to 70BCE. Failure of the 70CCE shows significant delamination at the interface (Fig.5.8.a). This could be attributed to poor wetting of the C-fibers in 70CCE. When, A_f-CNFs are present in the composite, they compete with the C-fibers in consuming the resin for wetting their surfaces. Hence, at such higher V_f, epoxy resin may not be sufficient to achieve

ideal wetting of C-fibers. This can be evidenced from the poor wetting of the C-fibers in 70CCE (Fig.5.8.b) as compared to the wetting for 40CCE (Fig.5.4.c).

Figure 5.7: SEM images of the 70CCE samples failed under flexural loads. (a) Mixed mode of failure with significant interlaminar crack propagation (indicated by arrows) coupled with ruptur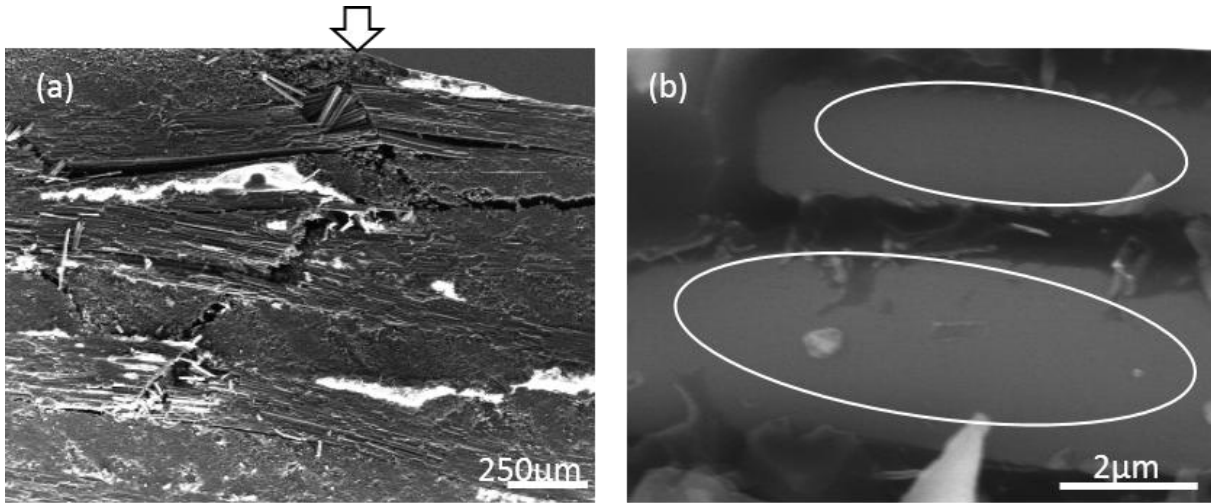e of carbon fabrics (b) Encircled zones showing glassy surface of the C-filament indicating poor wetting of C-filament surface.

Poor wetting at higher V_f of the A_f – CNF reinforced C-epoxy could be due to the fact that, carbon nanofibers due to high surface area may consume considerable proportion of the resin, which may fail to ensure an ideal bonding between fiber-matrix. This resulted in weak interface and facile crack propagation leading to reduction in the flexural strength. In case of 70BCE, there were no A_f -CNFs to compete with C-fibers for the resin. This leads to better

wetting of C-fibers, as well as the effective interlocking of alternate fabric layers with crimp zones of the fabrics. Hence, 70BCE has shown better flexural strength as compared to 70CCE. Failure of the 70CCE at lower elongation as compared to the 70BCE (Fig.5.5.b) also indicates that, the composite has failed before utilizing the maximum potential of the reinforcing fibers.

4.2. Tensile strength: Visible improvement in tensile strength due to A_f-CNF addition was observed for C-epoxy (Table.5.2). Reasons for this, can be understood from the fracture modes of the BCE and CCE samples. Figure.5.9. shows that, the tensile failure of the C-epoxy involved interfilament debonding at the micro level and interlayer debonding at the macro level. However, the magnitude of the interfiber and interlayer debonding varied significantly from BCE to CCE. It was observed that, A_f-CNFs improved both interfilament and interlayer strength. Reasons for these observations are discussed in detail in the following sections.
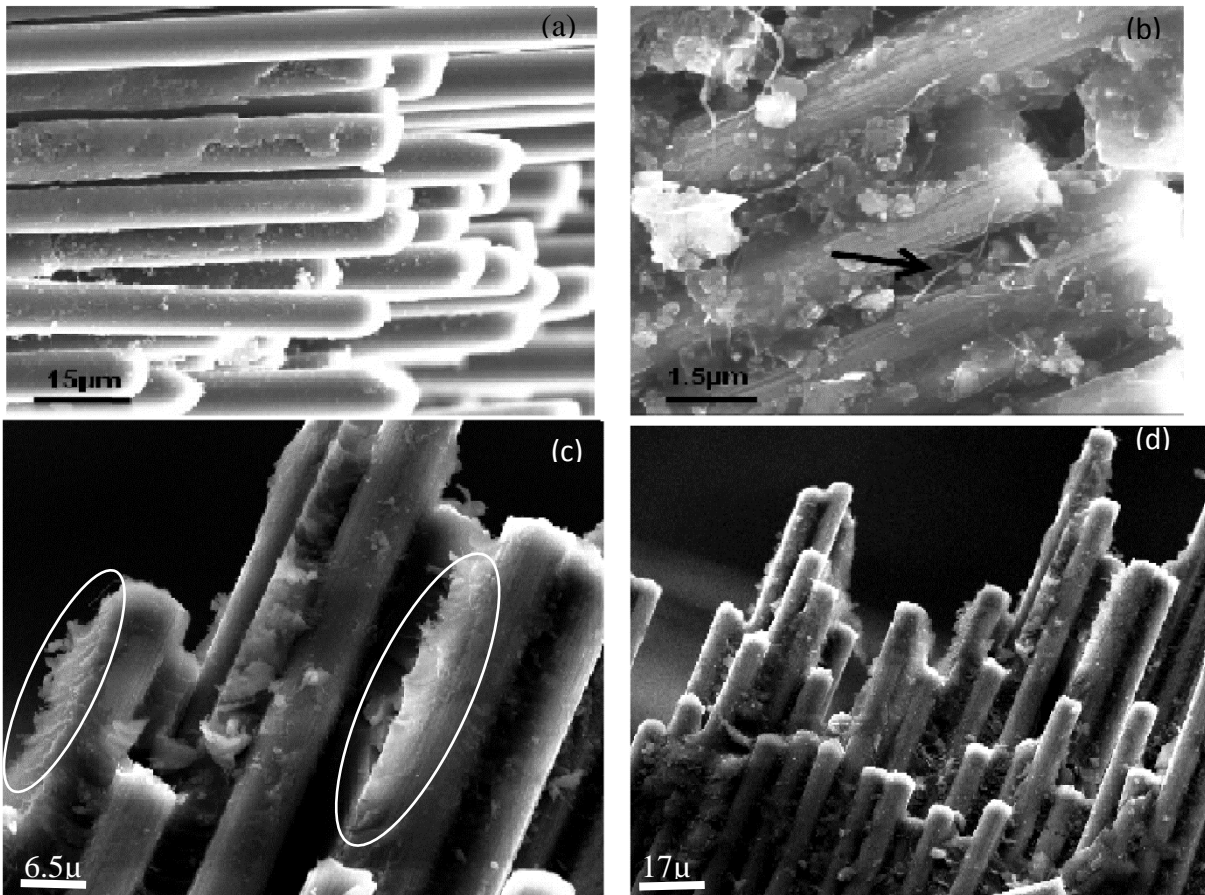
Fig.5.9: SEM images of C-epoxy samples failed under tensile loads (a) 40BCE showing interfilament debonding (b) 40CCE showing strong interfilament bonding due to interlocking of filaments by A_f –CNF (indicated by arrow) (c) & (d) 50CCE sample showing significant interface toughness (indicated by encircled zones) due to A_f -CNFs.

4.2.1. Interfilament bond strengthening: It was observed that the fractured surfaces of the BCE were smooth with complete interfilament debonding (Fig.5.9.a), with negligible matrix adhered to their surface. On the other hand, CCE have shown strong interfilament bonding with significant matrix adhered to their surfaces. A_f -CNFs are observed to lock the fiber matrix interface (Fig.5.9.b). It can also be seen that, the matrix that is adhered to the surfaces of the C-fibers is rough indicating significant interface toughness due to A_f -CNFs (Fig. 5.9.c & 5.9.d). Enhanced interface toughness could be due to the ability of A_f –CNFs to act as micro bridges/interlocks at the fiber – matrix interface, which enhances the toughness. However, as seen in Fig.5.10, significant surface roughness with hackle like features could also be seen at the interfaces where concentration of A_f -CNFs is minimum. This could be attributed to the enhanced interface crosslink density due to the addition of A_f-CNFs. Amino functional groups present on the surface of the CNFs can participate in the crosslinking reaction with the epoxy matrix resulting in enhanced interface crosslink density. Increased crosslink density at the interface results in enhanced interface toughness [15].
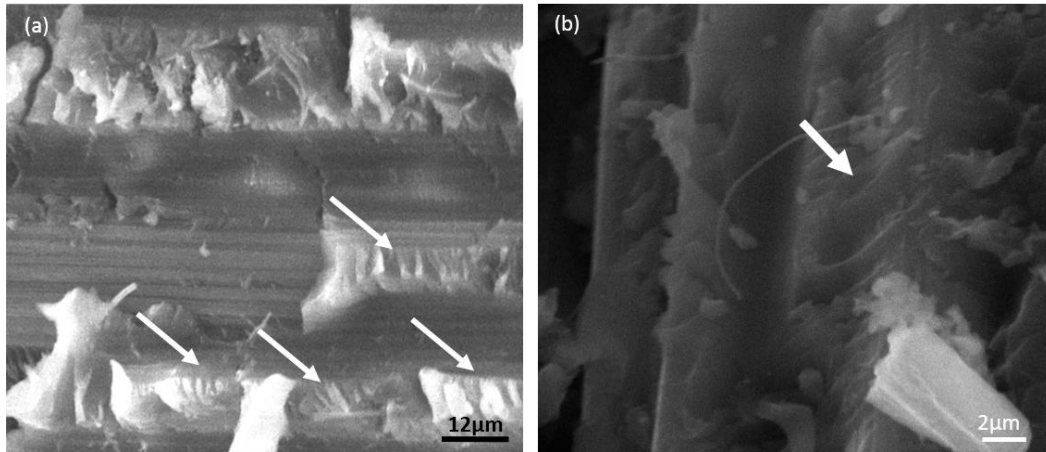
Figure 5.10: SEM images of the 60CCE sample failed under tensile loads. (a) & (b) 60CCE showing rough surface with hackle like features indicating interface toughening (indicated by arrows)

Influence of the enhanced interface toughness and the bridging at the interface resulted in involving more number of reinforcing fibers/ filaments during failure of the composite [16].

Thus for CCE, higher interface toughness coupled with strong interfilament bonding ensured a uniform load distribution across all the carbon fibers [17-18]. Hence, CCE samples show higher tensile strength.

4.2.2. Interlayer bond strengthening: When CFRP is subjected to external stress, a shear stress is generated between the fiber and matrix due to the elastic mismatch according to the shear lag theory [19]. Hence, beyond a critical stress, shearing of the fiber – matrix interface will occur, which may lead to generation of the microcracks at interface areas and debonding of layers. This could result in non - uniform load distribution across the sample and leads to a premature failure. This can be evidenced from the SEM images of BCE samples (Fig.5.11.a &5.11.b), which have shown a significant interlayer delamination during the tensile failure. However, for CCE, interlayer delamination decreased significantly (Fig.5.11.c & Fig.5.11.d.).
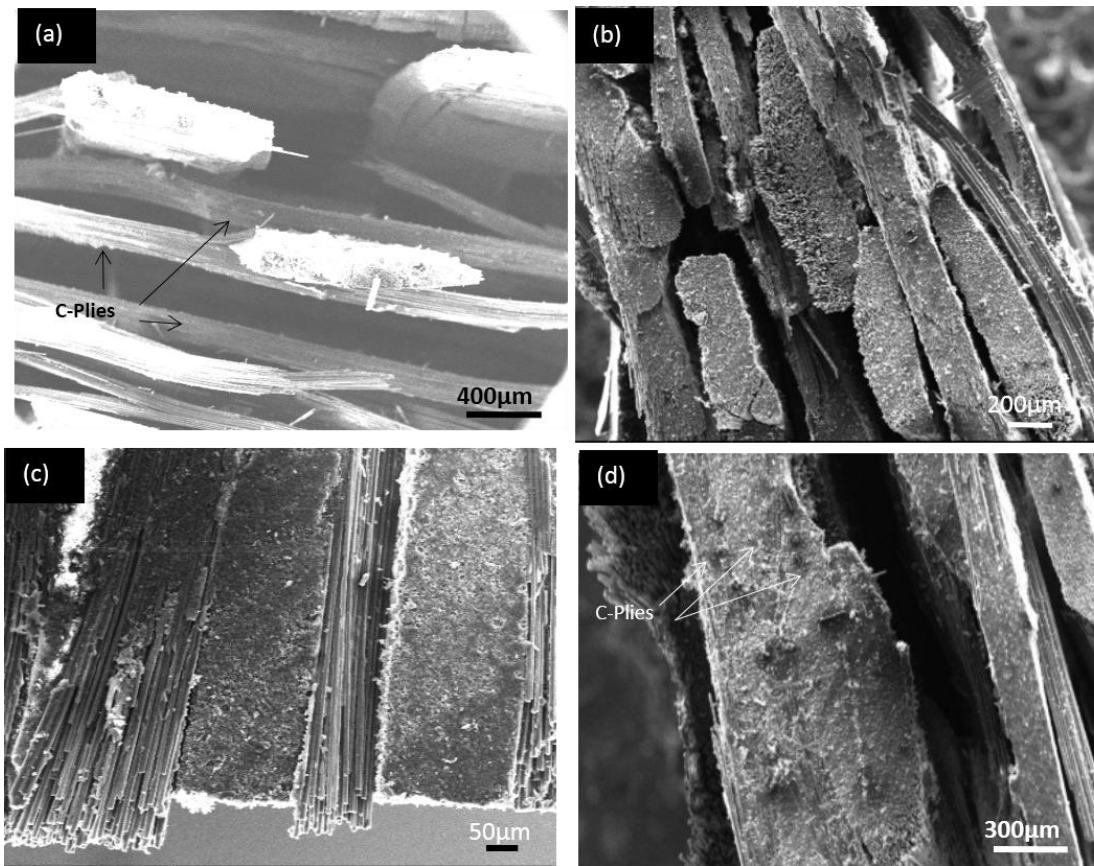
Figure.5.11: SEM images of the 60CCE sample failed under tensile loads. (a) 60BCE& (b)

40BCE showing interlayer (plies) delamination during tensile failure (c) & (d) 40CCE & 60CCE showing improved interlayer bonding (shown by arrow)

Observed variations in the failure mode of the BCE as compared to the CCE were reasoned as follows.

i) A_f-CNFs that are added to CFRPs preferentially assume the interface position of the C-fiber to the matrix (Fig.5.9.b &5.10.a) due to the filtration effects of the C-filaments. Hence they form a thin layer of A_f-CNF rich C-fiber surface. A_f-CNF dispersed epoxy is known to display higher stiffness. Hence, while moving from the fiber surface to the matrix at the interface and beyond, there will be a gradual transition from the stiff, isotropic C-fibers to the weaker epoxy matrix. This leads to reduction in the stress concentration across the C-fiber - matrix interface during the interface sliding. Due to this, A_f-CNF reinforced CFRPs, experiences less stress concentration at the interface leading to delayed crack initiation [20]. Besides this, long projections of A_f-CNFs from the C-fiber surfaces as shown in Fig.5.12. indicates possible Z-reinforcement of the various layers which can further minimize the interlayer debonding [21].
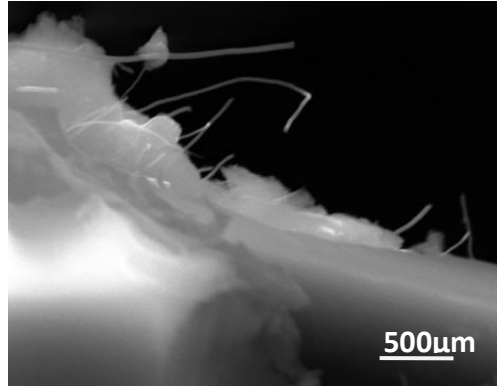
Fig5.12: SEM image of 60CCE showing A_f-CNF projections from C-filaments from the fracture zones.

Schematic tensile failure modes of CCE and BCE are shown in Fig.5.13.
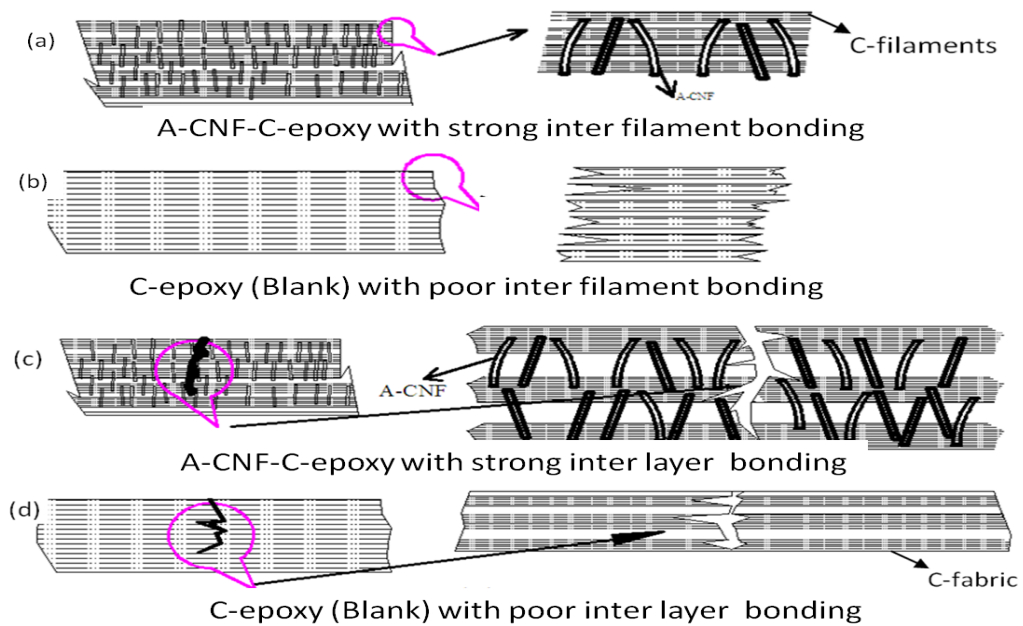
Figure.5.13: Showing schematic tensile failure modes of C-epoxy with and without amino functionalised CNFs (A-CNF/ A_f-CNF) (a) Interfilament bond strengthening by A_f-CNF there by involving more C-filaments/fibers during failure. (b) C-epoxy without A_f-CNF showing poor interfilament bonding (c) C-epoxy with A_f-CNF showing interply bonding due to Z- reinforcement of by A_f-CNF (d) C-epoxy without A_f-CNF showing more interply debonding.

Thus, the strengthened fiber – matrix bonding at the micro level and strengthened interlayer bonding at the macro level lead to a uniform load distribution across the sample under tensile load. This resulted in a higher tensile strength for CCE samples compared to that of BCE.

Similar to the trend observed for flexural properties, the tensile strength of 70CCE was observed to be lower as compared to 70BCE. Fracture mode of the 70CCE was observed to be predominantly with interlayer debonding as shown in Fig.5.14.a. As explained previously, A_f-CNF addition to $70V_f$ C-epoxy led to the resin insufficiency and thus inefficient wetting of the C-fiber surface as shown in fig.5.14.b &5.14.c. This in turn resulted in the generation of the interfacial cracks, interfilament debonding and interlayer debonding (Fig.5.15.a &5.15.b). Hence, the tensile strength of the 70CCE was lower than 70BCE.

Figure.5.14: 70CCE samples failed under tensile load (a) Significant interply debonding during tensile failure. (b) Encircled zone showing poor bonding of the C-fibers with matrix, and preferential matrix attachment with A_f-CNFs at interface (shown by arrows) (c) C-filaments with poor wetting (shown by encircled zone) indicating matrix insufficiency.
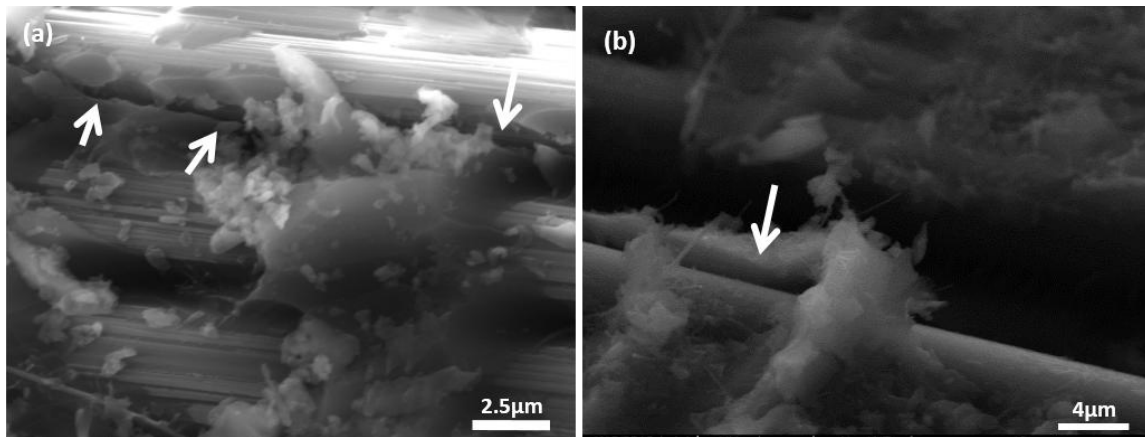
Figure.5.15: 70CCE samples failed under tensile loads showing debonding at the fiber-matrix interface (shown by arrows)

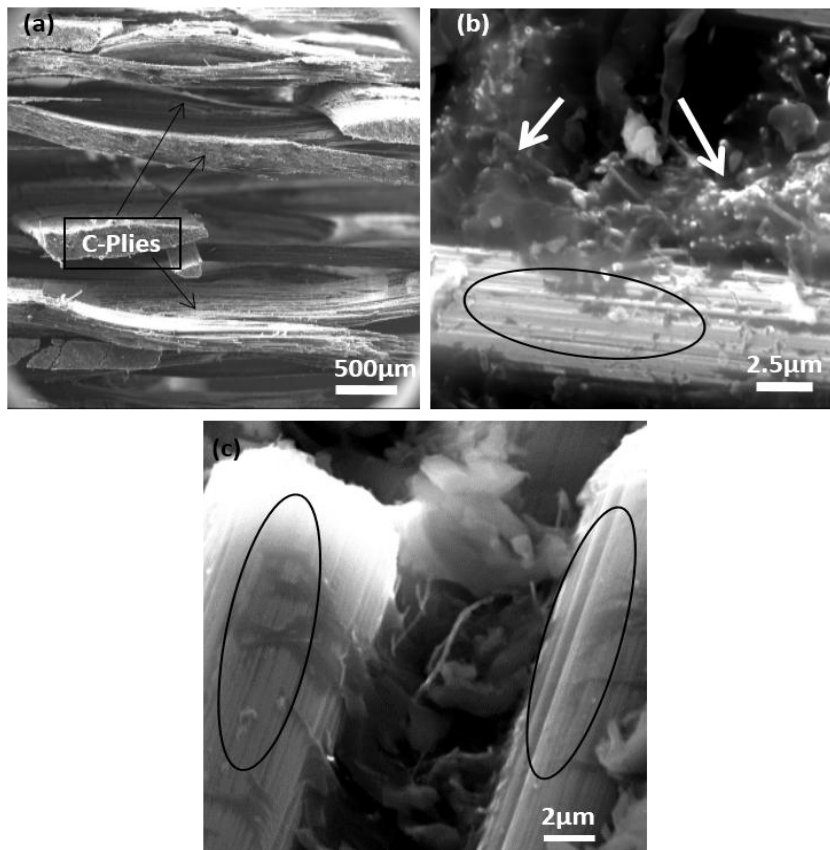**4.3. ILSS:** Interlaminar shear strength gives indication of the resistance to the initiation of the cracks at the interface. ILSS of the CCE samples are higher as compared to the BCE. However, percentage improvements in ILSS decreased with increasing V_f (Table.5.2). For instance, for 40CCE, ILSS was 28 % higher as compared to the 40BCE while it was only 2 % higher for 60CCE as compared to 60BCE. A_f-CNF addition results in more ILSS, because, CNFs provides more interfacial surface area and also act as interlocks at the fiber matrix interface, which effectively resists interface shearing [8]. Decrease in the percentage improvement of ILSS with increasing V_f of the composite can be attributed to the enhanced fiber surface area in the high V_f composite laminates, which seeks more bridging and anchoring with the matrix. This is because, as the fiber interface area increases, proportionately more number of A_f-CNFs are required to anchor them. However, as the fiber volume fraction increases, matrix volume fraction decreases. Since the A_f-CNFs are dispersed in the resin/ matrix, the reduction in the volume fraction of the matrix will bring down effective numbers of A_f-CNFs which are acting as anchoring sites. Hence, as the A_f-CNFs are coming down, their ability to anchor the interfaces also decreases leading to reduced ILSS for the composite. 70CCE has shown lower ILSS than 70BCE (Table.5.2), because of the matrix deficiency to wet the fiber and CNF surfaces.

5. Conclusions

i) A_f-CNF can impart significant enhancement in the flexural, shear and tensile
Strength for the laminated carbon-epoxy composites having lower fiber volume fractions (V_f around 40%). However, as the fiber volume fraction of the composite increased (around 60%), strengthening mechanisms due to A_f-CNF are losing their prominence and thus giving only marginal improvement in the above properties.

ii) Addition of A_f –CNF to C-epoxy composite laminates having very high fiber volume fraction (70% fiber volume fraction in present study) results in reduction in mechanical properties due to inability of the available matrix to form ideal bond with both A_f-CNF and C-fibers.

Referecnes

[1] G.G.Tibbetts, M.L.Lake ,K.L.Strong, B.P.Rice.A review of the fabrication and properties of vapour-grown carbon nanofiber/polymer composites. Composites. Sci. Technol 67(2007) 1709-1718

[2] Jiang Li, Mathew J.Vergne, Eric D.Mowles, Wei-Hong Zhong, David M.Hercules, Charles M.Lukehart. Surface functionalisation and characterization of graphitic carbon nanofibers (GCNFs). Carbon.40(2005) 2883-2893

[3]ProlongoS.G,Camp.M,Gude.M.R.,Chaos-Moran.R,Urena.A, Thermo physical characterization of epoxy resin reinforced by amino functionalised carbon nanofiber.Composite.Sci.Technol.69(2009) 349-357.

[4] SohelRana, RamsamyAlagirusamy, Mangala Joshi. Development of carbon nanofibre incorporated three phase carbon/epoxy composites with enhanced mechanical, electrical and thermal properties. Composites: Part A 42 (2011) 439-445.

[5] JianfengShen,W.Huang, L.Wu, Y.Hu,M.Ye. The reinforcement role of different amino-functionalised multi-walled carbon nanotubes in epoxy nanocomposites. Composite.Sci. Technol. 67(2007) 3041-3050

[6] Zhou.Y.PervinF.Pervin, S.Jeelani.S,P.K.Mallick. Improvement in the mechanical properties of carbon fabric-epoxy composites using carbon nanofibers. J.Mater.Proc. Technol 198(2008) 445-453.

[7] Y.Iwahori, Shin Ishiwata, T.Sumizawa, T.Ishikawa. Mechanical properties improvements in two-phase and three –phase composites using carbon nano-fiber dispersed resin. Composites: PartA36(2005) 1430-1439.

[8] Keith J.Green, D.R.Dean, U.K.Vaidya, E.Nyairo. Multiscale fiber reinforced composites based on a carbon nanofiber/epoxy nanophased polymer matrix: Synthesis, mechanical, and thermomechanical behavior. Composites : Part A 40(2009) 1470-1475.

[9] M.H.G.Wichmann,J.Sumfleth,F.H.Gojny,M.Quaresimin,B.Fielder,K.Schulte.Glass-fiber reinforced composites with enhanced mechanical & electrical properties and limitations of modified matrix. Engg.Fract.Mechanics.73(2006)2346-2359.

[10] S.S.Wicks. Roberto Guzman De villoria, Brian.L.Warde. Interlaminar and intra laminar reinforcement of composite laminates with aligned carbon nanotubes.Composites. Sci. Technol 70(2010) 20-28.

[11] A.Godara, L.Mezzo, F.Luizi, A.Warrier, S.V.Lomov, A.W.VanVuure, L.Gorbatick., P.Moldenaers, I.Verpoest, Influence of carbon nanotube reinforcement on the processing & mech.behavior of carbon-fiber epoxy composites.Carbon.47 (2009) 2914-2923

[12]F.H.Gojny,M.H.G.Wichmann.,U.Kopke,B.Fiedler,K.Schulte. Carbon nanotube-reinforced epoxy – composites: enhanced stiffness and fracture toughness at low nanotube content. Composite.Sci.Technol.64(2004) 2363-2371

[13] Y.Tomohiro, Y.Iwahori, Shin Ishiwata, KiyosiEnomoto. Composites Part A Mechanical properties of CFRP laminates manufactured from unidirectional prepregs using CSCNT-dispersed epoxy. Composites:Part A38 (2007) 2121-2130.

[14] G.Savage. Carbon-Carbon Composites, First edition, Chapman & Hall.1993.

[15] I.Srikanth, Suresh Kumar, Anil Kumar, P.Ghosal, Ch.Subrahmanyam. Effect of amino functionalised MWCNTs on the crosslink density and fracture toughness of epoxy and mechanical properties of carbon-epoxy composites. Composites:Part A 43(2012) 2083-2086

[16] S.Tsantzalis, P.karapappas, A.Vavouliotis, P.Tsotra, V.Kostopoulos, T.Tanimoto, K.Friedrich. On the improvement of toughnes of CFRPs with resin doped with CNF and PZT particles. Composites : Part A 38 (2007)1159-1162.

[17] P.Karapappas,A.Vavouliotis,P.Tsotra,V.Kostopoulos,A.Paipetis. Enhanced fracture properties of carbon reinforced composites by the addition of multi-walled carbon nanotubes. J.Compos.Mater.43(2009)977-985.

[18] Daniel C.Davis, Justin W. Wilkerson, Jiang Zhu and Viktor G.Hadjev.A Strategy for improving mechanical properties of a fiber reinforced epoxy composite using functionalised carbon nanotubes. Composite Sci. Technol. 71 (2011) 1089-1097

[19] S.U.Khan, G.Y.Li., Naveed.A.Siddiqui,.J.K.Kim. Vibration damping characteristics of carbon fiber-reinforced composites containing multi-walled carbon nanotubes. Composite.Sci and Technol 71 (2001):1486-1494.

[20] Larissa Gorbatikh, StepanV.Lomov, IgnaasVerpoest. Nano-engineered composites: A multiscale approach for adding toughness to fiber reinforced composites. Procedia Engineering 10 (2011) 3252-3258

[21] F.H.Gojny, M.H.G.Wichmann, B.Fiedler, W.Bauhofer, K.Schulte.Influence of nano-modification on the mechanical and electrical properties of conventional fiber-reinforced composites. Composites: Part A36 (2005) 1525-1534.

Chapter: VI

CNT-Zirconia Reinforced Carbon-Phenolic Composites

CNT-Zirconia Reinforced Carbon-Phenolic Composites

Carbon-Phenolic (C-Ph) composites having 0.5wt%, 1.0wt% and 1.5wt% of multiwalled carbon nanotube (CNTs) were fabricated (CNT-C-Ph) and tested for their flexural strength, ILSS and thermal conductivity. On the otherhand, Zirconium oxide (Zirconia) coating on carbon fabric (C-fabric) was developed by using zirconia sol. C-fabrics having different weight percentages(wt%) of zirconia namely 0 wt% (Blank), 3.5wt%, 6.5wt% and 9.5wt% were used to make Zirconia-Carbon-Phenolic (Zr-C-Ph) composites. Thermal conductivity, ILSS and flexural strength were measured for the prepared Zr-C-Ph composites. Based on the initial results, subsequently a functionally graded carbon – phenolic composite (FG-C-Ph) having CNT-C-Ph composition up to certain thickness followed by Zr-C-Ph composition for the remaining thickness was made. Thermal insulation and ablative properties for blank C-Ph, Zr-C-Ph, FG-C-Ph were studied using plasma arc jet test which was carried out at a heat flux of 4.0 MW/m^2 for 30 seconds. Results from the plasma arc jet test show that, the temperature drop across the Zr-C-Ph composite was found to be highest while it was least for the blank. However the ablation rate was found to be highest for the FG-C-Ph while it was least for the blank. Ablation mechanisms for all the tested composites are proposed based on the SEM and XRD studies

1. Introduction: Rayon carbon fabric reinforced phenolic (C-Ph) composites are widely used as thermal protection systems (TPS) in aerospace applications due to the low thermal conductivity of the rayon based carbon fabric and the high char yielding properties of the phenolic matrix [1-3]. Many research groups have attempted to reduce the thermal conductivity of the C-Ph composites further. It is reported that, the spun yarn carbon fibers carbonized at low temperature can decrease the thermal conductivity of C-Ph composites significantly besides imparting better interfacial and ablative properties [4]. Silicone based anti-ablation coatings on thermal protection systems can form oxidation resistant silica layer during ablation, whereas silicone polymer based ablative composites can undergo cermetisation during ablation forming oxidation resistant ceramic layer [5,6]. On the other hand, addition of various nanomaterials like, nanosilica, montmorillonite nanoclay, polyhedral oligomeric silsesquioxane (POSS) to C-Ph composites are reported to reduce their thermal conductivity besides reducing the ablation rate [7,8]. Though, zirconia (ZrO$_2$) is known as a better thermal insulator than silica, it was not explored so far, as an additive to C-Ph composites. Recently, Yaxi chen et al. reported that addition of zirconium diboride to C-Ph composites can significantly

improve their thermal insulation properties during ablation. The reason for this was assigned primarily to the formation of insulating zirconia layer by oxidative decomposition of zirconium diboride [9]. Though, it is now well established that, the ceramic additives can decrease the thermal conductivity of C-Ph composites, they pose problems such as poor interlaminar shear strength (ILSS), especially at higher loadings which results in the delamination of composites [7]. It is essential for TPS to have a good interlaminar shear strength to resist the mechanical erosion as they should withstand the harsh conditions like high velocity aerodynamic shearing loads. It has been reported that carbon nanotubes (CNTs) and carbon nanofibers enhance ILSS of the C-fiber reinforced polymer matrix composites [10,11]. So far limited studies have been carried out to understand the combined effects of ceramics and CNTs addition to C-Ph composites on the thermo-mechanical and ablative performance [7,12-14]. In general, introduction of ceramic additives to C-Ph composites was carried out by either direct addition of the ceramic powder or through a polymeric resin, which on thermal decomposition gives the intended ceramic. Developing ceramic coating/ zirconia coating on C- fabrics and using them as reinforcements to obtain low thermal conductive TPS and integrating it with CNT-CFRP is the novel concept of the present study.

1.1. Aims of the study: Aims of the study are as following:

(i)   To find out the optimum concentration of the A_f-MWCNTs to improve the flexural strength and ILSS of C-Ph composites with minimum improvements in the thermal conductivity

(ii)   To understand the effect of zirconia coating on the C-fabric, by studying the mechanical, thermal and ablative properties of carbon - phenolic composites made by zirconia coated C-fabrics.

(iii)   To prepare functionally graded CNT-Zr-C-Ph composites which can combine the advantages of CNTs and zirconia addition to C-Ph in imparting better mechanical properties and low thermal conductivity respectively.

(iv)   To study how CNTs addition to C-Ph composites can affect the flexural strength, shear strength and ablation rate.

2. Raw materials: Carbon fabric, phenolic resin and amino functionalised A_f-MWCNTs are the main raw materials. Detailed specifications of each of the raw materials is given below.

Phenolic resin:

1.	Chemical name	:	Resol
2.	Viscosity	:	200 cP at 30°C
3.	Density	:	1.2 g/cc
4.	Point of trouble	:	6-7 ml
5.	Solid content	:	65%
6.	Volatile content	:	35%
7.	Commercial name	:	Resol grade phenolic resin

Carbon fiber/fabric specifications: Rayon based woven carbon fabrics were used to make laminated (2D) CNT-C-Ph and Zr-C-Ph composites. Brief specifications of the fibers are as given below

1.	Tensile strength	:	1.0 GPa
2.	Tensile modulus	:	41 GPa
3.	Density	:	1.65 g/cc
4.	Diameter	:	8.5 µm

Carbon nanotubes (CNTs): Amino functionalised MWCNTs (A_f-MWCNTs) were used in the present study. MWCNTs synthesized by CVD method were procured from M/s Chemapol industries (Mumbai). These MWCNTs were purified and amino functionalised (as detailed in chapter–III). Brief specifications of the A_f-MWCNTs are as given below

1.	Purity	:	99.9%
2.	Metallic impurities	:	0.1%
3.	Diameter	:	20-30 nm
4.	Length	:	2-4 microns

3. Experimental Work: To meet the objectives/ aims of the work mentioned in section.1.1, experimental work is carried out in following steps.

3.1: Step (i): Optimisation of the CNT content in C-Ph composites: Amino functionalised MWCNTs (A_f-MWCNTs) reinforced C-Phenolic composites (CNT-C-Ph) were made by adding different weight percentages (wt%) of A_f-MWCNTs, namely 0wt% (blank), 0.5wt%, 1.0wt% and 1.5wt%. Thermal conductivity, flexural strength and ILSS were measured for the prepared CNT-C-Ph composites. Aim of this step is to optimise the

concentration of A_f-MWCNTs in C-Ph composites in order to obtain maximum improvement in flexural and shear strength with minimum improvement in the thermal conductivity. Fabrication procedure of CNT-C-Ph composites and the results obtained in the mechanical and thermal property evaluation are presented in section 3.4.

3.2: Step (ii): Optimisation the zirconia content in C-Ph composites: zirconia added C-Ph composites (Zr-C-Ph) were made by using zirconium oxide (Zirconia) coated carbon fabrics. To obtain zirconia coating on carbon fabric (C-fabric) zirconia sol was used. C-fabrics with different weight percentages (wt%) of zirconia namely 0wt% (Blank), 3.5wt%, 6.5wt% and 9.5wt% were used to fabricate Zr-C-Ph composites. Thermal conductivity, ILSS and flexural strength were measured for the prepared Zr-C-Ph composites. Aim of this step is to find out the optimum concentration of zirconia that gives the best reduction in thermal conductivity, while retaining good flexural and shear strength. Fabrication procedure of Zr-C-Ph composites and the results obtained in the mechanical, thermal property evaluation tests are presented in section 3.5, section.4 & section.5.

3.3: Step (iii): Realising functionally graded composite: Based on the mechanical and thermal properties of the CNT-C-Ph and Zr-C-Ph composites, a functionally graded carbon – phenolic composite (FG-C-Ph) was made with optimised composition of CNT-C-Ph (of step i) up to certain thickness followed by optimised composition of Zr-C-Ph composition (of step.ii) for the remaining thickness.
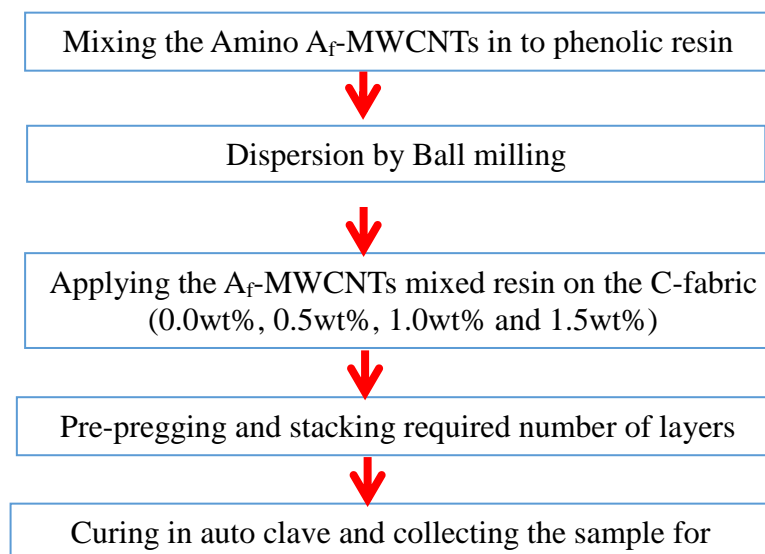
Finally, thermal insulation and ablative properties of the functionally graded C-Phcomposites were studied and compared with the blank C-Ph, Zr-C-Ph composites by using plasma arc jet test, which was carried out at a heat flux of 4.0 MW/m^2 for 30 seconds.

3.4.Fabrication and testing of CNT-C-Ph composites: Predecided weight of (0wt% /blank, 0.5wt%,1.0wt% and 1.5wt%) amino functionalised multiwalled carbon nanotubes (A_f-MWCNTs) were added to phenolic resin and ball milled for 3 hours at 250 rpm to ensure their dispersion in the resin. This A_f-MWCNT-resin mixture was applied on the C-fabric and allowed to dry at room temperature for 48h to allow partial curing to get prepregs (A_f-MWCNTs -C-Prepreg). A_f-MWCNTs-C-prepreg was cut in to 150 mm x 150 mm and stacked up in a die (job) followed by curing in an autoclave. Typical cure cycle involved raising the temperature of the job up to 120°C and then soaking the job for 120 minutes. 5 bar pressure was applied on the job at the time of gelling. Subsequently temperature was raised to 180°C and maintained for four hours under the same load. Thus, four different CNT-C-Ph composites of approximately 5 mm thickness were prepared with 0.0wt% (blank), 0.5wt%, 1.0wt% and 1.5wt% Af-MWCNTs. Representative samples were collected from the

laminates to measure density and fiber volume fraction (%V_f). %V_f was measured as per ASTM D 3171 by taking approximately 2g of the composite. ILSS and flexural strength were measured as per ASTM D 2344 (sample dimensions 50mm x 10mm x 5mm) and ASTM D 790(sample dimensions 100mm x 10mm x 5mm) whereas thermal conductivity was measured as per ASTM E 1225 using hot guard method (sample dimensions 25mm dia and 5mm height).

The following flow diagram gives a brief overview of the experimental work described in this section.

Flow diagram: Schematic flow of experimental work

Mixing the Amino A_f-MWCNTs in to phenolic resin

⬇

Dispersion by Ball milling

⬇

Applying the A_f-MWCNTs mixed resin on the C-fabric (0.0wt%, 0.5wt%, 1.0wt% and 1.5wt%)

⬇

Pre-pregging and stacking required number of layers

⬇

Curing in auto clave and collecting the sample for

3.4.1. Results: The following table (Table.6.1) gives the density and mechanical properties of the prepared composites

Table.6.1: Density and mechanical properties of the composites

Sample Description	Density g/cc	%Vf	[a] F.S (MPa)	ILSS (MPa)
Blank C-Ph	1.44	53	225(22)	20(1.0)
0.5wt%CNT C-Ph	1.42	52	262(21)	22(2.1)
1.0wt% CNT-C-Ph	1.49	59	221(14)	21(1.3)
1.5wt% CNT C-Ph	1.50	59	204(7)	22(3.2)

[a]Flexural strength, Values in the parentheses are standard deviations

From the results it can be seen that, 0.5wt% A_f-MWCNT-C-phenolic showed a significant improvement in the flexural strength. Beyond this loading of A_f-MWCNT to C-Ph composites, flexural strength and ILSS have come down significantly.

Thermal conductivity values obtained for CNT-C-Ph samples are shown in Table.6.2.

Table.6.2: Thermal conductivity values of the CNT-C-Ph composites

Sample Description	Thermal Conductivity (W/m-k)	[a]Percentage improvement
Blank C-Ph	0.59	-
0.5wt%CNT-C-Ph	0.69	17
1.0wt% CNT-C-Ph	0.71	20
1.5wt% CNT-C-Ph	0.71	20

[a][(Sample-Blank)/Blank]x100.

It can be seen that, as the A_f-MWCNTs concentration increases in the C-Ph composites, thermal conductivity increased which may be due to increased number of heat conducing path ways (MWCNTs) formed by bridging of C-fabric/ fibers by MWCNTs. C-fabric layers were previously sandwiched and separated with the insulating phenolic matrix layer. However, beyond 1.0wt% addition of A_f-MWCNTs, thermal conductivity improvement was not observed probably because of the threshold value obtained at 1.0wt% addition of A_f-MWCNTs. At some optimum loading of CNTs, interconnected network of CNTs will form in the matrix. At this loading thermal conductivity will be maximum and beyond this loading, further improvements in the thermal conductivity may not be observed. CNT-C-Ph composites that have shown best mechanical properties and lowest thermal conductivity are used further in making FG-C-Ph (CNT-Zr-C-Ph) composites as discussed in the section 3.5.2. Reasons for the observed trend in the flexural strength, ILSS and thermal conductivity due to A_f-MWCNTs addition is discussed in subsequent sections.

3.5. Fabrication and testing of Zr-C-Ph and FG-C-Ph composites:

3.5.1. Zr-C-Ph composite fabrication: Zirconia coated carbon fabrics were used to realise Zr-C-Ph composites. Zirconia coating on the C-fabric was obtained using zirconia sol. Zirconia sol was prepared by mixing zirconium oxy chloride, ethanol and demineralized water in the molar ratio of 0.05: 2.38: 1.1 and stirring the mixture for one hour with a magnetic stirrer at room temperature. This sol was applied on the surface of the carbon fabric (C-fabric) with the help of a spray gun and allowed to dry at room temperature (approximately 96 hours) till the coated fabric attained constant weight. Expected yield of the zirconia coating from the sprayed sol was calculated using equation-1.

$$ZrOCl_2 + H_2O \longrightarrow ZrO_2 + 2\ HCl \text{------------------(1)}$$

Thus, four different compositions of zirconia coated C-fabrics (Zr-C-fabrics) having zirconia weight percentages (wt %) of 0.0wt% (blank), 3.5wt%, 6.5wt% and 9.5wt% were made by selecting the amount of the sol sprayed. Morphologyof the coating on Zr-C-fabrics was studied with scanning electron microscope (ESEM-FEI Quanta 400, The Netherlands). Phenolic resin was applied on the Zr-C-fabrics followed by drying at room temperature for 48 hours to allow partial curing to get prepregs (Zr-C-prepregs). To fabricate the composites, Zr-C-prepregs were cut in to 150 mm x 150 mm pieces (approximately 60 layers) and stacked up (job) followed by curing in an autoclave. Curing cycle employed was same that was employed for fabricating CNT-C-Ph composites (Section: 3.4). Thus, four different Zr-C-Ph composites of approximate 20 mm thickness were prepared with 0.0wt% (blank), 3.5wt%, 6.5wt% and 9.5 wt% Zr-C- fabrics. Representative samples were collected from the laminates to measure density and fiber volume fraction (%V_f). %V_f was measured as per ASTM D 3171.

3.5.2. FG-C-Ph composite fabrication: Based on the thermal and mechanical characterization of the composites made (in the sections 3.4.1 and 3.5.1), a functionally graded carbon - phenolic (FG-C-Ph) composite was fabricated by using the combination of 0.5wt% A_f-MWCNTs-C-prepregs and 6.5wt% zirconia coated -C-prepregs. To prepare the FG-C-Ph composite, initially nine layers of A_f-MWCNTs - C- prepregs were stacked up, over which approximately 40 layers of Zr-C-prepregs were stacked. Curing cycle employed was similar to the curing cycle that was employed adopted for CNT-

C-Ph composites (Section: 3.4).In the finished composite, approximately 3 mm from the top was having 0.5wt%A_f-MWCNT-C-Ph composition while the rest 17 mm of the composite was having 6.5wt% Zr-C-Ph composition. Samples from this composite were tested only for ablation properties. Schematic representation of the FG-C-Ph composite that was fabricated is shown in Fig.6.1.
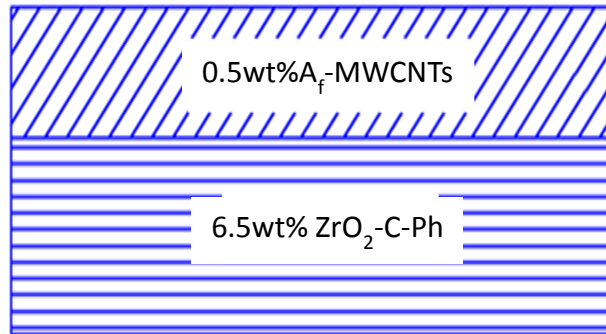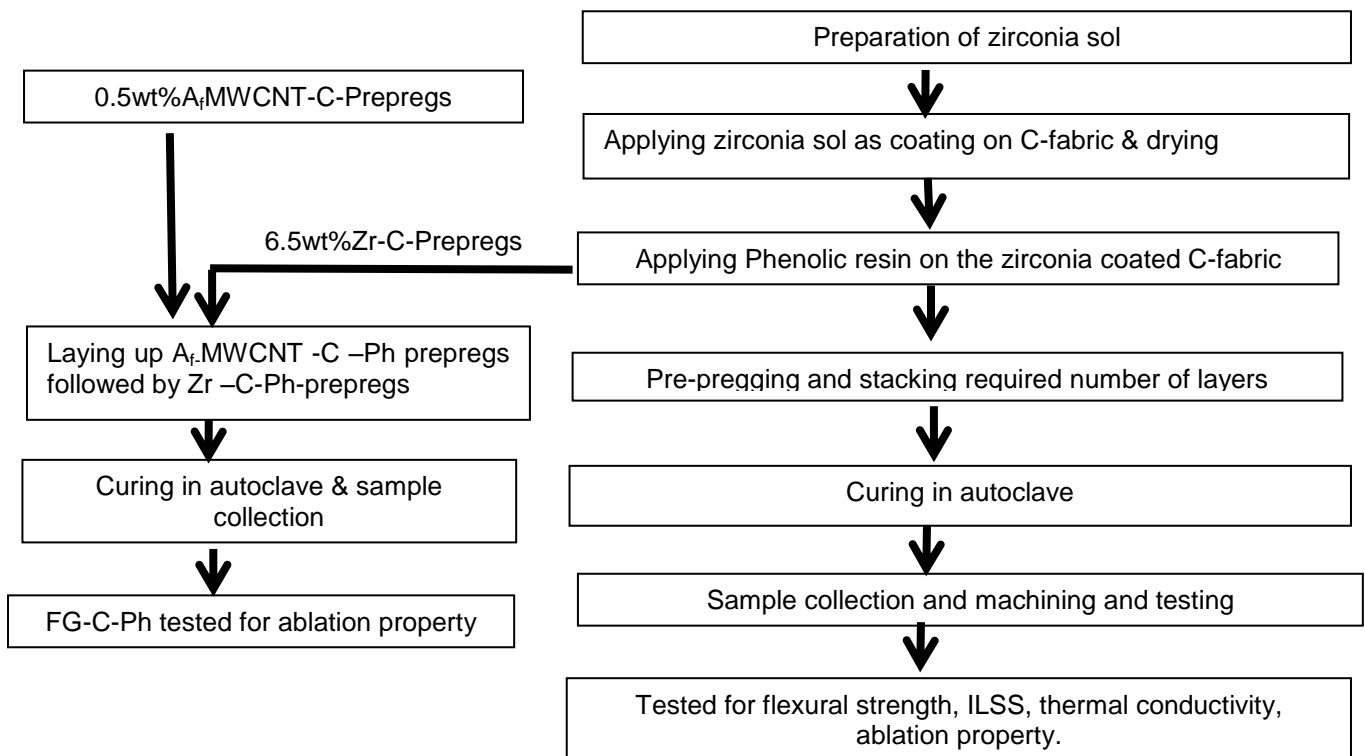

Figure: 6.1: Schematic of the FG-C-Ph composite made with A_f-MWCNT-C-prepregs and zirconia coated C-prepregs.

Following flow diagram shows the experimental work described in section 3.5 at a glance.

Flow diagram: Schematic flow of experimental work

Carbon fabric which was used as the reinforcement, die made from mild steel in which the prepregs were layed up, cured and typical fabricated composite are shown in Fig.6.2.

4. Characterization

4.1. Flexural strength and ILSS: Specimens having dimensions of 5 mm x 10 mm x 100 mm and 5 mm x 10 mm x 50 mm were collected for flexural strength and ILSS respectively from the prepared Zr-C-Ph composites. Flexural strength was measured as per ASTM D 790 while ILSS was measured as per the ASTM D 2344 using universal testing machine (United, Model STM 50 KN, US). Minimum five number of samples were tested for each property and the average values are shown in Table.6.3.

4.2. Thermal Conductivity: Cylindrical specimens having 25 mm diameter and 5 mm height were machined from the prepared composites. Thermal conductivity in the through thickness direction was measured at 300^0C under steady state conditions as per ASTM E 1225 using hot guard method. Two samples from each of the composite were tested and the average values of the thermal conductivity of the two samples is shown in Table.6.4.
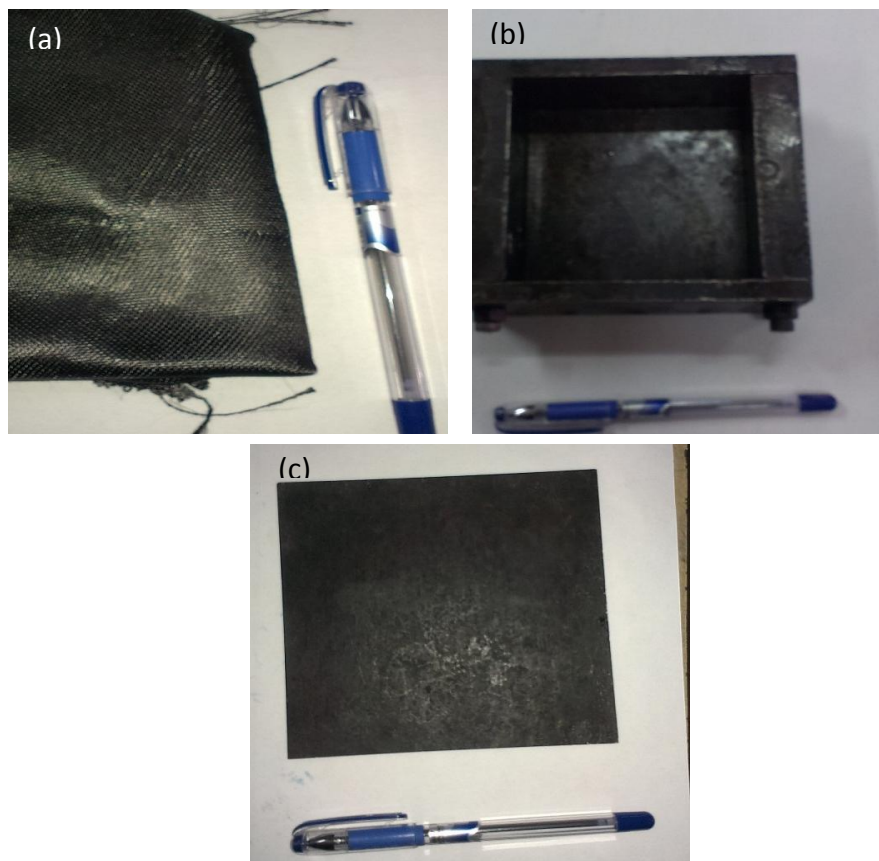

Figure.6.2: (a) Carbon fabric (b) Die for stacking prepregs (c) Fabricated C-Ph composite.

4.3. Plasma arc jet test: Cylindrical specimens having 10 mm diameter and 17.6 mm height were machined from the blank C-Ph, Zr-C-Ph and FG-C-Ph composites. Length of the specimens was kept perpendicular to the direction of the fabric layup. Test specimen was encircled with the guard ring which was also machined out from the same composite. Guard ring was employed to ensure unidirectional exposure of the test specimen to the plasma arc jet. 'K' type thermo couple was bonded to the rear surface (away from the surface facing the plasma arc jet) of each specimen to measure the back face temperature. A schematic of the test specimen configuration is shown in Fig.6.3.a.
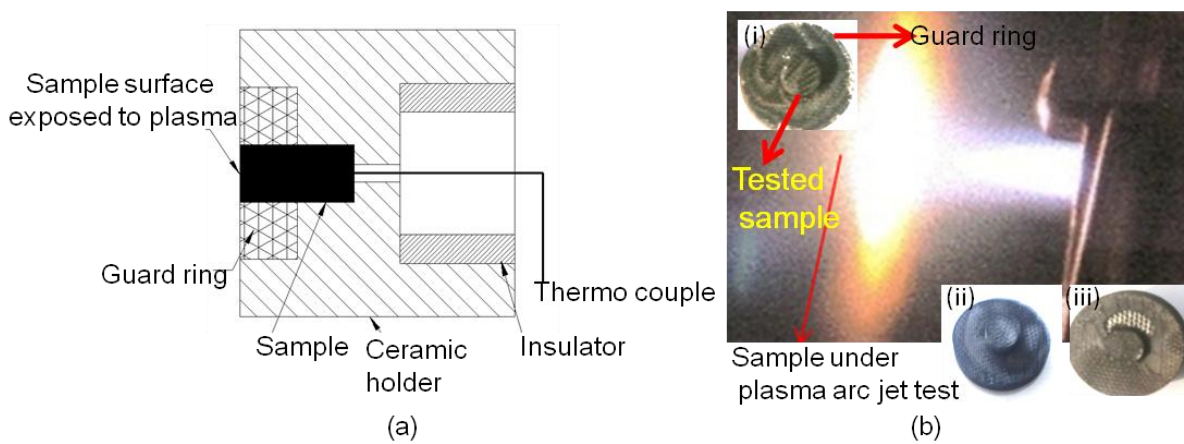

Figure 6.3:Plasma arc jet test a) Schematic configuration of the sample and the holder used for plasma arc jet testing b) Plasma arc jet testing under progress; i) Blank C-Ph after test ii) 6.5wt% Zirconia C-Ph after test iii) FG-C-Ph after test

Specimens were exposed to the plasma arc jet at a flame velocity of about 1 mach having a stagnant flux of 4MW/m^2 for 30 seconds (Fig 6.3.b). Raise in back face temperature is continuously recorded as a function of time. Though the plasma jet was switched off after 30 seconds of test duration, back face temperature was recorded up to 70seconds. In case of FG-C-Ph, test specimen was oriented in such a way that, CNT-C-Ph part of the composite faced the plasma jet while the back face temperature measured was for Zr-C-Ph part of the composite. Ablation rate was determined by dividing the reduction in length of the specimen with the test durationin seconds. Averageback face temperature and ablation rate were determined based on the average of two samples and typical values are shown in the Table.6.5. Microstructure of the ablated surfaces was studied with FESEM (FEI,Quanta 200), where as compositional changes resulted due to ablation was studied with X-ray

diffraction (XRD-Philips PWD, Model 1830, The Netherlands). Representative samples are shown in Fig.6.3.b (i – iii).

5. Results and discussion

5.1. Microstructure of the coated fabric and prepregs: Microstructure of the representative C-fabric samples coated with zirconia are shown in Fig.6.4. Thickness of the coating was observed to be approximately 700 nm to 900 nm for 3.5wt% zirconia coating (Fig.6.4.b).
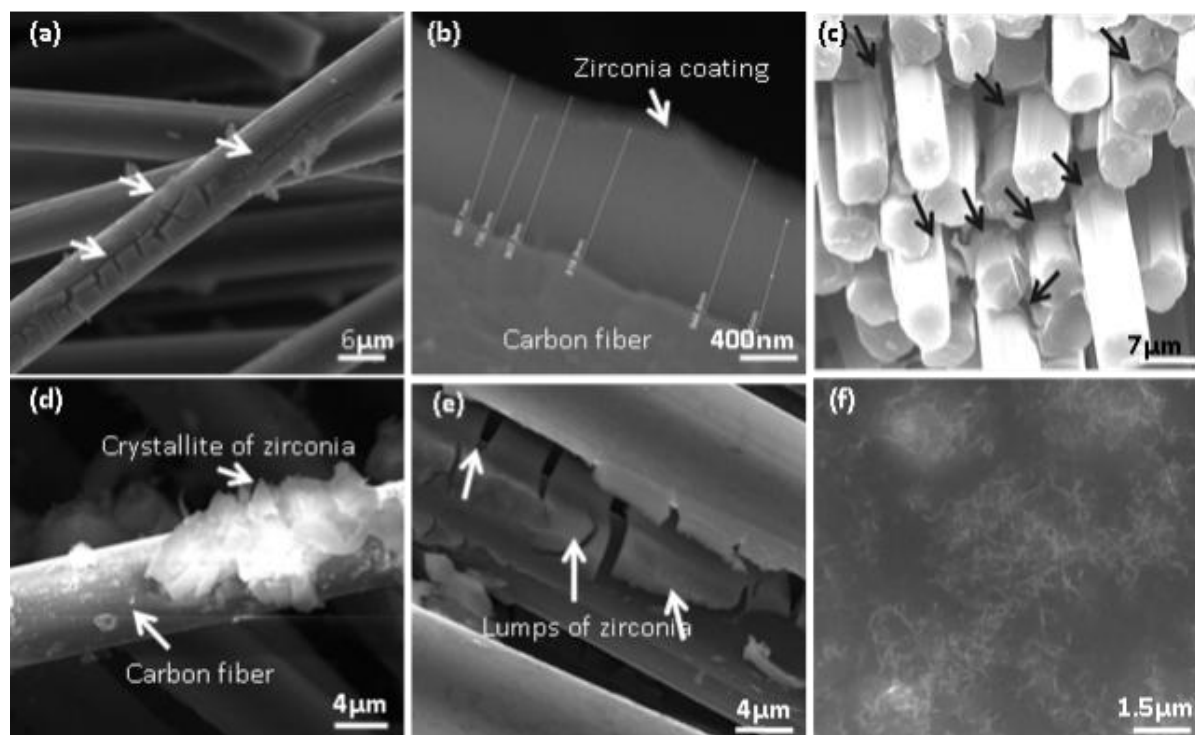

Figure 6.4: Microstructure of the zirconia coated fabrics and CNT-C-Prepregs a) C-fibers coated with 3.5wt% of zirconia showing thin layer of coating (indicated by arrows) b) 3.5wt% zirconia coating on C-fibers showing approximate thickness of 700-900nm c) 3.5wt% zirconia coating on C-fibers showing coating formation on all carbon filaments d) 6.5wt% zirconia coating on C-fibers with growth of large crystallites e) 9.5wt% of zirconia coating on C-fiber having lumps of zirconia f) 0.5wt%A_f-MWCNT-C-prepregs showing good dispersion of A_f-MWCNTs.

It can be seen from the Fig.6.4.a,6.4.b & 6.4.c, that the precursor based coating method employed in the present study can develop a uniform coating around filament surface. However, as the wt% of zirconia increased, lumps of zirconia coating were observed (Fig.6.4d,6.4.e). On the other hand, A_f-MWCNTs were observed to be well dispersed on the C-fabric surface. (Fig.6.4.f).

5.2. Density, %V$_f$: It is observed that, as the wt% of the zirconia on the C-fabric increased, density and %V$_f$ of the composites have come down (Table.6.3). This is due to the increased coating thickness that is deposited over the C-fabric with increased wt% of the zirconia which seeks more space during compaction of the C-fabric layers. In contrast to this, A$_f$-MWCNTs -C-Ph composites have shown slightly increasing trend in the density and %V$_f$ as compared to blank C-Ph, indicating better compressibility of the A$_f$-MWCNTs -C-Ph prepregs (Table.6.1).

5.3. Flexural strength and ILSS: It is observed that, Zr-C-Ph composites have shown poor flexural and ILSS properties as compared to the blank C-Ph composites. Reduction in these properties is more with increasing wt% of zirconia (Table.6.3).

Table.6.3: Physical and mechanical properties of the composites

Sample Description	Density g/cc	%Vf	[a] F.S (MPa)	ILSS (MPa)
Blank C-Ph	1.44	53	225 (22)	20 (1.0)
3.5 wt%Zr- C-Ph	1.40	50	222 (36)	19 (2.8)
6.5 wt% Zr-C-Ph	1.25	37	146(10)	14(2.9)

[a]Flexural strength, Values in the parentheses are standard deviations

Samples cannot be machined out from the 9.5wt% Zr-C-Ph composite due to delamination during machining, which indicates poor ILSS properties. Hence physical and mechanical property data cannot be generated for this composition. Reason for the reduced ILSS for Zr-C-Ph composites can be attributed to the fact that, once the zirconia layer is deposited on the C-fiber, effective interfacial interaction between the matrix and the fibers comes down. This leads to poor interfacial bond strength, resulting in lower ILSS. Significantly poor ILSS at higher loading could be attributed to the large crystallites of the zirconia (Fig.6.4.d,6.4.e) which could have acted as defect zones in the composite. Besides this, reduction in %V$_f$ of the composites made with Zr-C-prepregs is also responsible for the reduction in the mechanical properties of the C-Ph composites. On the other hand, A$_f$-MWCNT-C-Ph composite displayed enhanced flexural and shear properties. It can be seen that,

well dispersed A_f-MWCNTs present in C-Ph composites, are strengthening the fiber - matrix interface by bridging the interfacial microcracks (Fig.6.5.a) leading to enhanced ILSS for the CNT-C-Ph. Similar strengthening mechanisms for the ILSS improvement of CFRPs due to A_f-MWCNTs were reported [15,16]. Enhanced flexural strength due to A_f-MWCNTs addition may be due to strengthening of the fiber matrix interface (Fig.6.5.b) and stiffening of the matrix, which can effectively resist the bending forces [17].
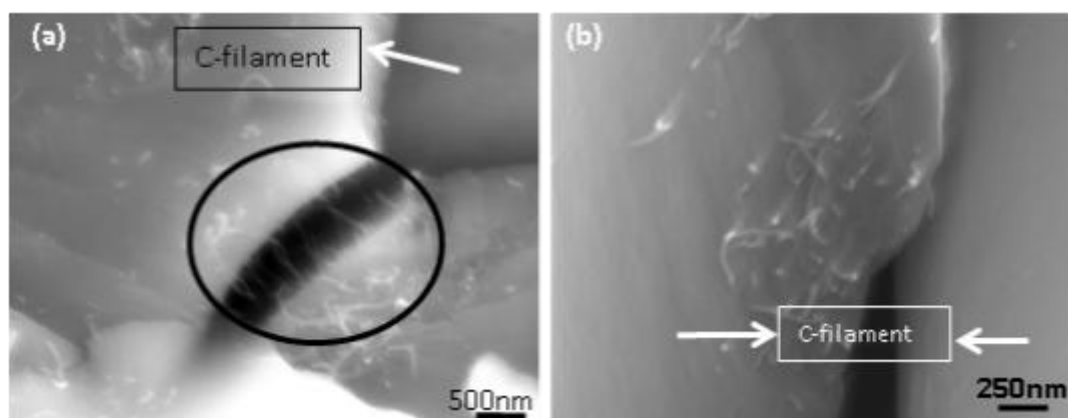

Figure.6.5: FESEM images of the A_f-MWCNT-C-Ph composites failed under shear and flexural loads (a) Image showing well dispersed A_f-MWCNTs bridging the matrix micro cracks at the C-fiber-matrix interface (encircled zone) during shear failure (b) Image showing A_f-MWCNT reinforced matrix holding the C-fibers together during flexural failure.

5.4. Thermal conductivity: Thermal conductivity of Zr-C-Ph composites is found to be significantly less as compared to the blank C-Ph (Table.6.4). This is due to the fact that, significant proportion of the advancing heat energy is consumed in generating lattice vibrations (phonons) in the zirconia layer [7]. Drop in the thermal conductivity is significantly more at higher wt% of zirconia probably due to increased thickness of insulating layer.

Table.6.4: Thermal conductivity values of the composites

Sample Description	Thermal Conductivity (W/m-k)	[a]Percentage Change
Blank C-Ph	0.59($\pm$0.05)	-
3.5wt% Zr-C-Ph	0.41($\pm$0.15)	- 30
6.5wt%Zr-C-Ph	0.33($\pm$0.10)	-44

[a][(Sample-Blank)/Blank]x 100. Values in the parentheses are average deviation

On the other hand, A_f-MWCNT-C-Ph composite displayed more thermal conductivity as compared to the blank C-Ph (Table.6.2). This can be attributed to following aspects [18, 19].

i) A_f-MWCNTs increases thermal conductivity of matrix which was originally insulating.

ii) A_f-MWCNTs provides increased contact area at the fiber matrix interface which enables a facile heat transfer from the fiber to the matrix. This is because, A_f-MWCNTs acts as interfilament/ fiber thermal bridges resulting in more conducting pathways in the composites.

5.5. Back face temperature and ablation rate: Observed back face temperatures with respect to time, for the samples that were subjected to plasma arc jet test are shown in Fig.6.6.
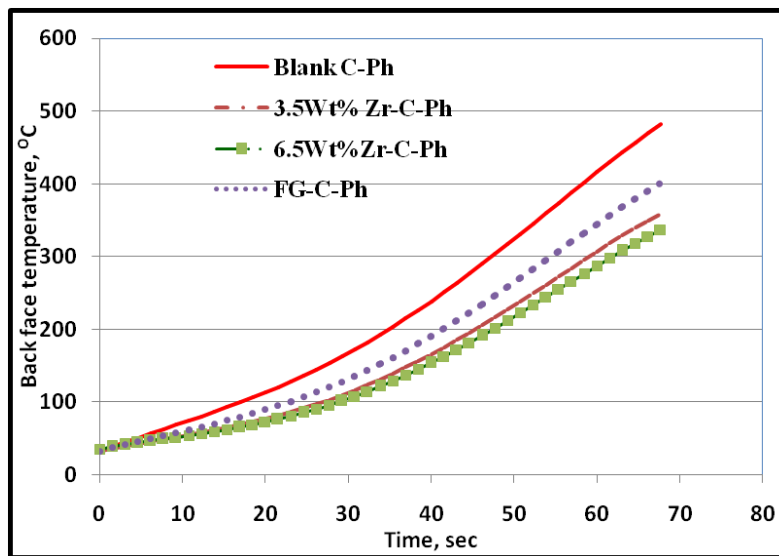

Figure.6.6: Back face temperatures of the blank C-Ph, Zr-C-Ph and FG-C-Ph composites

As seen in the Fig.6.6, back face temperature of the test specimens continued to raise even after the plasma jet was switched off after 30 seconds of test duration. This is due to the dissipation of heat energy from the ablated surface to the back face. Back face temperature at the end of the test (30 seconds after the plasma jet hit the front face of the specimen) and ablation rate of the test specimens are shown in Table.6.5.

Results show that, there is a significant reduction in the back face temperature of the Zr-C-Ph composites as compared to the blank. It indicates that, the insulating coating layer of the zirconia present on the C-fabric layers is able to reduce the back face temperature significantly under harsh testing environment.

Table.6.5: Ablation rate and back face temperature of composites in plasma arc jet test

122

Sample Description	Ablation rate (mm/s)	[a] Temp (^{0}C)
Blank C-Ph	0.054	169
3.5wt% Zr-C-Ph	0.078	114
6.5 wt% Zr-C-Ph	0.105	104
FG-C-Ph	0.103	135

[a]Back face temperature at the end of test (30seconds)

It is observed that, as the wt% of zirconia increased in Zr-C-Ph composites, there is more reduction in the back face temperature (Table.6.5) as the ceramic skin (zirconia coating) structure present on the C-fibers, can effectively insulate the virgin material beneath the ablation surface [20]. More thermal insulation capability of the Zr-C-Ph composites, is also evidenced by the lower depth of penetration of pyrolytic decomposition zone (char zone) in the through thickness direction from the ablated surface as compared to the blank C-Ph composites (Fig.6.7).

Effective thickness of the insulating Zr-C-Ph layers is less in FG-C-Ph composite as compared to the other Zr-C-Ph composites. Hence, back face temperature is observed to be more for FG-C-Ph as compared to the Zr- C-Ph composites (Table.6.5). On the other hand, ablation rate has increased for the Zr-C-Phas well as for FG-C-Ph composites as compared to the blank C-Ph. These observed trends in ablation rate are explained as follows.
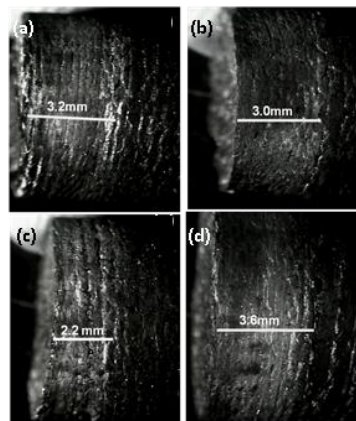

Figure 6.7: Stereo microscope images of samples after plasma arc jet test. Left end of the sample surfaces in each figure is ablated surface (surface exposed to plasma). Measured char depths are shown on the images. a) Blank C-Ph b) 3.5wt% Zr-C-Ph c) 6.5wt% Zr-C-Ph d) FG-C-Ph

5.5.1. Ablation mechanism in Zr-C-Ph composites: Two major degradation processes may have operated simultaneously during the ablation. The first one is the chemical degradation of composite which involves endothermic pyrolysis of the phenolic matrix (charring of the matrix) as shown in equation-2.

$$\text{Phenolic matrix} \longrightarrow C\ (\text{Char}) + CH_4 + CO + H_2 - \text{heat} \ldots\ldots\ldots (2)$$
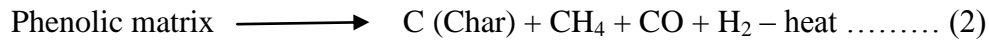
The second major degradation process is mechanical erosion due to high aerodynamic shear forces of the plasma jet which removes char and C-fibers from the ablating surface. Microstructure of the ablated surfaces shown in Fig.6.8 indicates that the matrix charring and its subsequent removal is taking place before the fiber erosion (Fig.6.8.a, 6.8.b).

Fiber damage and their erosive losses will be significantly low, when the char that is forming during ablation is retained for long durations. This is due to the fact that, char not only offers radiative cooling to the surface, but also projects an unidirectional fiber face to the plasma jet by encircling the individual fibers. Ablated surface of the blank C-Ph shows less matrix removal (Fig.6.8.a) as compared to the matrix removal from Zr-C-Ph composites (Fig.6.8.b).

The reason for more matrix removal from Zr-C-Ph composite during ablation can be due to additional reaction as shown in equation-3, that is taking place.

$$ZrO_2 + 3C\ (\text{Solid char}) \longrightarrow ZrC\ (\text{Solid}) + 2CO\ (\text{Gaseous}) \text{ ------- } (3)$$

In essence, zirconia present on the C-fibers reacting with the charred matrix, leading to the formation of zirconium carbide (ZrC) with the evolution of carbon monoxide. Formation of ZrC is confirmed from the XRD studies of the ablated surfaces of the Zr-C-Ph composites (Fig.6.9).

Formation of ZrC results in the net reduction of the solid (char) volume by a significant proportion with the evolution gaseous by products leading to highly porous network formation (Fig.6.8.b) in the remaining matrix. Similar observations regarding enhanced matrix removal for C-Ph composites in presence of zirconia (derived from high temperature oxidative decomposition of ZrB_2) was made by Y.Chen et al.[9].
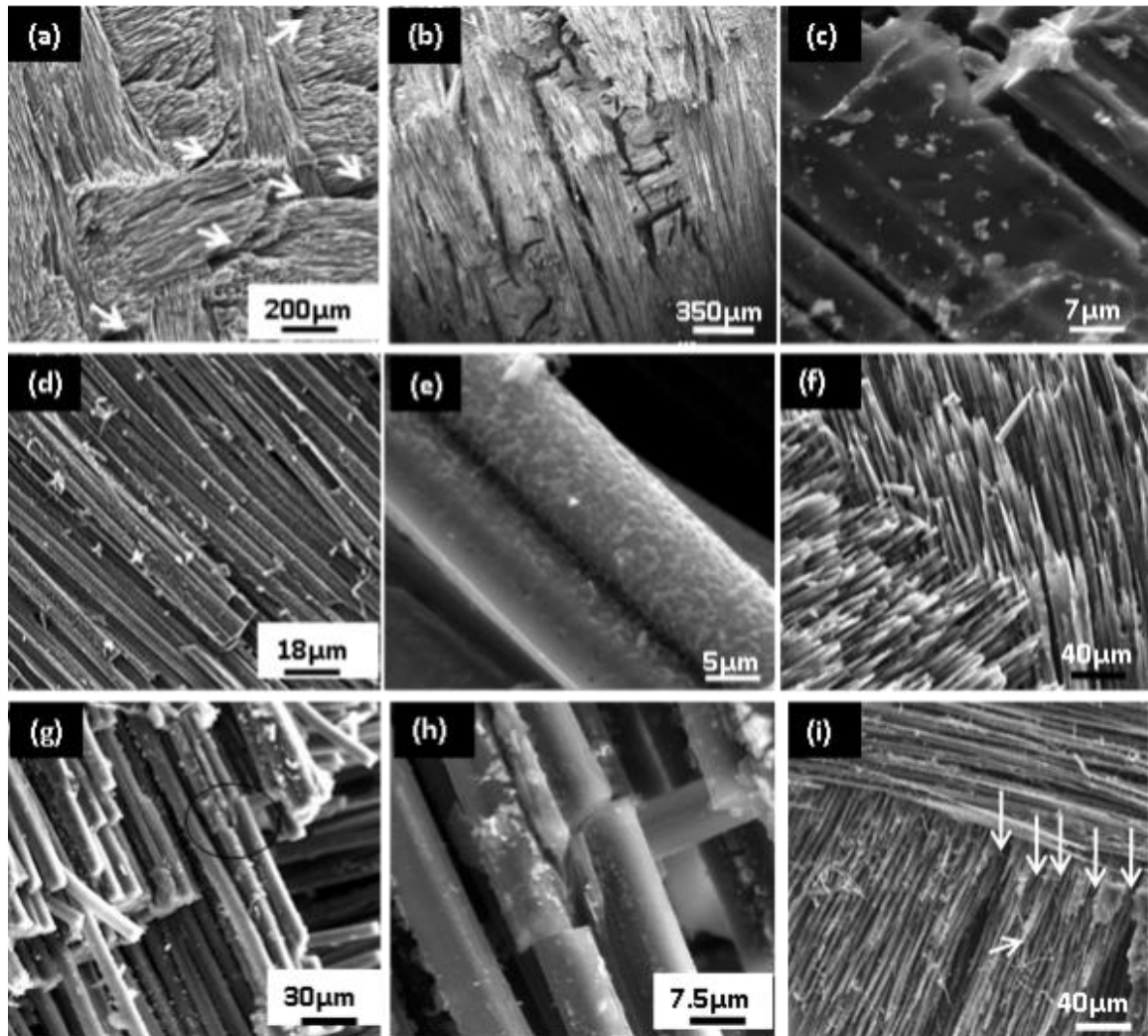
124

Figure.6.8: SEM images of samples after plasma arc jet test a) Blank C-Ph showing matrix removal ahead of fiber damage (pockets of matrix removed zones indentified by arrows)   b) 3.5wt% Zr-C-Ph showing more matrix removal up to considerable depth   c) Blank C-Ph showing low matrix porosity in the char zone (approximately 0.3mm behind the ablated surface) with good interfiber bonding. d&e) 3.5wt% Zr-C-Ph showing high level of matrix porosity in the char zone with poor interfiber bonding   f) Blank C-Ph showing needle like structure formation for C-fibers   g) 3.5wt% Zr-C-Ph showing broken fibers without needle like structure formation   h) Magnified view of the encircled zone of fig.g. showing initiation of fiber breaking   i) 6.5wt% Zr-C-Ph showing lumps of broken fibers.
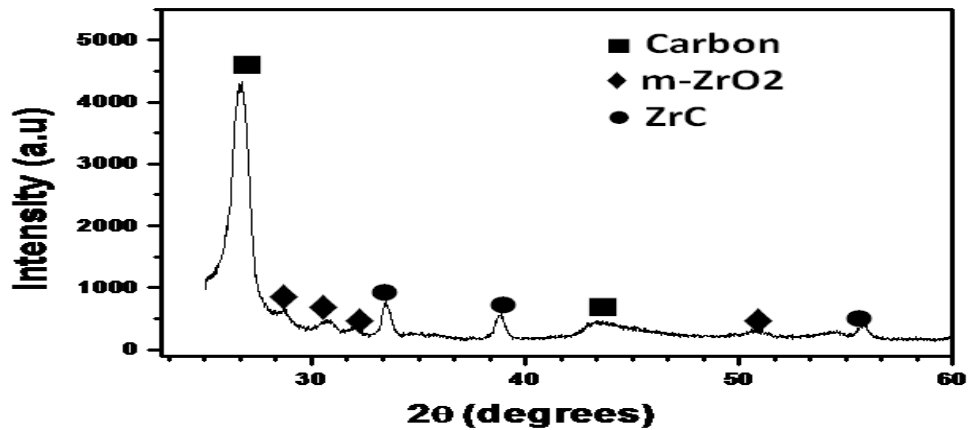
Figure.6.9: XRD of the ablated surface of Zr- C-Ph composite showing formation of ZrC

The above proposed reaction, showing consumption of the solid char by ZrO_2 giving gaseous by products (reaction-3) is also validated by carrying out through thickness SEM studies of the char zone of the tested samples (Approximately 0.3 mm behind the ablated surface). It was observed that, compared to the blank C-Ph composites (Fig.6.8.c), porosity in Zr-C-Ph composite is significantly high (Fig.6.8.d, 6.8.e). Lower rate of matrix removal from the blank resulted in better protection of the fibers as evidenced by the formation of needle like structure with less fiber breakage (Fig.6.8.f) [21]. Higher rate of matrix removal in Zr-C-Ph composites made the fibers under protected from the high velocity shear forces of plasma jet, which resulted in a severe breakage of lumps of fibers (Fig.6.8.g &6.8.h). The cumulative effect of enhanced rates of matrix and fiber removal resulted into enhanced ablation rate for Zr-C-Ph composite. As the wt% of zirconia in C-Ph increased, net reduction in solid char volume has become more prominent, which resulted in more fiber damage (Fig.6.8.i) with further enhancement in the ablation rate.

5.5.2. Ablation mechanism in FG-C-Ph composites: FG-C-Ph composite which was exposed to the plasma jet towards the surface having CNT-C-Ph composition, has shown the highest ablation rate among the tested composites. Considerable damage to the fibers on the ablated surface is observed (Fig.6.10).

It is clearly visible that, the fibers near the crossover points eroded higher than the fibers from the other areas (Fig.6.10.a). This is because CNT reinforcement in the C-Ph composite lead to increased thermal conductivity of the composite (Table.6.2).
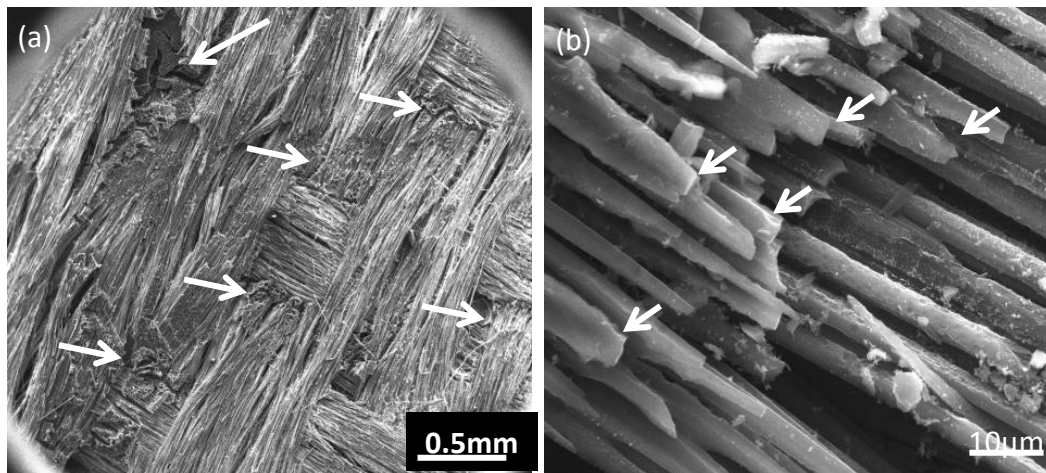
Figure.6.10: SEM images of FG-C-Ph samples after plasma arc jet test a) Significant erosive loss at the crossover points (indicated by arrows) b) Arrows indicating broken C fibers

 Enhanced thermal conductivity of the composite resulted in a faster rate of the heat front advancement which in turn led to the accelerated charring and degradation of the matrix along the thickness. Similar observations on enhanced rate of matrix pyrolysis for CNT reinforced phenolics was reported by Natali et al.[14]. As the crossover points are matrix rich areas in composites, they will become char rich areas during the ablation. Hence degradation at the crossover points is observed to be more severe. Accelerated charring and subsequent erosion of the matrix resulted in enhanced fibber breaking (Fig.6.10.b) and ablation rate [21]. Enhanced flexural, shear strength of C-Ph due to A_f-MWCNTs could not result into enhanced resistance to erosive loss of composite, primarily due to the fact that, the room temperature mechanical property improvements due to A_f-MWCNTs may have lost their significance in the charred matrix.

6. Conclusions:

i)   0.5wt% addition of A_f-MWCNT to C-Ph composites gives better improvement in the flexural strength and ILSS of C-Ph composites with minimum improvement in the thermal conductivity as compared to the 1.0wt% and 1.5wt% A_f-MWCNT addition.

(ii)   Zirconia addition to C-Ph composites (through coating of Zirconia on C-fabric) can bring down their thermal conductivity significantly. This resulted in reduced back face temperature when exposed to high temperature and high flux environments. However, zirconia addition to C-Ph composites reduces their flexural strength and ILSS.

iii)   Presence of zirconia in C-Ph composites has increased the ablation rate, primarily due to enhanced conversion of solid char in to zirconium carbide (ZrC) and carbon monoxide (gaseous product) leading to under protection of the carbon fibers facing the plasma jet.

iv)   Feasibility of integrating A_f-MWCNTs and zirconia in C-Ph composite and realizing a functionally graded composites is established.

v)   It is observed that A_f-MWCNTs can improve the room temperature flexural and shear strength of C-Ph composites. However enhancement in these properties lost their prominence in the charred matrix. Enhanced thermal conductivity due to A_f-MWCNTs improved the ablation rate of C-Ph composites.

References

[1] G.Savage, Carbon-Carbon Composites, First edition, Chapman & Hal, London,1993.

[2] G.F.D'Aelio, J.A.Parke blative plastics. Marcel Dekker, New York, 1971.

[3] K.A.Trick,T.E.Saliba, Mechanisms of the pyrolysis of phenolic resin in a carbon/ phenolic composite. Carbon 33(1995) 1509-1515.

[4] J.K.Park, D.Cho, T.J.Kang. A comparison of the interfacial, thermal and ablative properties between spun and filament yarn type carbon fabric/phenolic composites. Carbon 42(2004) 795-804.

[5] J.Xiao, J.M.Chen, H.D.Zhuo, Q.Zhang. Study of several organic resin coatings as anti-ablation coatings for supersonic craft control actuator. Mater.Sci.Engg.A. 452-453(2007) 23-30.

[6] Joseph H. Koo, Mark J. Miller, Jon Weispfenning, Charles Blackmon. Silicone Polymer Composites for Thermal Protection of Naval Launching System, Journal of Spacecraft and Rockets 48 (2001). 904-919.

[7] I.Srikanth, Alex Daniel, Suresh Kumar, N.Padmavathi, VajinderSingh,P.Ghosal, Anil Kumar,G.Rohini Devi. Nano silica modified carbon – phenolic composites for enhanced ablation resistance. ScriptaMaterialia63 (2010) 200-203.

[8] Joseph.H.Koo, Holly Stretz, Alan Bray, Jon Weispfenning, Z.P.Luo, Rusty Blanski, Nanostructured Materials for Rocket Propulsion System: Recent Progress. AIAA :2003:1769.

[9] Yaxi Chen, Ping Chen, Changqing Hong, Baoxi Zhang, David Hui. Improved ablation resistance of carbon–phenolic composites by introducing zirconium diboride particles. Composites: Part B 47 (2013) 320–325.

[10] G.Lubineau, A.Rahaman. A review of strategies for improving the degradation properties of laminated continuous fiber/epoxy composites with carbon based nanoreinforcements. Carbon 50 (2012) 2377-2395.

[11] J.M.Park, Z.J. Wang, D.J.Kwon, G.Y.Gu, W.I.Lee.J.K.Park. Interfacial properties and self sensing of single carbon fiber reinforced CNT-Phenolic nanocomposites using electro-micro mechanical and wettability tests. Composites : B 43(2012) 1171-1177.

[12] Maurizio Natali, Marco Monti, José Maria Kenny, Luigi Torre. A nanostructured ablative bulk molding compound: Development and characterization. Composites A 2011;42: 1197-1204.

[13] R.D.Patton,C.U.Pittman,L.Wang.Jr,J.R.Hill.A.Day, Ablation, mechanical and thermal conductivity properties of vaporgrown carbonfiber/ phenolic matrix composites. Composites: Part:A 33 (2002) 243-251.

[14] M.Natali, M.Monti, D.Puglia, J.M.Kenny, L.Torre. Ablative properties of carbon black and MWNT/phenolic composites: a comparative study. Composites: Part A. 43(2011) 174-182.

[15] K.J.Green,D.R. Dean., U.K.Vaidya,E.Nyairo, Multiscale fiber reinforce composites based on a carbon nanofiber/epoxy nanophased polymer matrix: synthesis, mechanical, and thermo mechanical behavior. Composites A 40 (2009) 1470-75.

[16] J.Cho, I.M.Daniel,D.A. Dakin . Effects of block copolymer dispersant and nanotube length on reinforcement of carbon/epoxy composites. Composites: Part A 39 (2008) 1844–1850.

[17] F.H.Gojny, M.H.G.Wichmann, U.Kopke, B.Fiedler, K.Schulte.. Carbon nanotube-reinforced epoxy – composites: enhanced stiffness and fracture toughness at low nanotube content. Compos Sci Technol. 64(2004) 2363-2371.

[18] C.Gau, S.Y.Chen, H.L.Tsai, Syh-Tsang Jenq, Cheng-Ching Lee, Yu-Der Chen, and Ting-Hua Chien. Synthesis of functionalized carbon nanotubes/phenolic nanocomposites and its electrical and thermal conductivity measurements. Jap.J.App.Phys.48(2009) 06FF10-1-4.

[19] Y.A.Kim, S.Kamio, T.Tajiri, T.Hayashi.,S.M.Song,M.EndoM.Terrones,M.S.Dresselhaus. Enhanced thermal conductivity of carbon fiber/phenolic resin composites by the introduction of carbon nanotubes.Appl. Phys. Lett. 90 (2007) doi.org/10.1063/1.2710778

[20] W.K.Ho, J.H.Koo, O.A.Ezekoye. Thermo plastic polyurethane elastomer nanocomposites: Morphology,thermo physical and flammability properties. Journal of nanomaterials.2010 (2010). doi:10.1155/2010/583234

[21] Donghwan Cho, Byung Il Yoon. Microstructural interpretation of the effect of various matrices on the ablation properties of carbon-fiber –reinforced composites. Compos Sci Technol. 61(2001) 271-280.

Chapter: VII

Concluding Remarks and

Future Scope of Work

1. Concluding remarks: In this chapter, the major conclusions listed at the end of chapter III to chapter VI are reviewed and the implications of the results obtained are over viewed.

High temperature heat treatment (2600^0C) of MWCNTs is an efficient method to obtain ultra high pure MWCNTs. This method also ensures enhanced structural perfection to MWCNTs. However the duration of heat treatment should be optimised, otherwise the process can render MWCNTs with distorted structures.

Amino functionalised MWCNTs (A_f-MWCNTs) are increasing the crosslink density of epoxy matrix due to the participation of amine groups of MWCNTs in crosslinking reaction. Toughness of the matrix increases up to optimum crosslink density. Hence, beyond certain weight percentage (wt%) addition of MWCNTs to matrix (epoxy), they start to embrittle it.

When the A_f-MWCNTs added epoxy resin is used to fabricate C-epoxy composites, Af-MWCNTs settles at the interface of carobn fiber and epoxy matrix. Their ability to enhance the crosslink density results in increased toughness of interface. Toughened interface can better resist the matrix microcracks that initiates at the interface when the C-epoxy is subjected to mechanical loads. This results in uniform load distribution across the area of the composite subjected to loading. As the strength of all the reinforcing carbon filaments/ fibers is harnessed completely, the mechanical properties of A_f-MWCNT-C-epoxy will be better than the blank C-epoxy (C-epoxy without A_f-MWCNTs). However, beyond optimum concentration of A_f-MWCNTs, they embrittle the interface. This leads to facile generation and propagation of interface cracks and premature failure of the composites. Present study reveals that, MWCNTs are not acting as load bearing reinforcements in the composites. Even if A_f-MWCNTs are well dispersed they bring down the mechanical properties beyond optimum concentration.

Flexural strength and shear strength improvements to C-epoxy composites due to amino functionalised carbon nanofibers (A_f-CNFs) are significant when C-epoxy composite is having lower fibre volume fraction. As the fiber volume fraction of the composite is increasing the strengthening mechanisms due to A_f-CNFs are losing their prominence. A_f-CNFs are observed to strengthen the matrix. Hence, fiber dominated properties like tensile strength are not increasing significantly due to A_f-CNFs.

In case of CFRPs used for thermal protection systems (Carbon - Phenolic composites), it was observed that, flexural strength and shear strength increases significantly with A_f-MWCNTs

132

addition. However, thermal conductivity was also observed to be increasing due to A_f-MWCNT addition. Considering the applications of thermal protection systems (TPS) which seeks increased flexural and shear strength with reduced thermal conductivity, efforts were made to introduce zirconia to C-phenolic composites through sol – gel method. Introduction of zirconia to CFRP has brought down the thermal conductivity. Feasibility of integrating both CNT reinforced C-Ph and Zirconia added C-Ph into a single structure (FG-C-Ph) is established. Both zirconia added C-Ph and FG-C-Ph phenolic were found to give significant reduction in back face temperature when they were exposed to high temperature and high flux (4 MW/m^2) environments.

2. Contributions: Additional mechanisms (other than conventionally proposed mechanisms) involved in strength improvements to CFRPs due to CNTs/CNFs addition are proposed. These mechanisms were supplemented with suitable characterisation methods. Besides understanding the need for introducing optimised concentrations of CNTs/CNFs to CFRPs, this work has highlighted the need for using CFRPs having optimised volume fractions to tap the potential of CNTs/CNFs as additional reinforcements. Mechanisms which define the thermal and ablative properties of CNT reinforced CFRPs are understood. Feasibility to offset the increased thermal conductivity of CNT reinforced CFRPs by introducing zirconia is established. The findings of the study, offers scope for increasing the specific strength of the presently used CFRPs with CNTs/CNFs addition. The major findings of this work and the insights of the science generated from this work indicates certain guidelines for the future research

3. Future scope of work:. Present study gives evidence of interface toughening by CNTs and CNFs to CFRPs. Hence, applications which seek toughened interfaces can be explored in future, to gain maximum advantage of these reinforcements. For example impact properties of laminated CFRPs will improve if the interface can dissipate applied load to longer distances at faster rates. It was observed in the present study that, network of CNTs/CNFs which are present at the interface are able to generate diffuse cracks much away from the point of loading. This mechanism can enhance the impact resistance of CFRPs/FRPs, as CNTs/CNFs can minimising the localised damages and back face trauma (Damage at the back face). This can find applications in composite armour used for defence systems.

Similarly damping properties of CFRPs can also increase significantly as CNT/CNF reinforced CFRPs can dissipate more energy at the interface. This will have significance in reducing the noise of the composite subsystems. Hence, impact and damping properties of CNT/CNF reinforced CFRPs can be explored further.

On the other hand, functionally graded CNT - ceramic CFRPs in different compositional sequences can be explored in future. For instance, blank carbon - phenolic (C-Ph) on the top which will experience the hot gases, followed by zirconia addition to C-Ph in the middle and CNTs addition to C-Ph at the bottom could give low thermal conductivity, high strength without compromising on the ablation rate.

Research studies can be taken up to understand what should be the critical length required for MWCNTs/CNFs to act as load bearing reinforcements. Possibility of using continuous CNT fibers as reinforcements by completely eliminating the conventional C-fibers could offer scope for realising the full potential of CNTs/CNFs as reinforcements.

Publications

List of publications

i) I.Srikanth, Suresh Kumar, Anil Kumar, P.Ghosal, Ch.Subrahmanyam. Effect of amino functionalised MWCNT on the crosslink density, fracture toughness of epoxy and mechanical properties of carbon – epoxy composites. *Composites: Part A*: 43:2012:2083-2086.

ii) I.Srikanth, N.Padmavathi, Suresh Kumar, P.Ghosal, Anil Kumar, Ch.Subrahmanyam. Mechanical, thermal and ablative properties of zirconia, CNT modified carbon/phenolic composites. *Composites Science and Technology*. 80:2013:1-7

iii) I.Srikanth, Suresh Kumar, Vajinder Singh, Rangababu, ParthaGhosal,Ch.Subrahmanyam. Studies on carbon nanofiber addition effect on the mechanical properties of different V_f carbon – epoxy composites. *Bulletin of Materials Science.* Accepted for publication.

iv) I.Srikanth, N.Padmavathi, Anil Kumar, P.Ghosal, Ch.Subrahmanyam. Effect of high temperature heat treatment duration on the purity and microstructure of MWCNTs. *Bulletin of Materials Science.* Accepted for publication.